JACS
JOURNAL OF THE AMERICAN CHEMICAL SOCIETY
Article
Cite This: J. Am. Chem. Soc. 2019, 141, 10684−10701
pubs.acs.org/JACS

GTP Hydrolysis Without an Active Site Base: A Unifying Mechanism for Ras and Related GTPases

Ana R. Calixto,[†,‡] Cátia Moreira,[†,‡] Anna Pabis,[§] Carsten Kötting,[∥] Klaus Gerwert,[∥] Till Rudack,*[,∥] and Shina C.L. Kamerlin*[,†]

[†]Department of Chemistry-BMC, Uppsala University, Box 576, S-751 23 Uppsala, Sweden
[§]Department of Cell and Molecular Biology, Uppsala University, BMC Box 596, S-751 24, Uppsala, Sweden
[∥]Department of Biophysics, Ruhr University Bochum, 44801 Bochum, Germany

Supporting Information

ABSTRACT: GTP hydrolysis is a biologically crucial reaction, being involved in regulating almost all cellular processes. As a result, the enzymes that catalyze this reaction are among the most important drug targets. Despite their vital importance and decades of substantial research effort, the fundamental mechanism of enzyme-catalyzed GTP hydrolysis by GTPases remains highly controversial. Specifically, how do these regulatory proteins hydrolyze GTP without an obvious general base in the active site to activate the water molecule for nucleophilic attack? To answer this question, we perform empirical valence bond simulations of GTPase-catalyzed GTP hydrolysis, comparing solvent- and substrate-assisted pathways in three distinct GTPases, Ras, Rab, and the $G_{\alpha i}$ subunit of a heterotrimeric G-protein, both in the presence and in the absence of the corresponding GTPase activating proteins. Our results demonstrate that a general base is not needed in the active site, as the preferred mechanism for GTP hydrolysis is a conserved solvent-assisted pathway. This pathway involves the rate-limiting nucleophilic attack of a water molecule, leading to a short-lived intermediate that tautomerizes to form $H_2PO_4^-$ and GDP as the final products. Our fundamental biochemical insight into the enzymatic regulation of GTP hydrolysis not only resolves a decades-old mechanistic controversy but also has high relevance for drug discovery efforts. That is, revisiting the role of oncogenic mutants with respect to our mechanistic findings would pave the way for a new starting point to discover drugs for (so far) "undruggable" GTPases like Ras.

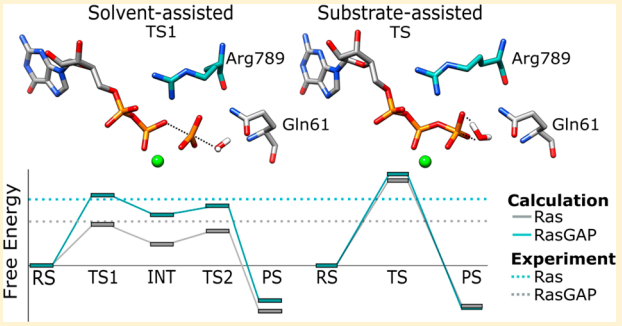

INTRODUCTION

Phosphate esters are essential to life, facilitating cellular signaling, energy production, and protein synthesis and maintaining the integrity of the genetic material.[1] Their central role in biology has made them the topics of almost a century of extensive computational and experimental research effort.[1−4] However, the mechanisms of even the uncatalyzed hydrolysis of phosphate esters are highly complex due to the availability of competing pathways for the same reaction,[1] with the precise choice of the mechanism being highly sensitive to esterification state, protonation state, and leaving group.[1,4] In addition, uncatalyzed phosphoryl transfer reactions in aqueous solution are among the slowest biochemical reactions known, with half-lives into the billions of years,[5] whereas their enzymatic counterparts can occur on the submillisecond time scale.[5] Therefore, the enzymes that catalyze phosphoryl transfer reactions are the most proficient known to man[1,5] compared to many enzymes catalyzing other reactions.[5−7] Finally, enzymes that catalyze phosphoryl transfer reactions play a central role in facilitating some of the most important processes in biology. Consequently, knowledge of the chemical mechanisms of these enzymes, as well as how they function and are regulated, provides a window into the regulation of life itself at the most intimate molecular level.

GTPases, in turn, are a large superclass of hydrolytic enzymes, which are divided into various classes, families, and subfamilies.[8−18] The enzymes of this superclass are structurally and mechanistically diverse hydrolytic enzymes which catalyze the conversion of guanosine triphosphate (GTP) to guanosine diphosphate (GDP) and inorganic phosphate (P_i). In doing so, these enzymes regulate all stages of cellular function, from signaling cascades to cell migration, polarity, adhesion, cytoskeletal organization, proliferation, and apoptosis (e.g., ref 19).

A key feature of GTPases is their role as "molecular switches", harnessing conformational transitions between active GTP-bound "ON" states and inactive GDP-bound "OFF" states to control various cellular processes.[20] This transition is observed in a range of GTPases such as Ras and its

Received: March 24, 2019
Published: June 14, 2019

DOI: 10.1021/jacs.9b03193
J. Am. Chem. Soc. 2019, 141, 10684−10701

homologues, as well as in elongation factors and in heterotrimeric G proteins, and generally involves fairly significant conformational changes. The overall catalytic rates of many GTPases are affected by interaction with different external regulatory proteins,[20] which substantially enhance the rates of GTP hydrolysis by GTPases by up to a 10^5-fold increase,[21] depending on the specific GTPase/regulator combination.[21−24] In addition, the rates of biological GTP hydrolysis run the gamut from GTPases such as Rab1b GTPase, which regulates vesicular transport and has an intrinsic turnover rate as slow as 1.5×10^{-5} s^{-1} at 20 °C,[25] to Ras GTPase, which is involved in cellular signaling, having a turnover rate as fast as 19.1 s^{-1} at 25 °C when activated by its GTPase activating protein (GAP),[27] and Cdc42, which has a turnover rate as fast as 90 s^{-1} at 25 °C when activated by its GTPase activating protein GRAF1.[28]

Finally, phosphate esters are mechanistically versatile: even though the reaction is superficially a trivial inline nucleophilic substitution reaction using a water nucleophile, this reaction can proceed through multiple different pathways. That is, this reaction can, in generalized terms, proceed through three different mechanisms, as shown in Figure 1. The first of these

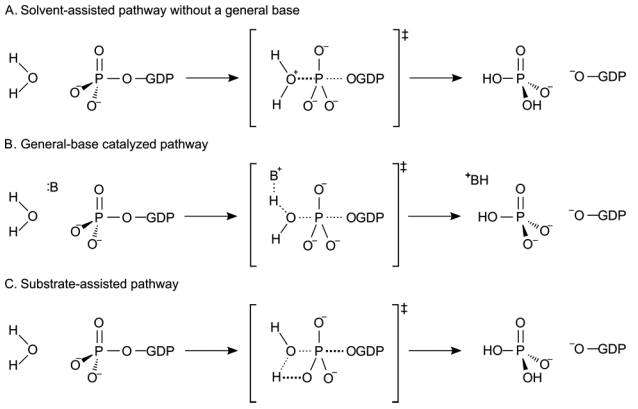

Figure 1. Overview of different potential mechanisms for GTP hydrolysis by GTPases to yield GDP and inorganic phosphate. (A) Solvent-assisted pathway in which deprotonation of the incoming nucleophile occurs after the initial nucleophilic attack. (B) General base-catalyzed pathway. (C) Substrate-assisted pathway involving direct proton transfer to the substrate itself. Note in the case of C that as quantum chemical studies of the nonenzymatic reaction have suggested that the barriers for direct proton transfer to the substrate and for proton transfer to the substrate via intervening water molecules are similar,[26] only the direct mechanism has been considered in this work. Finally, we have not considered mechanism B in this work due to the absence of an obvious general base in the active site.

is a solvent-assisted pathway with a loose dissociative transition state with very little bond formation to the incoming nucleophile ($P-O_{nuc}$) and advanced bond cleavage to the departing leaving group ($P-O_{lg}$), as shown, for example, in refs 26, 29, and 30. Here, the nucleophile is not yet deprotonated at the transition state, but rather, deprotonation of the nucleophile occurs in a fast step after the initial rate-limiting attack of H_2O (solvent-assisted pathway, Figure 1A). Once the $P-O_{nuc}$ bond has been substantially formed, the pK_a of this oxygen will be so low that this proton transfer can occur either to the γ-phosphate oxygen atom through a fast tautomerization step to a nearby proton acceptor in the active site (if available, in the case of enzymatic phosphate hydrolysis) or to bulk solvent. In the present work, we consider only proton transfer to the γ-phosphate oxygen atom due to lack of other obvious proton acceptors in the GTPase active site, as well as experimental evidence for this proton transfer occurring.[31] The reaction could also proceed via a general base-catalyzed pathway (Figure 1B), which can have either a loose or a tight transition state, or through a more associative substrate-assisted pathway (Figure 1C) with a much tighter transition state involving substantial bond formation to the incoming nucleophile and little bond cleavage to the departing leaving group, together with proton transfer from the nucleophilic water molecule to the γ-phosphate oxygen, as suggested in, e.g., refs 27, 32, and 33. We have previously considered an additional mechanistic option involving a substrate-as-base-type mechanism involving an intervening water molecule that deprotonates the nucleophile in the case of the nonenzymatic phosphate monoester hydrolysis but found it to be energetically essentially identical to the direct substrate-assisted mechanism.[26] Therefore, we have not considered this option in the present work. Overall, the choice of mechanism is highly sensitive to the precise electrostatic environment of the reaction, and as these different pathways can be energetically very similar, this leads to significant challenges to both theory and experiment to unambiguously distinguish between them.[1,19,26]

Therefore, despite being extensively studied from a *biological* point-of-view,[20,21,33−39] apart from the exceptions of enzymes such as Ras, some Rab GTPases[25,34] and EF-Tu[40−46] and more recently work on role of the intrinsic arginine finger in heterotrimeric G-proteins,[47] the precise *chemical* mechanisms of GTP hydrolysis by many of the different members of this biologically central enzyme superfamily remain largely unknown. The challenge here is that although all GTPases catalyze the same chemical reaction (Figure 1) and many have similar active site architectures (Figure 2), they can use vastly different regulatory strategies to achieve efficient catalysis[21,48] and thus could plausibly also use different catalytic mechanisms to hydrolyze GTP.

For example, in the case of Ras GTPase (Figure 2A) the formation of a complex with the GAP provides a key catalytic arginine residue, the "arginine finger", which is highly conserved among several GAP proteins for small GTPases[21] and has been argued to provide electrostatic stabilization in the active site of the Ras in complex with its GAP. In addition, the GAP is believed to stabilize the position of the nucleophilic attacking water molecule.[52] From here onward, we refer to the complex of Ras together with its GAP solely as RasGAP.

In addition to the arginine finger, there has been substantial discussion about the catalytic role of a conserved glutamine in the active site of small GTPases (Gln61 in Ras). There is an ongoing debate whether it is directly involved in acid−base catalysis or merely helps to stabilize the transition state for GTP hydrolysis (e.g., refs 1, 4, 27, 33, 34, and 52−66). Whereas in Ras and Rho the catalytic glutamine belongs to the GTPase, there exists another group of small GTPases, namely, members of the Rab GTPase subfamily (Figure 2B), in which the GAP protein (in most cases known to possess a Tre2/Bub2/Cdc16 (TBC) domain) provides both the glutamine and the arginine. Interestingly, it has been shown that the "glutamine finger" provided by the TBC domain displaces the intrinsic glutamine in Rab GTPases.[25] This "dual finger" motive of RabGAP, which accelerates the intrinsic rate of GTP

DOI: 10.1021/jacs.9b03193
J. Am. Chem. Soc. 2019, 141, 10684−10701

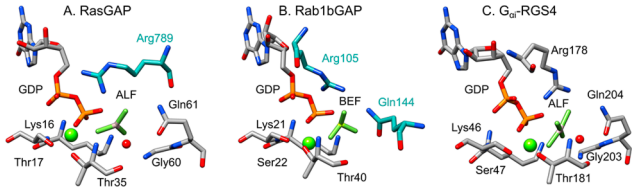

Figure 2. Active sites of (A) RasGAP in complex with GDP and AlF_3 (ALF) (PDB ID 1WQ1[49,50]). (B) Human Rab1 in complex with the GTPase activating protein (GAP) domain of TBC1D20 and BeF_3^- (BEF) (PDB ID 4HLQ[25,50]). (C) α-Subunit of the heterotrimeric G_i protein in complex with the RGS4 activating protein, GDP, and AlF_4^- (ALF) (PDB ID 1AGR[50,51]). Residues from each GTPase are highlighted in gray, and those from the corresponding GAP/RGS protein are shown in cyan. Catalytic water molecule and magnesium ion are shown as green and red balls, respectively. Note that in PDB ID 4HLQ, the position of the catalytic water molecule is not resolved in the X-ray structure and is therefore omitted from this panel. Residues inserted by the regulatory proteins are, specifically, (A) the arginine finger in the RasGAP complex and (B) the arginine and glutamine fingers in the RabGAP complex. In case C, the arginine (Arg178) and glutamine (Gln204) are both intrinsic to the GTPase itself, and the catalytic stimulation by the regulatory protein is thus entirely allosteric.

hydrolysis by up to 10^5-fold,[67] is critical to catalysis and intolerant to mutations.[22] Rab GTPases regulate membrane trafficking within cells. They also play a key role in many bacterial pathogeneses, making these enzymes and their regulators important targets for the design of novel antibiotics.

Other GTPases using a similar Arg/Gln constellation in their active sites are heterotrimeric G proteins (Figure 2C). Heterotrimeric G proteins are large, membrane-associated enzymes that are activated by G protein-coupled receptors[68] and that form a bimodal GTP-hydrolyzing switch, which plays an important role in regulating cellular signaling.[35] They are composed of three independent subunits (labeled the α-, β-, and γ-subunits), with the α-subunit sharing strong structural similarity with small GTPases such as Ras.[35] However, in contrast to Ras and Rab GTPases, the key catalytic Arg/Gln residues are both intrinsically present in the active site of the α-subunit of the heterotrimeric G-protein. Thus, the stimulatory effect on the rate of GTPase hydrolysis of the Regulator of G protein signaling (RGS) proteins, which are the GAPs of heterotrimeric G proteins,[69] is purely allosteric[70] (see also ref 47 which discusses the role of the intrinsic arginine residue).

As shown above, GTPases use different catalysis strategies, despite similar active site architectures, which raises the curious question of how much of an influence these differences have on the preferred reaction pathway(s) for GTP hydrolysis. In particular, a long-standing question in understanding GTP hydrolysis by small GTPases and related enzymes has been how GTP hydrolysis can occur in the absence of an obvious general base in the active site.[1,4,19,34] Computational studies have focused on either substrate-assisted GTP hydrolysis pathways (with the involvement of either one or two active site water molecules[27,31,43,71,72]) as shown in Figure 1C or general-base catalyzed pathways involving the side chain of the active site Gln as a general base,[52,61,62,73,74] as shown in simplified fashion in Figure 1B. However, the extremely low pK_a of the carbonyl group (estimated to be about −2[75]) makes it extremely unlikely that this side chain fulfills the role of a general base during the reaction (see, e.g., refs 56, 72, 75, and 76 for discussion), and therefore we have not considered this mechanism from a computational perspective in the present work. Considering instead the elevated pK_a of the nonbridging oxygens of the GTP γ-phosphate (p$K_a \approx 6.5$[77]), substrate-assisted catalysis would in principle be viable. However, we recently performed detailed studies of the mechanisms of the hydrolysis of phosphate monoester dianions,[26,29] acetyl phosphate,[30] and GTP analogues, demonstrating that a solvent-assisted pathway, such as that shown in Figure 1A, is substantially energetically preferred over the corresponding substrate-assisted pathway.

Having a solvent-assisted pathway without a general base is in principle possible, and it has been questioned whether a general base is actually needed during GTP hydrolysis[4] on the basis of analysis of kinetic isotope effects[78−80] and linear free energy relationships,[27,81] that is, it was suggested in ref 4 that the catalytic advantage to the reaction of generating a hydroxide nucleophile is, at best, ∼60-fold in contrast to the 10^5-fold rate acceleration observed relative to the non-enzymatic reaction. Therefore, based on the analysis in ref 4, a solvent-assisted pathway in which the nucleophile is deprotonated *after* the rate-limiting transition state (Figure 1A) would be in agreement with the experimental data. In such a mechanism having an active site base present becomes less relevant, and once the group transfer has occurred tautomerization leads to a $H_2PO_4^-$, as shown by FTIR spectroscopic measurements in the case of Ras.[31] However, the solvent-assisted mechanism, which does not require an explicit general base (Figure 1A), has been largely ignored in computational studies. The only exception to this is an optimized transition state for GTP hydrolysis by Rho GTPase, which appears similar to the transition state that would be expected in a solvent-assisted pathway but without consideration of the full reaction pathway leading to this transition state.[82]

In the present work, we explore for the first time computationally and in a systematic way whether such a solvent-assisted pathway is a viable mechanism for enzymatically catalyzed GTP hydrolysis and, if so, whether it is conserved, not only among the small GTPases Ras, Rho, and Rab but also within other GTPase families such as heterotrimeric G proteins. In light of this, we also revisit the role of the corresponding GAP/RGS proteins for these enzymes and show that their role is 2-fold: (1) to maintain the structural preorganization of the active site, through rigidification of catalytically unfavorable protein motions at both the local and global levels, and (2) to sequester the active site from solvent, thus increasing the strength of short-range electrostatic interactions between the substrate and the polar residues in the active site, allowing them to provide greater transition state stabilization. Taken together, these data are key to our broader understanding of enzyme catalysis and regulation in these biologically critical systems.

METHODOLOGY

Parameterization of the Empirical Valence Bond Potentials. The empirical valence bond (EVB) approach[83−85] has been used extensively to model enzymatic reactivity in general and phosphate hydrolysis in particular. This approach is a hybrid EVB/MM approach, based on classical force fields, that allows for the description of chemical reactivity within a valence bond-based quantum mechanical framework.[85] The main advantages of this approach in studies of enzymatic reactivity are that, on one hand, as the dynamical behavior of the system is described classically, it is a very computationally

DOI: 10.1021/jacs.9b03193
J. Am. Chem. Soc. 2019, 141, 10684−10701

inexpensive approach, allowing for the extensive conformational sampling allowed to obtain convergent free energies while taking into account dynamical changes along the chemical reaction coordinate during the chemical step of catalysis. At the same time, a well-parametrized EVB potential carries a tremendous amount of chemical information, allowing for bond-breaking and bond-forming processes to be described in a physically meaningful manner.[84,85] The main shortcomings of this approach are that the quality of the results obtained are dependent on the quality of the parametrization of the EVB potentials describing the different valence bond states (which can be checked, for example, against the fidelity of the model in reproducing relevant experimental observables, as in the present work) and also that by predefining the different valence bond states, one does not allow unexpected alternate processes to occur spontaneously. However, this approach has an excellent track record of reproducing and rationalizing key experimental observables[86−88] and compensates for these limitations by the ability to perform sufficient sampling to capture the conformational flexibility of the enzyme along the EVB reaction coordinate. It should also be emphasized that in the EVB framework parametrization is only performed once against a predefined reference state (either the nonenzymatic reaction in vacuum or in solution or the wild-type enzyme against a series of mutations). These parameters are then transferred unchanged to all other systems being studied, allowing for direct comparison of multiple systems without prejudice.

Here, we modeled both enzymatic and nonenzymatic GTP hydrolysis proceeding via each solvent- and substrate-assisted mechanism (Figure 1A and 1C), without the involvement of an external general base, using the valence bond states shown in Figures S1 and S2 (note that although Figure S1 depicts three valence bond states, the process is modeled in two sequential steps from **State 1** to **2** and **2** to **3** and two valence bond states are used simultaneously). Both mechanisms were modeled as a single concerted step, based on our previous DFT studies of the corresponding nonenzymatic reaction in aqueous solution, using different model reactions.[26,29,89] We note that in the case of the solvent-assisted pathway our QM calculations have suggested that the rate-limiting phosphoryl transfer reaction results in the formation of a high-energy transient intermediate that then tautomerizes to form the actual final product (Figure S3). As this step will be very fast and clearly not rate limiting, we only modeled it explicitly in the case of GTP hydrolysis in water and catalyzed by Ras and RasGAP.

All simulations in this work have been performed using the Q simulation package,[90] version 5.10, and the OPLS-AA force field.[91] The GTP and GDP molecules were described in our simulations using OPLS-AA compatible force field parameters derived in previous work,[92] and the magnesium ion was modeled using a multisite cationic dummy model, as described in detail in ref 93. The use of a multisite model greatly improves the stability of the metal center in the simulations while correctly describing the key thermodynamic properties of the metal and without the need for any artificial restraints or bonds between the metal and ligands.[93] Parameters describing the different tautomers of inorganic phosphate ($H_2PO_4^-$, Figure S3) were obtained using Macromodel 9.1, version 11.[94] In the case of the bonded parameters for the transient intermediate ($P-O_{nuc}$ = 1.88 Å), based on our previous quantum chemical calculations,[30] these were calculated using the Seminario method.[95] The partial charges of both species were calculated using the standard RESP procotol,[96] and both the RESP and the Seminario procedures were performed using Gaussian 09 Rev. E01[97] in conjunction with AMBER tools.[98] Both GTP and GDP charges were obtained from the revised parameters published by Carlson and co-workers, for use with the AMBER force field, for consistency.[99] Finally, the bonds breaking or forming during the reaction were described using Morse and soft-pair potentials, which were specifically parametrized to reproduce the $P-O_{nuc}$ and $P-O_{lg}$ distances obtained at the transition states in our recent DFT study of methyl triphosphate hydrolysis[30] in the corresponding EVB reaction in aqueous solution. The same parameters were then transferred unchanged from the reaction in aqueous solution to the active sites of the different GTPases studies in this work. All EVB parameters used in this work are provided in the Supporting Information.

System Setup. Initial coordinates for the simulations were taken from crystal structures in the Protein Data Bank[50] with the following accession numbers: 1QRA[50,100] (Ras), 1WQ1[49,50] (RasGAP), 1GIA[50,101] ($G_{\alpha i}$-subunit), 3NKV[50,102] (Rab), chains I and J from 4HLQ[25,50] (Rab1GAP), 621P[50,54] (Ras Q61H variant). In the case of the $G_{\alpha i}$−RGS4 complex, a refined crystal structure was used as a starting point for the simulations.[47] Where available in the crystal structure, the GTP molecule in the active site was kept in the same position as in the initial structure. In the other cases, the terminal group of the GTP analogue present in the crystal structure was manually replaced by the γ-phosphate to generate a GTP ligand. The magnesium multisite cationic dummy model center was superimposed with crystal magnesium coordinates, and the dummy atoms were aligned with the coordination sphere atoms of magnesium ion to optimize the description of the interactions between the metal and protein. A full list of the different analogues present in each structure used in this work is presented in Table S1.

In all cases, the system was solvated in a 30 Å radius droplet of TIP3P[103] water molecules centered on the P atom of the γ-phosphate group of the GTP. All crystallographic water molecules within this 30 Å sphere were retained for the simulations and also described using the TIP3P model. This water droplet was then simulated subject to surface-constrained all-atom solvent (SCAAS) boundary conditions[104] in a multilayered approach in which all atoms within the inner 85% of the solvent sphere were allowed to move freely, while atoms in the external 15% and outside of the solvent sphere where subject to 10 and 200 kcal mol^{-1} $Å^{-2}$ harmonic position restraints, respectively. All residues outside of the explicit water sphere were kept in their neutral forms in order to prevent instabilities due to the presence of charged residues outside the explicitly solvated region and were kept restrained to their crystallographic coordinates by the aforementioned 200 kcal mol^{-1} $Å^{-2}$ harmonic position restraints. All other residues were protonated based on their expected protonation states at physiological pH, as estimated using PROPKA 3.1[105] (Table S2).

Simulation Details. All simulations were performed with the leapfrog integrator using a 1 fs time step unless stated otherwise. Temperature control was maintained using the Berendsen thermostat[106] with separate coupling of the solute and solvent to individual heat baths. The nonbonded interactions were calculated with a 10 Å cutoff, except for the reacting atoms, to which a 99 Å (in principle infinite)

DOI: 10.1021/jacs.9b03193
J. Am. Chem. Soc. 2019, 141, 10684−10701

cutoff was applied for the nonbonded interactions. Long-range electrostatic effects were described using the local reaction field (LRF) approach.[107] All bonds involving hydrogen atoms were constrained using the SHAKE algorithm.[108] All systems were initially simulated for 3 ps at 1 K with a 0.1 fs step size in order to remove steric clashes and close contacts in the system. The positions of all atoms were fixed during this initial stage of the simulation by use of a 200 kcal mol^{-1} $Å^{-2}$ harmonic restraint on all atoms in the system. The step size was subsequently increased to 1 fs, and the temperature was gradually increased to 300 K while steadily removing the positional restraints on the system over a total of 210 ps of simulation time. After reaching the target temperature of 300 K, each system was subjected to a further 50 ns of unrestrained equilibration (not taking into account the restraint on atoms outside the flexible simulation sphere). For each system, the equilibration was repeated 20 times with different sets of initial velocities, obtained by assigning different initial random seeds to the different replicas. The end points of the 20 × 50 ns equilibration runs were used as starting points for the empirical valence bond (EVB) simulations[83] of each of the solvent- and substrate-assisted pathways, respectively. In the case of the solvent-assisted mechanism, an additional EVB simulation was performed for the tautomerization reaction in water, Ras and RasGAP systems, using as the starting point intermediate obtained from EVB simulations of the phosphoryl transfer, depicted as the step between **State 1** and **State 2** in Figure S1.

The GTP and nucleophilic water molecule were subjected to weak 0.5 kcal mol^{-1} $Å^{-2}$ positional restraints during the EVB simulations in order to keep them close to the center of the explicit simulation sphere. Additionally, a harmonic distance restraint of 10.0 kcal mol^{-1} $Å^{-2}$ was applied at the Michaelis complex to prevent the nucleophilic water from moving farther than 4 Å away from the P atom of the γ-phosphate of the GTP. This restraint was only activated when this 4 Å distance cutoff was exceeded (i.e., this restraint was effectively only applied to the Michaelis complex as this bond is either partially or fully formed in subsequent transition and intermediate/product states). All EVB simulations of the phosphate hydrolysis step (moving between **States 1** and **2** in the solvent- and substrate-assisted pathways, respectively, see Figures S1 and S2) were initiated at the approximate transition state of the reaction, corresponding to the equal mixing of the two states in the EVB-FEP/US approach ($\lambda = 0.5$). Note that equilibrating the system at the transition state leads to the additional advantage of needing shorter equilibration times for system convergence (Figures S4 and S5), as the transition state is highly polarized (allowing the system to preorganize easily) and there are already partial bonds to the nucleophile and leaving group. This allows us to run a much larger number of individual trajectories.

The EVB free energy perturbation/umbrella sampling (EVB-FEP/US) simulations of both the substrate- and the solvent-assisted mechanisms were performed using the valence bond states shown in Figures S1 and S2 with 51 individual mapping windows per EVB trajectory. Each window was simulated for 200 ps of simulation time, leading to a total of 10.2 ns of simulation time per individual EVB trajectory. Each simulation was repeated in 20 individual replicas, leading to a total of 18 μs of equilibration time over all systems, 204 ns of EVB simulation time per system and reaction mechanism (408 ns in the case of the solvent-assisted Ras- and RasGAP-catalyzed reactions where the tautomerization step was explicitly included in the simulations), and a total of 3.7 μs of EVB simulation time over all systems.

Calibration of the Empirical Valence Bond Parameters. The EVB gas-phase shift and coupling parameters (α and H_{ij}, respectively) were calibrated using the background reaction in aqueous solution as a reference system for each of the substrate- and solvent-assisted mechanisms. For a detailed description of these parameters, see, e.g., refs 83 and 85. In the case of the nonenzymatic reaction, the substrate- and solvent-assisted hydrolyses of GTP, respectively, were used as reference states for the corresponding enzymatic mechanisms. The nonenzymatic reaction was modeled using the same protocol as the enzymatic reaction, with the exception that a shorter 20 ns equilibration was performed prior to the EVB simulations. The EVB parameters were then adjusted to reproduce activation free energies of 27.9 kcal mol^{-1} for the solvent-assisted mechanism and 37.2 kcal mol^{-1} for the substrate-assisted mechanism. The value for the preferred (in aqueous solution) solvent-assisted mechanism is based on the experimentally measured activation free energy for GTP hydrolysis in aqueous solution at 25 °C,[109] whereas that for the substrate-assisted mechanism is adjusted based on the energy difference found between the two pathways in our detailed DFT study of nonenzymatic methyl triphosphate hydrolysis (averaging over the values obtained from two different DFT functionals).[30] In the case of the overall reaction free energy, this was set to −7.4 kcal mol^{-1} for the substrate-assisted pathway (based on experimental data).[109] In the case of the solvent-assisted pathway, as quantum chemical calculations suggest that this pathway proceeds via the high-energy intermediate shown in Figures S1 and S3,[26,30] the free energy of this intermediate was set to 19.0 kcal mol^{-1} as an estimate of the energy of this intermediate.

Finally, for the tautomerization step, as we assumed this step would be fast, we calibrated our simulations to reproduce an activation free energy ($\Delta G^{\ddagger}$) of 4 kcal mol^{-1} as an estimated upper limit for the tautomerization step and a reaction free energy (ΔG^{0}) of −26.4 kcal mol^{-1} to result in an overall reaction free energy of −7.4 kcal mol^{-1} between the initial reactant state and the final product state, in agreement with experiment.[109] We note that the intermediate formed after the phosphoryl transfer step in the solvent-assisted pathway has an elongated $P-O^{+}H_2$ bond, and therefore, as discussed in ref 29, this is very likely to be a high-energy metastable species that is formed only transiently prior to deprotonation of the nucleophile, either by deprotonation to bulk water or by tautomerization as modeled here. On the basis of this and also considering the fact that the equilibrium for this process so strongly favors the product of the tautomerization step, we believe that 4 kcal mol^{-1} provides a comfortable upper limit for the likely activation free energy for this step, allowing us to obtain an approximation of the energetics of this step in our EVB simulations. The parameters obtained from the EVB calibration were then used unchanged to describe also the corresponding enzymatic hydrolysis of GTP via solvent- and substrate-assisted pathways, respectively, in all systems studied in this work. These parameters are provided in the Supporting Information alongside all other EVB parameters used in our simulations

Analysis. All simulation analyses were performed using the Q fep and Q calc modules of the Q simulation package,[90] combined with the Q tools package (DOI 10.5281/zenodo.842003) and using VMD 1.9.3.[110] Finally, all structure

DOI: 10.1021/jacs.9b03193
J. Am. Chem. Soc. 2019, 141, 10684−10701

depictions in this work were generated using Chimera.[111] Active site volumes for Ras and RasGAP were calculated from 20 × 50 ns of MD equilibration performed at the respective Michaelis complexes using Pocket Volume MEasurer (POVME) 3.0,[112,113] with snapshots taken every 100 ps of the simulations. RMSD calculations were performed using MDTraj,[114] with snapshots taken every 100 ps of the simulations. Finally, the loss of conformational entropy of the catalytic glutamine residue upon protein folding was calculated using the initial crystal structures used for the simulations and the Predicting Loss of Protein S(entropy) (PLOPS)[115] Web server.

RESULTS AND DISCUSSION

To explore the viability of the solvent-assisted pathway for GTP hydrolysis we first performed EVB simulations to calculate the free energy barriers during GTP hydrolysis based on the solvent-assisted and the substrate-assisted pathway. In order to validate the simulations and determine the preferred pathway, the calculated barriers were compared to the experimental values. Following from this we analyzed the detailed role of the catalytically important Gln in the active site and also investigated the effect of its mutation to a histidine, which would be analogous to the corresponding residue in translational GTPases such as EF-Tu.[41,42,71] We first discuss the results for the most prominent small GTPase, Ras, with and without its GAP. Then we demonstrate that our findings are of general relevance and conserved among GTPases by studying proteins of the Rab family as well as the $G_{\alpha i}$ subunit.

Substrate- vs Solvent-Assisted GTP Hydrolysis in the Reaction Catalyzed by Ras and RasGAP. There have been a number of computational studies of the nonenzymatic hydrolysis of triphosphates, GTP and ATP in vacuum and solution.[116−122] In the case of nonenzymatic methyl triphosphate hydrolysis, detailed quantum chemical calculations have shown that the activation free energy for the substrate-assisted pathways is ∼9 kcal mol^{-1} higher in energy than for the corresponding solvent-assisted pathway,[30] a trend also seen in the hydrolysis of analogous compounds such as a range of phosphate monoesters.[29] Therefore, the solvent-assisted pathway is intrinsically favorable compared to the substrate-assisted pathway except for compounds with very poor leaving groups (pK_a > 8.4, see discussion in ref 29), and the enzyme must overcome a much higher free energy barrier for the reaction to proceed via the substrate-assisted pathway.

In order to check whether these findings also hold true for enzyme-catalyzed GTP hydrolysis, we prepared EVB models of both substrate- and solvent-assisted GTP hydrolysis catalyzed by Ras and RasGAP. As quantum chemical studies of the nonenzymatic reaction have suggested that the barriers for the direct proton transfer and for proton transfer via intervening water molecules are similar,[26] only the direct mechanism of the substrate-assisted pathway (Figure 1C) has been compared to the solvent-assisted pathway (Figure 1A) in this work. In addition, due to the extremely low pK_a of the carbonyl group of the active site Gln (estimated to be about −2[75]), we disregarded the possibility of this residue acting as a proton acceptor and consider only the mechanisms shown in Figure 1A and 1C in this work.

The free energy profiles derived from our EVB simulations are shown in Figure 3A and 3B and Tables S3 and S4, and structures of the corresponding key stationary points during

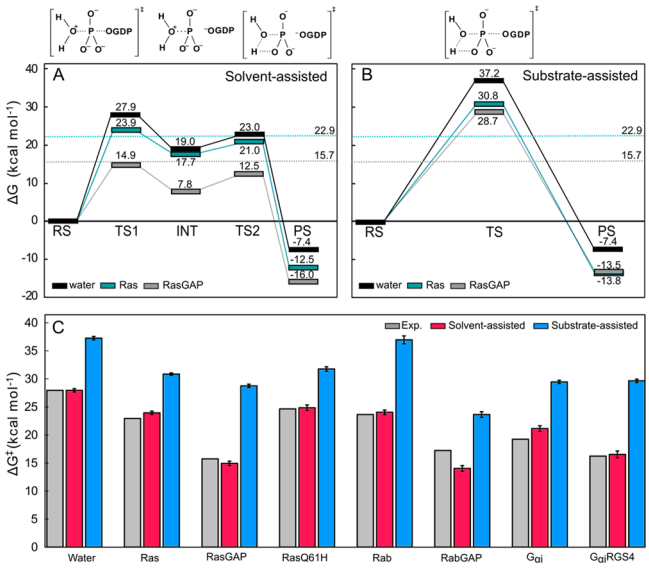

Figure 3. Calculated free energies of GTP hydrolysis in aqueous solution or catalyzed by different GTPases obtained from our empirical valence bond simulations. Shown are free energy profiles for the (A) solvent- and (B) substrate-assisted hydrolysis of GTP in aqueous solution and in the Ras and RasGAP active sites. Corresponding experimental values for Ras- and RasGAP-catalyzed GTP hydrolysis are shown as dashed green and dashed gray lines, respectively. (C) Activation free energies for each of the two mechanisms in the active site of a range of GTPases, both with and without their GAPs, are compared with available experimental data (based on data presented in refs 25, 27, 109, 123, and 124). The raw data for this figure is provided in Tables S3 and S4. The free energy profile for the solvent-assisted hydrolysis of GTP (A) presents the rate-limiting step involving the formation of a short-lived intermediate (INT), which will then tautomerize as shown in Figures S1 and S3 to yield the final product, which is chemically identical to the final product state for the substrate-assisted pathway (note that as we reach this final product state from different trajectories, our results are similar but not identical for the two pathways). As discussed in ref,[26,30] this tautomerization is expected to be very fast and not rate-limiting, and therefore the calibration performed in the nonenzymatic reaction (shown in Figure 3A) was simply to an estimated upper limit of the activation free energy of this tautomerization step. RS, TS1, INT, TS2, and PS in Figure 3A refer to the Michaelis complex (reactant state in the case of the nonenzymatic reaction), transition state, short-lived intermediate, tautomerization reaction transition state and product states for the solvent-assisted hydrolysis of GTP, and RS, TS and PS in Figure 3B refer to the Michaelis complex (reactant state in the case of the nonenzymatic reaction), transition state and product state for the substrate-assisted hydrolysis of GTP, respectively.

our simulations are shown in Figures 4, 5, and S6−S15. The free energy calculations yield activation free energies of 23.9 and 14.9 kcal mol^{-1} for the solvent-assisted hydrolysis of GTP catalyzed by Ras and RasGAP, respectively, which are in excellent agreement with the corresponding experimental values of 22.9 (Ras)[27] and 15.7 kcal mol^{-1} (RasGAP).[27] In contrast, in the case of the substrate-assisted pathway, we obtain much higher activation free energies of 30.8 and 28.7 kcal mol^{-1} for Ras and RasGAP, respectively, which is higher than the solvent-assisted pathway by 6.9 and 13.8 kcal mol^{-1}, respectively, for Ras and RasGAP. Therefore, the substrate-assisted pathway is not energetically viable in either system. We note here that the experimental values were derived from the measured k_{cat} values, which do not correspond necessarily

DOI: 10.1021/jacs.9b03193
J. Am. Chem. Soc. 2019, 141, 10684−10701

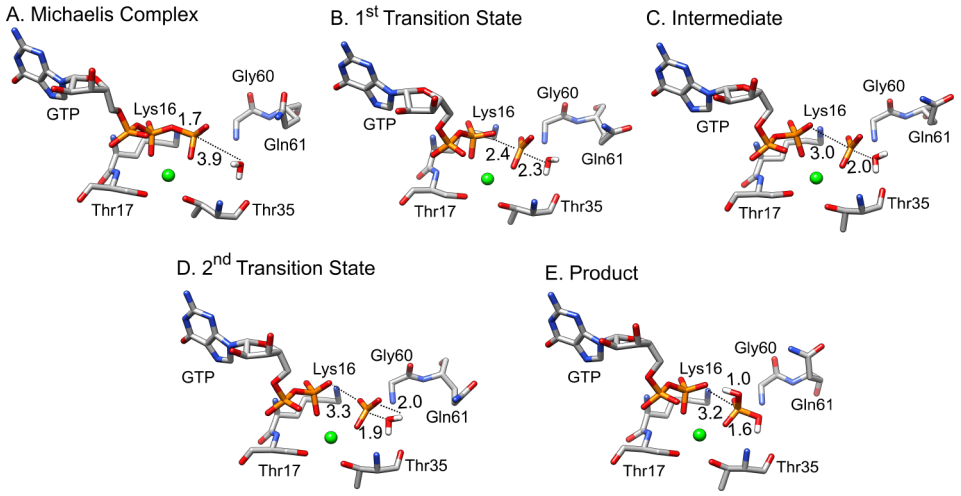

Figure 4. Structures of key stationary points extracted from our empirical valence bond simulations of the Ras-catalyzed solvent-assisted hydrolysis of GTP. (A) Michaelis complex. (B) Transition state for the phosphoryl transfer reaction. (C) Short-lived intermediate. (D) Transition state for the tautomerization step (Figure S3). (E) Product complex. P−O distances annotated on this figure (in Angstrsoms) are average distances over all replicas, as presented in Table 1, and the structures shown in this figure were selected because they have P−O distances that are very similar to the average distances across all of the EVB trajectories. Corresponding free energies for this reaction can be found in Figure 3 and Tables S3 and S4. Shown here are the substrate, nucleophilic water molecule, Mg^{2+} ion, and key catalytic residues. The remainder of the protein has been omitted for clarity.

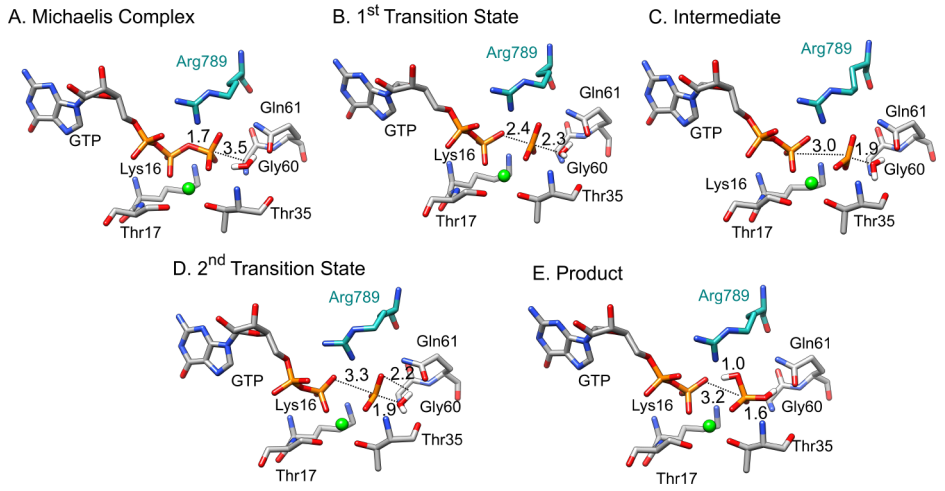

Figure 5. Structures of key stationary points, extracted from our empirical valence bond simulations of the RasGAP-catalyzed solvent-assisted hydrolysis of GTP. (A) Michaelis complex. (B) Transition state for the phosphoryl transfer reaction. (C) Short-lived intermediate. (D) Transition state for the tautomerization step (Figure S3). (E) Product complex. P−O distances annotated on this figure (in Angstroms) are average distances over all replicas, as presented in Table 1, and structures shown in this figure were selected because they have P−O distances that are very similar to the average distances across all of the EVB trajectories. Corresponding free energies for this reaction can be found in Figure 3 and Tables S3 and S4. Shown here are the substrate, nucleophilic water molecule, Mg^{2+} ion, and key catalytic residues. The remainder of the protein has been omitted for clarity.

to the calculated chemical step. However, they do provide a lower limit for the reaction rate of this step (and thus are an upper limit for its activation free energy) against which to compare our calculations. Finally, as can be seen in this data, in all cases, the substrate-assisted pathway fails to reproduce the large experimentally observed free energy barrier reduction caused by the complexation with the GAP/RGS protein.

Is the Preference for Solvent-Assisted GTP Hydrolysis Conserved Among Different GTPases? Our simulations of the Ras and RasGAP-catalyzed hydrolysis of GTP clearly demonstrate that a solvent-assisted pathway is favorable over the substrate-assisted pathway commonly put forward in the literature.[27,32,43,55,73] The next question, therefore, is how conserved this mechanistic preference is and if it is a general motive in GTPases with a glutamine at the analogous structural position as Q61 in Ras. We therefore decided to compare substrate- and solvent-assisted catalysis in four more systems: Rab1 and Rab1GAP as well as the $G_{\alpha i}$-subunit, both in the presence and absence of the RGS protein (Figure 3C and Table S3). Because we demonstrated in the case of Ras that the final tautomerization step (Figures S1 and S3) does not affect the rate-limiting formation of the transition state, to save computational time, we did not model the final tautomerization step for the four systems considered here but rather focus on the energetics of the rate-limiting phosphoryl transfer step.

DOI: 10.1021/jacs.9b03193
J. Am. Chem. Soc. 2019, 141, 10684−10701

Table 1. Average Calculated Phosphorus−Oxygen Distances to the Departing Leaving Group ($P-O_{lg}$) and to the Incoming Nucleophile ($P-O_{nuc}$) at the Michaelis Complexes as Well as the First Transition States and Intermediate States for GTPase-Catalyzed GTP Hydrolysis via a Solvent-Assisted Pathway[a]

	Ras	RasGAP	Ras Q61H	Rab	RabGAP	$G_{\alpha i}$	$G_{\alpha i}$−RGS4
Michaelis complex							
$P-O_{lg}$	1.69 ± 0.00	1.74 ± 0.01	1.70 ± 0.00	1.66 ± 0.00	1.67 ± 0.00	1.69 ± 0.00	1.70 ± 0.00
$P-O_{nuc}$	3.91 ± 0.02	3.54 ± 0.01	3.94 ± 0.02	3.43 ± 0.01	3.50 ± 0.01	3.67 ± 0.02	3.73 ± 0.02
$O_{nuc}-O_{lg}$	5.55 ± 0.03	5.01 ± 0.02	5.60 ± 0.02	3.56 ± 0.02	4.94 ± 0.02	5.30 ± 0.03	5.33 ± 0.03
first transition state							
$P-O_{lg}$	2.40 ± 0.01	2.38 ± 0.01	2.46 ± 0.01	2.17 ± 0.01	2.28 ± 0.01	2.34 ± 0.01	2.32 ± 0.01
$P-O_{nuc}$	2.29 ± 0.01	2.32 ± 0.01	2.28 ± 0.01	2.17 ± 0.01	2.36 ± 0.01	2.29 ± 0.01	2.35 ± 0.01
$O_{nuc}-O_{lg}$	4.69 ± 0.01	4.69 ± 0.01	4.73 ± 0.01	4.33 ± 0.01	4.64 ± 0.01	4.63 ± 0.01	4.67 ± 0.01
intermediate state							
$P-O_{lg}$	3.00 ± 0.01	2.98 ± 0.01	3.35 ± 0.02	2.50 ± 0.01	2.87 ± 0.01	2.84 ± 0.01	2.82 ± 0.01
$P-O_{nuc}$	1.98 ± 0.01	1.90 ± 0.01	1.88 ± 0.00	1.93 ± 0.01	1.89 ± 0.01	1.91 ± 0.01	1.92 ± 0.01
$O_{nuc}-O_{lg}$	4.89 ± 0.01	4.87 ± 0.01	5.22 ± 0.02	4.43 ± 0.01	4.76 ± 0.01	4.74 ± 0.01	4.74 ± 0.01

[a]All values are averages and standard error of the mean over 400 individual snapshots, extracted from 20 independent empirical valence bond simulations, obtained as described in the Methodology section. For the corresponding values for the nonenzymatic reaction in aqueous solution as well as the GTPase-catalyzed reaction proceeding through a substrate-assisted mechanism, see Tables S5−S7.

In all four cases (Figure 3C and Table S3) we obtain similar observations as in the case of Ras-catalyzed GTP hydrolysis, that is, the absolute values of the activation free energies for the solvent-assisted pathway are in good qualitative and quantitative agreement with the experimental values, with the largest deviations being in the case $G_{\alpha i}$, where our calculated value is higher than the experimental value by 1.9 kcal mol^{-1} as well as in the case of RabGAP where we underestimate the experimental value by 3.2 kcal mol^{-1}, at least in part likely due to the lower resolution of the crystal structure used (PDB ID 4HLQ,[25,50] 3.3 Å resolution, *R* value free 0.274). However, even with these exceptions, in all cases, the solvent-assisted pathway is clearly substantially energetically favorable over the substrate-assisted pathway by between 6.9 and 13.8 kcal mol^{-1}. In addition, in the case of the solvent-assisted pathway, the calculated barrier reductions compared to the nonenzymatic reaction are in all cases in good agreement with experiment.

Exploring the Effect of Mutating Q61 in Ras on the Solvent- and Substrate-Assisted Pathways. To further validate the reliability of our simulations in correctly describing GTP hydrolysis catalyzed by Ras and RasGAP, we modeled the effect of a key active site mutation: Q61H (Figure 3C and Table S3), which replaces the catalytically important glutamine in Ras, with the analogous histidine found in the corresponding structural position in elongation factors such as EF-Tu[41,42] and EF-G[125] (Figure S16). In the case of EF-Tu and EF-G, on the basis of crystallographic evidence, this histidine has been argued to be the general base in the reaction.[42] In the case of Ras, experimental data on the catalytic activity of this enzyme variant is available for only the Ras-catalyzed reaction; however, curiously, both the Q61H substitution in Ras[54] and the H84Q substitution in EF-Tu[126] have been shown to be detrimental to the catalytic activity of the corresponding enzyme, and therefore, the residues at these positions are not interchangeable. In the case of Ras, if Q61 were acting as a general base, as has been suggested in the literature,[52,61,73,127,128] one would expect a histidine rather than a glutamine at position 61 to be more catalytically favorable, as a histidine side chain is a much better candidate for a general base than the Q61 amide group, due to the substantially higher pK_a of the imidazole. In addition, one would expect a solvent-assisted mechanism to be less impacted by whether there is a histidine or a glutamine present at position 61, as this pathway does not require a general base. Despite this, however, in the case of the solvent-assisted pathway, our calculations predict a 0.9 kcal mol^{-1} increase in the activation free energy of the Ras-catalyzed reaction, relative to wild type, in agreement with experiment[54] (for the substrate-assisted pathway the activation free energy is also increased by 0.9 kcal mol^{-1} but starting from a much higher activation free energy of 30.8 kcal mol^{-1} for wild-type Ras). This is primarily due to the fact that Q61 in Ras plays an important role in positioning the catalytic water molecule both in the Michaelis complex but also in the transition state, which has an elongated $P-O_{nuc}$ distance of 2.3 Å in the case of the solvent-assisted pathway (Table 1) and 2.1 Å in the case of the substrate-assisted pathway (Table S7), and therefore, removal of this stabilizing interaction is the likely cause for the increase in the activation free energy upon this residue substitution.

Exploring the Origins of the Catalytic Effect of the GAP and RGS Proteins. Having clearly established the mechanistic preference for a solvent-assisted pathway and the reliability of our simulations, as a final point, we explored the origins of the catalytic effect of the GAP and RGS proteins by examining several key parameters including the nature of the transition states involved in the different systems and reaction pathways studied here, key interaction distances, the electrostatic contributions of individual residues to the calculated activation free energies, and the degree of solvent exposure of the active site during the reactions in the different enzymes. In the main text we focus on discussion of these parameters in the context of the energetically preferred solvent-assisted pathway. However, the corresponding data for the substrate-assisted pathway is provided for comparison in the Supporting Information.

In terms of transition state geometries (Table 1), there does not appear to be any clear trend either between systems or between the same system with and without its regulatory protein. In the case of Ras, the calculated transition states are very similar in both wild-type Ras, the Q61H variant, and RasGAP. In the case of Rab, there is a very small elongation of $P-O_{nuc}$ at the transition state for the RabGAP complex compared to Rab in the absence of its GAP, and in the case of $G_{\alpha i}$ with and without RGS, the transition states are once again

DOI: 10.1021/jacs.9b03193
J. Am. Chem. Soc. 2019, 141, 10684−10701

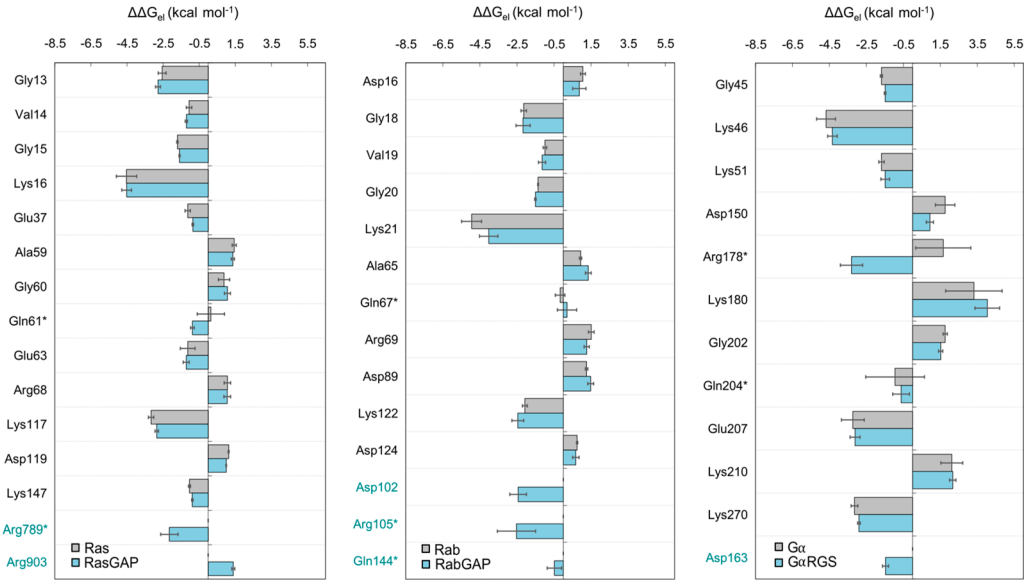

Figure 6. Electrostatic contributions from individual residues to the activation free energies for solvent-assisted GTP hydrolysis by different GTPases studied in this work. All values were obtained by applying the linear response approximation[130,131] to our calculated EVB trajectories, as in our previous work.[89,132,133] Key catalytic Arg and Gln residues are denoted on the *y* axis for each panel with an asterisk (*).

very similar to Ras. Overall, the variations are too small to conclusively reveal any trend but do show that in all cases the transition state is loose and dissociative in nature,[129] with advanced bond cleavage to the leaving group, although all transition states are more compact than that for the corresponding nonenzymatic reaction in aqueous solution ($P-O_{lg}$ = 2.56 ± 0.01 Å, $P-O_{nuc}$ = 2.26 ± 0.01 Å, and $O_{nuc}-O_{lg}$ = 4.82 ± 0.01 Å). This is in contrast to the much tighter (more associative) transition states we obtain in the case of the substrate-assisted pathway (see Table S7).

Curiously, in the case of the Rab-catalyzed solvent-assisted hydrolysis of GTP (Table 1), the reaction proceeds through a perfectly symmetrical transition state with more compact $O_{nuc}-O_{lg}$ distances in each of the Michaelis complex, first transition state, and intermediate states than in any of the other systems studied here. It is not immediately clear what the origin of this shift toward a tighter transition state is. However, the Rab active site contains two serine residues (Ser17 and Ser39) that are not present in either Ras (where they are replaced by Gly12 and Pro34 at the same position, respectively) or $G_{\alpha i}$ (where they are replaced by Gly42 and Lys147, respectively). In the case of Rab, these two serine side chains form hydrogen-bonding interactions with the non-bridging oxygen atoms of the γ-phosphate and may speculatively be leading to the more compact transition state compared to other GTPases studied in this work. Note that in our RabGAP simulations the interaction with Ser39, which is located on the Switch I loop, is lost and replaced by an interaction with the arginine finger provided by the GAP, thus creating a more similar active site environment (and thus transition state) to other GTPases studied here.

Following from this we also calculated the electrostatic contributions of different residues to the calculated activation free energies, both with and without the presence of the GAP or RGS proteins (Figure 6), calculated by postprocessing of the EVB trajectories using the linear response approximation,[130,131] as in our previous work.[89,132,133] These data indicate that in all cases one of the largest stabilizing contributions when comparing the different enzymes with and without their corresponding activator proteins is from the active site arginine either provided by the GAP protein or intrinsically present in $G_{\alpha i}$[47,134−136] and from an active site lysine, highlighted in Figure 2 (Lys16 in Ras and RasGAP, Lys21 in Rab and RabGAP, and Lys46 in $G_{\alpha i}$ and $G_{\alpha i}$−RGS4). In the case of the active site lysine, as this residue is present both in the presence and in the absence of the GAP/RGS, it does not contribute to the additional catalytic effect of the regulatory protein. However, the relatively large contribution of this residue illustrates that it is important for the overall barrier reduction compared to the nonenzymatic reaction in aqueous solution in all systems studied. In the case of $G_{\alpha i}$ the mutations of this lysine to alanine lead to a ∼100-fold decrease of the hydrolysis rate.[92] The contribution from this residue is interesting, as having a lysine in this position is not uncommon among enzymes that catalyze phosphoryl transfer. For example, in the case of enzymes from the alkaline phosphatase superfamily, the active site typically contains either two metal ions or a single metal ion and a lysine in the position of the "missing" metal ion.[137,138] This lysine then interacts with the leaving group and provides electrostatic stabilization to the leaving group during the reaction, similarly to the active site lysine in these GTPases (see Figure 2). Other residues that appear to be catalytically important are Lys117 in the case of Ras and RasGAP, Lys122 in the case of Rab and RabGAP, and Lys270 in the case of $G_{\alpha i}$ and $G_{\alpha i}$−RGS4. Once again, this lysine makes significant but similar contributions both in the absence and in the presence of the GAP/RGS proteins. An exception is Asp102, which is provided by RabGAP, and makes a significant stabilizing contribution that is not present in the Rab alone. This residue forms a bridge between the arginine and the glutamine fingers in the RabGAP active site and therefore plays a role in stabilizing both of their positions during the catalytic mechanism.

In the case of the arginine finger, this residue provides up to 3.3 kcal mol^{-1} of additional stabilization when the regulatory protein is bound in all systems studied (Figure 6), which is primarily due to stabilization of the negative charge building up on the leaving group oxygen, facilitated by the formation of a

DOI: 10.1021/jacs.9b03193
J. Am. Chem. Soc. 2019, 141, 10684−10701

Table 2. Average Distances between the Arg Finger Provided by the GAP (or the intrinsic Arg, in the case of $G_{\alpha i}$) and the Leaving Group Oxygen (O_{lg}) at the Michaelis Complexes, First Transition States, and Intermediate States for GTPase-Catalyzed Solvent-Assisted GTP Hydrolysis[a]

	RasGAP	RabGAP	$G_{\alpha i}$	$G_{\alpha i}$–RGS4
Michaelis complex				
Arg:H_{ε}–O_{lg}	5.99 ± 0.02	5.98 ± 0.02	4.17 ± 0.05	5.57 ± 0.02
Arg:$H_{\eta 11}$–O_{lg}	**2.73 ± 0.01**	3.22 ± 0.01	7.37 ± 0.05	**2.15 ± 0.01**
Arg:$H_{\eta 12}$–O_{lg}	2.78 ± 0.01	**2.12 ± 0.02**	7.44 ± 0.05	3.20 ± 0.01
Arg:$H_{\eta 21}$–O_{lg}	4.61 ± 0.02	5.16 ± 0.02	**4.03 ± 0.05**	4.77 ± 0.02
Arg:$H_{\eta 22}$–O_{lg}	5.78 ± 0.02	3.53 ± 0.02	5.63 ± 0.05	3.28 ± 0.01
first transition state				
Arg:H_{ε}–O_{lg}	5.83 ± 0.02	5.75 ± 0.02	4.12 ± 0.05	5.54 ± 0.02
Arg:$H_{\eta 11}$–O_{lg}	2.76 ± 0.01	3.09 ± 0.01	7.39 ± 0.05	**1.77 ± 0.01**
Arg:$H_{\eta 12}$–O_{lg}	**2.32 ± 0.02**	**1.77 ± 0.01**	7.44 ± 0.05	3.10 ± 0.01
Arg:$H_{\eta 21}$–O_{lg}	4.16 ± 0.02	4.92 ± 0.02	**4.11 ± 0.05**	4.67 ± 0.01
Arg:$H_{\eta 22}$–O_{lg}	5.42 ± 0.02	3.32 ± 0.01	5.70 ± 0.05	3.23 ± 0.01
intermediate state				
Arg:H_{ε}–O_{lg}	5.60 ± 0.02	5.65 ± 0.02	4.11 ± 0.05	5.52 ± 0.02
Arg:$H_{\eta 11}$–O_{lg}	2.87 ± 0.01	3.05 ± 0.01	7.09 ± 0.07	**1.63 ± 0.01**
Arg:$H_{\eta 12}$–O_{lg}	**1.74 ± 0.01**	**1.65 ± 0.01**	7.21 ± 0.06	3.06 ± 0.01
Arg:$H_{\eta 21}$–O_{lg}	3.61 ± 0.01	4.80 ± 0.02	**4.04 ± 0.05**	4.62 ± 0.01
Arg:$H_{\eta 22}$–O_{lg}	4.94 ± 0.02	3.26 ± 0.01	5.44 ± 0.07	3.23 ± 0.01

[a] H_{ε} is the hydrogen at the N^{ε} nitrogen atom of Arg.$H_{\eta 11}$ and $H_{\eta 12}$, and $H_{\eta 21}$ and $H_{\eta 22}$ are the hydrogen atoms at $N_{\eta 1}$ and $N_{\eta 2}$ nitrogens of Arg. All values are averages and standard error of the mean over 400 individual snapshots, extracted from 20 independent empirical valence bond simulations, obtained as described in the Methodology section. The corresponding values for the substrate-assisted mechanism can be found in Table S8. The closest interactions, in each case, are highlighted in bold.

tighter Arg–O_{lg} interaction, which is formed upon moving from the Michaelis complex to the transition state (see the distances shown in Tables 2 and S8). Interestingly, (1) in the solvent-assisted mechanism, in the case of the $G_{\alpha i}$-subunit, there is little interaction between the intrinsic Arg and the leaving group oxygen in the absence of the RGS protein, whereas in the presence of the RGS protein, a much tighter interaction is formed with the leaving group oxygen, and therefore, the RGS protein appears to play a role in the positioning of this residue. The consequences of this difference are also observed in Figure 6, where a stabilizing contribution from the intrinsic arginine is only seen in this system when the RGS protein is bound. Also, (2) with the exception of $G_{\alpha i}$–RGS4, where the two mechanisms appear to be similar, these interactions in general are tighter in the case of the solvent-assisted mechanism than in the case of the substrate-assisted mechanism (Tables 2 and S8). This is likely due to greater charge build-up at the leaving group in the transition state for the dissociative transition state for the solvent-assisted mechanism (where the bond to the leaving group is substantial) than for the more associative transition state for the substrate-assisted mechanism (which has much less bond cleavage to the leaving group at the transition state). Therefore, optimal positioning of this residue clearly plays an important role in providing some (but not all) of the additional transition state stabilization provided by the GAP and RGS proteins in addition to the suggested role of this residue in organizing the active site and positioning the phosphate group for efficient catalysis.[141]

Following from this, the electrostatic contribution from the active site Gln appears to be negligible in all system without the GAP or RGS proteins but becomes slightly stabilizing in RasGAP, $G_{\alpha i}$, and $G_{\alpha i}$-RGS. More important, however, is the impact of the active site Gln on the positioning of the nucleophile. As can be seen in Figure 7, in the case of Ras, in the absence of the GAP, the Gln61 side chain is extremely "floppy" and samples many different conformations, analogous to observations made during 50 ns all-atom MD simulations in a previous study.[142] The presence of the GAP heavily restricts the conformational space of this residue, leading to the side chain to sample a single conformation that interacts directly with the nucleophilic water molecule at the Michaelis complex and transition states for the phosphoryl transfer step (note that as shown in Figures 7 and S17, the conformational space of both the water molecule and the Gln side chain is greatly reduced at the Michaelis complexes for Ras both with and without GAP). As a consequence, the lower entropy of the Michaelis complex in the case of RasGAP reduces the activation barrier compared to the intrinsic reaction (for a broader discussion of the issue of conformational sampling and entropy in enzyme catalysis, see, e.g., refs 87 and 143–157 among others). The average RMSD of this side chain at the Michaelis complex is 1.26 ± 0.08 and 0.28 ± 0.02 Å in the case of Ras and RasGAP, respectively. This restriction in the conformational space of the Gln side chain therefore appears to be absolutely critical for nucleophile positioning, although the catalytic impact of this restriction in conformational space can manifest itself in different ways, either through an entropic effect or through destabilization of the reactants or a reduction in the reorganization energy of the process.

To estimate the catalytic impact of restricting the conformational space of the Gln side chain, we placed a 10 kcal mol^{-1} $Å^{-2}$ positional restraint on all atoms of the Q61 side chain in our EVB simulations of the Ras-catalyzed hydrolysis of GTP via both substrate and solvent-assisted mechanisms (Table S9). In the case of the substrate-assisted pathway, the effect of this restraint is very small, reducing the activation free energy by only 1.2 kcal mol^{-1}. In the case of the solvent-assisted pathway, however, inclusion of this restraint drops the calculated activation free energy from 23.9 to 17.6 kcal mol^{-1}, thus

DOI: 10.1021/jacs.9b03193
J. Am. Chem. Soc. 2019, 141, 10684–10701

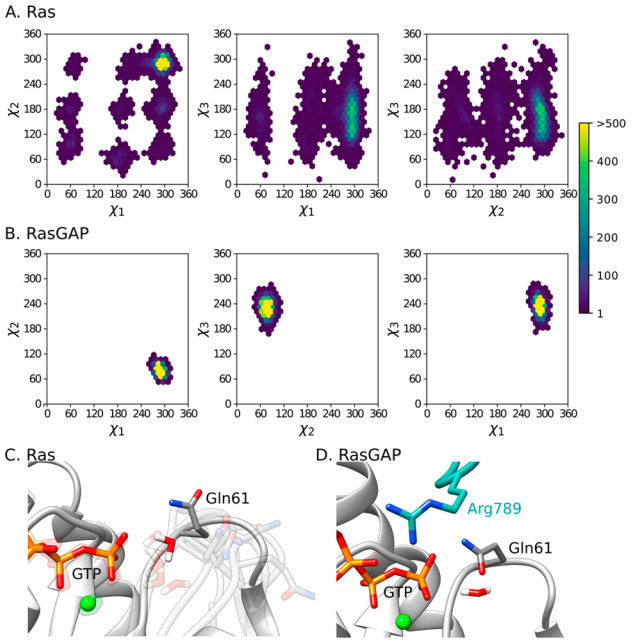

Figure 7. Conformational space sampled by the Gln61 side chain in 20 × 50 ns (1 μs total) simulations of the Michaelis complexes of (A) Ras and (B) RasGAP, defined as a function of the χ_1−χ_3 dihedral angles of this side chain. Simulations at the Michaelis complex were performed using the same protocol as for the equilibrations at the transition state, as described in the Methodology section, and using the same restraints as were applied in our EVB simulations (again, see the Methodology section). Snapshots were extracted every 100 ps for analysis. The joint distribution of side chain dihedral angles was obtained using MDTraj[114] and Matplotlib.[139] (C and D) Representative conformations sampled by the Gln61 side chain in simulations of Ras and RasGAP, respectively. Shown here also are the nucleophilic water molecule and the Mg^{2+} ion (green ball). In these panels, structures corresponding to the centroid of the most populated cluster, obtained from Ward clustering performed measuring the Gln61 side chain RMSD after protein backbone alignment, using TTClust,[140] are shown as a solid structure, and other conformations of the Gln61 side chain are shown as shaded structures in the background. In the case of RasGAP, this also corresponds to the centroid of the single populated cluster shown in panel D; hence, only one structure is shown in this panel.

reproducing a significant amount (6.3 kcal mol^{-1}) of the 7.2 kcal mol^{-1} catalytic impact of GAP on Ras[27] (Table S3, see also discussion in ref 158). One can also see an entropic effect in restricting the conformational space of the Gln side chain from simple calculations of per-residue entropy loss upon protein folding using the Predicting Loss of Protein S(entropy) (PLOPS)[115] Web server, which were performed on the initial crystal structures used for the simulations as described in the Methodology section and which suggest greater entropy loss for the catalytic Gln in the presence of the GAP/RGS protein than in its absence (Table S10). Therefore, rather than acting as a general base, this residue appears to play an important role in positioning the nucleophilic water molecule for efficient catalysis, thus creating a more stable encounter complex prior to subsequent hydrolysis of GTP through a dissociative, solvent-assisted transition state (similar to that observed in the absence of the enzyme[30]). Following from this, part of the role of the GAP appears to be the reduction in the flexibility of the Gln side chain (Figure 7) which in turn would allow for more stable positioning of the nucleophilic water molecule (Figure S17), in agreement with a prior qualitative study based on analysis of crystallographic data.[32] This is coupled with a general reduction of the volume of the active site pocket from 538.0 ± 93.8 $Å^3$ in the case of Ras to 268.0 ± 33.5 $Å^3$ in the case of RasGAP, calculated from the same simulations of the Michaelis complex used for the analysis presented in Figure 7 using POVME 3.0,[112,113] as described in the Methodology section.

Another question of interest is the role of the catalytic Mg^{2+} ion in our simulations. There have been a number of computational studies that have attempted to identify the general mechanisms of nucleophile activation in metal-aided enzymes (see, e.g., refs 159−166). One would expect the Mg^{2+} ion to provide a strong catalytic effect, and indeed, previous computational analyses of GTP hydrolysis have explored the role of the metal ion on charge storage during the reaction (and its impact on the geometry of the GTP molecule when bound to the active site),[118] the impact of the metal ion on the nature of the transition states involved, arguing that the Mg^{2+} ion contracts the transition state for GTP hydrolysis making it more associative,[72] or the impact of the metal ion on weakening the P−O bond to the leaving group, as well as transition state stabilization through enhanced electrophilicity of the metal group.[122] We note here that as our EVB simulations used a fixed-charge metal model, we are unable to capture the charge transfer effects observed in ref 118; however, our EVB parameters are based on the parametrization of ref 118 which implicitly included the impact of this charge transfer on fine geometric details of the GTP conformation in the parametrization. In addition, the original goal of the parametrization of the multipoint model used to describe Mg^{2+} in this work was to avoid the need for restraints or artificial bonds in the simulation while simultaneously retaining key thermodynamic properties of the metal ion.[93] As can be seen from Figure 3 and Table S11, the metal ion maintains a stable coordination sphere in all enzyme simulations, while at the same time our model reproduces the catalytic effect of the different systems studied with good quantitative and qualitative accuracy.

What complicates interpretation of the role of the metal ion in these systems is the fact that, as we discussed in previous work,[30] experimental work has suggested that the presence of a magnesium ion has minimal effect on stabilizing either the transition state or on perturbing the transition state geometry for nonenzymatic GTP hydrolysis. That is, Admiraal and Herschlag examined the kinetics of phosphoryl transfer from GTP, ATP, and a series of pyrophosphates to a series of alcohols in detail,[167] obtaining only a small β_{nuc} value, which is consistent with a dissociative transition state with very little bond formation between the incoming nucleophile and the phosphate. Curiously, inclusion of Mg^{2+} ions had minimal effect on either β_{nuc} or the reaction rates (for example, the activation barrier for ATP hydrolysis was reduced by only 0.7 kcal mol^{-1} at 60 °C). Similarly, Kötting and Gerwert studied GTP hydrolysis over a range of temperatures, both in the presence and in the absence of Mg^{2+}.[109] As in the case of the previous work by Admiraal and Herschlag,[167] they found minimal impact from inclusion of the Mg^{2+} ion: at 25 °C, there was no difference in rate between when the Mg^{2+} was present or absent (both scenarios yielded an experimental activation free energy of 27.9 kcal mol^{-1}). The presence of the Mg^{2+} did accelerate the reaction at higher temperatures, but this was mainly due to a higher enthalpy of activation. This makes it

DOI: 10.1021/jacs.9b03193
J. Am. Chem. Soc. 2019, 141, 10684−10701

extremely unclear what the role of the Mg^{2+} ion actually is. We demonstrated in the case of triphosphate hydrolysis in aqueous solution[30] that while the energetic and structural impact of including an Mg^{2+} ion in our simulations is not large, the presence of Mg^{2+} increases the energy difference between substrate- and solvent-assisted pathways, creating a greater preference for a solvent-assisted pathway than in its absence. In the case of enzymatic GTP hydrolysis, the situation appears to be more complex and system dependent, as can be seen from Table S3. Therefore, while the Mg^{2+} clearly has an impact in the enzyme environment, its role is highly complex and it remains unclear why the impact of the Mg^{2+} ion on the nonenzymatic reaction is minimal (and therefore why it would be needed for the enzymatic reaction, beyond a structural role during catalysis).

Finally, we examined the impact of the formation of the GTPase-GAP(RGS) complex on the solvation of the active site. Specifically, we considered (1) the average number of hydrogen bonds formed between the γ-phosphate and protein atoms/water molecules during these simulations and (2) the average number of water molecules within 6 Å of the γ-phosphate of GTP during EVB simulations of the GTPases studied here both with and without their activating proteins (Figure 8 and Tables S12 and S13). These data show that

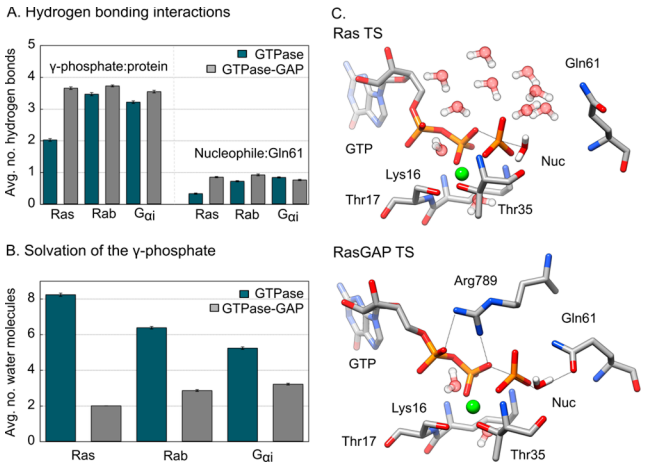

Figure 8. Solvation of the active site during solvent-assisted GTP hydrolysis catalyzed by Ras and RasGAP. (A) Average number of hydrogen bonds formed between key species (γ-phosphate:protein and catalytic Gln:nucleophile). (B) Average number of water molecules found within 6 Å of phosphorus atom of the γ-phosphate group of GTP. (C) Representative snapshots depicting the water molecules in the vicinity of the γ-phosphate group of GTP at the transition states of GTPase-catalyzed GTP hydrolysis. Associated raw data for this figure is shown in Table S12.

there is a small increase in substrate−protein and catalytic Gln:nucleophile hydrogen-bonding interactions upon complexation with the GAP or RGS proteins. However, a much larger effect (Figure 8B and 8C) is that the GAP/RGS proteins drastically reduce the number of water molecules in the vicinity of the γ-phosphate, thus strengthening protein−substrate interactions at the expense of water−substrate interactions. The importance of creating such hydrophobic cages in both enzyme catalysis and enzyme evolution has been discussed in detail elsewhere,[89,168−174] although this concept has also been met with criticism.[175−178] Our simulations show that, as a final puzzle piece, one role of the GAP and RGS proteins in catalysis appears to be to exclude solvent from the active site, thus accelerating the rate of the chemical reaction.

CONCLUSIONS

GTPases are biologically critical regulatory proteins and major drug targets, because they are involved in almost all vital cellular processes (e.g., ref 19). As a result, their mechanisms and regulation have been the topics of substantial research effort, both in order to understand a problem of fundamental biological importance and for design of novel therapeutics to target GTPases and regulate their vital cellular processes.[179−181]

The precise mechanism by which small GTPases (and related enzymes such as the $G_{\alpha i}$-subunit of heterotrimeric G-proteins) hydrolyze GTP has been controversial for decades,[1,4] due to the absence of an obvious candidate serving as a general base to deprotonate the nucleophilic water molecule. Here we demonstrate explicitly, for the first time, that a general base is not needed in the active site. The preferred mechanism for GTP hydrolysis by the proteins studied in this work is a solvent-assisted pathway (Figure 1A), in which proton transfer occurs *after* the rate-limiting transition state of the nucleophilic attack of a water molecule at the γ-phosphate. This result is in agreement with analogous studies of both phosphate monoester dianion[26] and triphosphate hydrolysis in water,[30,182] and the resulting protein-bound $H_2PO_4^-$ product state is in agreement with experimental IR spectroscopic data.[183] In addition, kinetic isotope effects[129,184] are consistent with GTP hydrolysis in Ras and RasGAP proceeding via a loose transition state. Finally, the solvent-assisted pathway is also consistent with the transition state structure suggested based on ^{19}F NMR studies of Rho GTPase.[82]

Through detailed empirical valence bond simulations of GTP hydrolysis in Ras, Rab1b, and the $G_{\alpha i}$-subunit, both in the presence and in the absence of the corresponding GAP/RGS protein, we demonstrate that our mechanistic findings are a common motive in GTPases with a Gln in the active site. As shown in Figure 3, in all cases, the calculated free energy barriers and the barrier reduction by the GTPase activating proteins for the solvent-assisted pathway are clearly in closer agreement with the experimental values. In addition, the activation free energies derived for the substrate-assisted pathway are between 6.9 and 13.8 kcal mol^{-1} higher than those for the solvent-assisted pathway. Thus, we conclude that a general base is not needed in the active site as the preferred mechanism for GTP hydrolysis is a conserved solvent-assisted pathway. This is similar to the loose, dissociative transition state that has been argued for in the case of phosphate monoester hydrolysis,[79−81] in contrast to the tighter transition states typically observed for phosphate di- and triester hydrolysis (for reviews, see, e.g., refs 1, 4, and 185). Interestingly, despite the mechanistic differences between different types of phosphate esters, a related solvent-as-base mechanism has been suggested in the case of the splicing mechanism of group II introns, which are Mg^{2+}-dependent ribozymes with phosphodiester transition states.[166] Note that such a mechanism has not been observed in other nuclease enzymes employing a Mg^{2+}-aided function.[165]

Following from this, experimental mutagenesis studies have verified the critical catalytic importance of the active site Gln to the GTPase-catalyzed reaction.[54] We show here computationally that restricting the Gln position in a GAP-like conformation achieves significant barrier reduction in the

DOI: 10.1021/jacs.9b03193
J. Am. Chem. Soc. 2019, 141, 10684−10701

solvent-assisted pathway without the actual GAP protein present. This Gln position optimizes the position of the nucleophilic water molecule for formation of the loose transition state involved in the solvent-assisted pathway. The stabilizing role of the GAP/RGS proteins is observed in all three systems. In addition, the Arg finger is also stabilized, which improves the interaction between this arginine and the leaving group oxygen of the GTP substrate, thus increasing the electrostatic stabilization provided by the Arg finger (Figure 6). Lastly, we show that GAP/RGS proteins facilitate a general tightening of the binding pocket through reducing its volume, allowing for greater precision in electrostatic interactions in the active site, which is then further enhanced by solvent exclusion from the active site upon binding of the regulatory protein, thus increasing the strength of these interactions in a reduced dielectric local environment.

In conclusion, our work resolves a decades-old mechanistic controversy[1,4] of how GTPases can hydrolyze GTP in the absence of a viable general base in the active site. Our revised mechanism for GTP hydrolysis by Ras GTPase and related enzymes also has the potential to shed new light on another long held secret, namely, understanding the mechanism of crucial oncogenic Ras mutants like G12 and G13 mutations, which are assumed to affect the transition state of the GTPase reaction.[186] Finally, an improved understanding of the nature of the transition states for this reaction provides new entry points for drug development.

■ ASSOCIATED CONTENT

Supporting Information

The Supporting Information is available free of charge on the ACS Publications website at DOI: 10.1021/jacs.9b03193.

Additional simulation analysis (RMSD, distances, structures of key stationary points) all empirical valence bond parameters necessary to reproduce the simulations (PDF)

■ AUTHOR INFORMATION

Corresponding Authors

*E-mail: till.rudack@rub.de.
*E-mail: lynn.kamerlin@kemi.uu.se.

ORCID

Ana R. Calixto: 0000-0002-1123-0413
Cátia Moreira: 0000-0002-6904-2511
Anna Pabis: 0000-0002-7705-5371
Carsten Kötting: 0000-0002-3599-9657
Till Rudack: 0000-0003-2693-9561
Shina C.L. Kamerlin: 0000-0002-3190-1173

Author Contributions

The manuscript was written through contributions of all authors. All authors have given approval to the final version of the manuscript.

Author Contributions

‡A.R.C. and C.M.: These authors contributed equally.

Notes

The authors declare no competing financial interest.

■ ACKNOWLEDGMENTS

This work was funded by Stiftelsen Olle Engkvist Byggmästare (grant 190-0335), the Wenner-Gren foundations (postdoctoral scholarship to A.P.), and the Knut and Alice Wallenberg Foundation (Wallenberg Academy Fellowship to S.C.L.K., KAW 2013.0124). C.K. and K.G. acknowledge funding by the DFG (Project number 321722360). All computational work was performed on the Rackham cluster at UPPMAX, the Kebnekaise cluster at HPC2N Umeå, and the Tetralith Cluster at NSC Linköping through computational resources provided by the Swedish National Infrastructure for computing (SNIC 2017/12-11 and 2018/2-3). We thank Jürgen Schlitter for fruitful discussions and Malin Lüking for initial assistance with the simulations.

■ REFERENCES

(1) Kamerlin, S. C. L.; Sharma, P. K.; Prasad, R. B.; Warshel, A. Why Nature Really Chose Phosphate. *Q. Rev. Biophys.* **2013**, *46*, 1−132.
(2) Williams, N. H. Models for Biological Phosphoryl Transfer. *Biochim. Biophys. Acta, Proteins Proteomics* **2004**, *1697*, 279−287.
(3) Cleland, W. W.; Hengge, A. C. Enzymatic Mechanisms of Phosphate and Sulfate Transfer. *Chem. Rev.* **2006**, *106*, 3252−3278.
(4) Lassila, J. K.; Zalatan, J. G.; Herschlag, D. Biological Phosphoryl-Transfer Reactions: Understanding Mechanism and Catalysis. *Annu. Rev. Biochem.* **2011**, *80*, 669−702.
(5) Wolfenden, R.; Snider, M. J. The Depth of Chemical Time and the Power of Enzymes as Catalysts. *Acc. Chem. Res.* **2001**, *34*, 938−945.
(6) Benkovic, S.; Hammes-Schiffer, S. A Perspective on Enzyme Catalysis. *Science* **2003**, *301*, 1196−1202.
(7) Garcia-Viloca, M.; Gao, J.; Karplus, M.; Truhlar, D. G. How Enzymes Work: Analysis by Modern Rate Theory and Computer Simulations. *Science* **2004**, *303*, 186−195.
(8) Bourne, H. R.; Sanders, D. A.; McCormick, F. The GTPase Superfamily: Conserved Structure and Molecular Mechanism. *Nature* **1991**, *349*, 117−127.
(9) Caldon, C. E.; Yoong, P.; March, P. E. Evolution of a Molecular Switch: Universal Bacterial GTPases Regulate Ribosome Function. *Mol. Microbiol.* **2001**, *41*, 289−297.
(10) Leipe, D. D.; Wolf, Y. I.; Koonin, E. V.; Aravind, L. Classification and Evolution of P-loop GTPases and Related ATPases. *J. Mol. Biol.* **2002**, *317*, 41−72.
(11) Boureux, A.; Vignal, E.; Faure, S.; Fort, P. Evolution of the Rho Family of Ras-Like GTPases in Eukaryotes. *Mol. Biol. Evol.* **2007**, *24*, 203−216.
(12) Benelli, D.; Londei, P. Begin at the Beginning: Evolution of Translational Initiation. *Res. Microbiol.* **2009**, *160*, 493−501.
(13) Hartman, H.; Smith, T. F. GTPases and the Origin of the Ribosome. *Biol. Direct* **2010**, *5*, 36.
(14) Diekmann, Y.; Seixas, E.; Gouw, M.; Tavares-Cadete, F.; Seabra, M. C.; Pereira-Leal, J. Thousands of Rab GTPases for the Cell Biologist. *PLoS Comput. Biol.* **2011**, *7*, No. e1002217.
(15) Rojas, A. M.; Fuentes, G.; Rausell, A.; Valencia, A. The Ras Protein Superfamily: Evolutionary Tree and Role of Conserved Amino Acids. *J. Cell Biol.* **2012**, *196*, 189−201.
(16) Klöpper, T. H.; Kienle, N.; Fasshauer, D.; Munro, S. Untangling the Evolution of Rab G Proteins: Implications of a Comprehensive Genome Analysis. *BMC Biol.* **2012**, *10*, 71.
(17) Gabernet-Castello, C.; O'Reilly, A. J.; Dacks, J. B.; Field, M. C. Evolution of Tre-2/Bub2/Cdc16 (TBC) Rab GTPase Activating Proteins. *Mol. Biol. Cell* **2013**, *24*, 1574−1583.
(18) Wuichet, K.; Søgaard-Andersen, L. Evolution and Diversity of the Ras Superfamily of Small GTPases in Prokaryotes. *Genome Biol. Evol.* **2015**, *7*, 57−70.
(19) Carvalho, A. T. P.; Szeler, K.; Vavitsas, K.; Åqvist, J.; Kamerlin, S. C. L. Modeling the Mechanisms of Biological GTP Hydrolysis. *Arch. Biochem. Biophys.* **2015**, *582*, 80−90.
(20) Sprang, S. R. G Protein Mechanisms: Insights from Structural Analysis. *Annu. Rev. Biochem.* **1997**, *66*, 639−678.
(21) Kötting, C.; Gerwert, K. The Dynamics of the Catalytic Site in Small GTPases, Variations on a Common Motif. *FEBS Lett.* **2013**, *587*, 2025−2027.

(22) Pan, X.; Eathiraj, S.; Munson, M.; Lambright, D. G. TBC-Domain GAPs for Rab GTPases Accelerate GTP Hydrolysis by a Dual-Finger Mechanism. *Nature* **2006**, *442*, 303−306.
(23) Dong, N.; Zhu, Y.; Lu, Q.; Hu, L.; Zheng, Y.; Shao, F. Structurally Distinct Bacterial TBC-Like GAPs Link Arf GTPase to Rab1 Inactivation to Counteract Host Defenses. *Cell* **2012**, *150*, 1029−1041.
(24) Gerwert, K.; Mann, D.; Kötting, C. Common Mechanisms of Catalysis in Small and Heterotrimeric GTPases and their Respective GAPs. *Biol. Chem.* **2017**, *398*, 523−533.
(25) Gavriljuk, K.; Gazdag, E.-M.; Itzen, Y.; Kötting, C.; Goody, R. S.; Gerwert, K. Catalytic Mechanism of a Mammalian Rab*RabGAP Complex in Atomic Detail. *Proc. Natl. Acad. Sci. U. S. A.* **2012**, *109*, 21348−21353.
(26) Duarte, F.; Åqvist, J.; Williams, N. H.; Kamerlin, S. C. L. Resolving Apparent Conflicts Between Theoretical and Experimental Models of Phosphate Monoester Hydrolysis. *J. Am. Chem. Soc.* **2015**, *137*, 1081−1093.
(27) Schweins, T.; Geyer, M.; Scheffzek, K.; Warshel, A.; Kalbitzer, H. R.; Wittinghofer, A. Substrate-Assisted Catalysis as a Mechanism for GTP Hydrolysis of p21Ras and Other GTP-Binding Proteins. *Nat. Struct. Biol.* **1995**, *2*, 36−44.
(28) Amin, E.; Jaiswal, M.; Derewenda, U.; Reis, K.; Nouri, K.; Koessmeier, K. T.; Aspenstrom, P.; Somlyo, A. V.; Dvorsky, R.; Ahmadian, M. R. Deciphering the Molecular and Functional Basis of RHOGAP Family Proteins: A Systematic Approach Toward Selective Inactivation of RHO Family Proteins. *J. Biol. Chem.* **2016**, *291*, 20353−20371.
(29) Duarte, F.; Barrozo, A.; Åqvist, J.; Williams, N. H.; Kamerlin, S. C. L. The Competing Mechanisms of Phosphate Monoester Dianion Hydrolysis. *J. Am. Chem. Soc.* **2016**, *138*, 10664−10673.
(30) Barrozo, A.; Blaha-Nelson, D.; Williams, N. H.; Kamerlin, S. C. L. The Effect of Magnesium Ions on Triphosphate Hydrolysis. *Pure Appl. Chem.* **2017**, *89*, 715−727.
(31) Kötting, C.; Blessenohl, M.; Suveyzdis, Y.; Goody, R. S.; Wittinghofer, A.; Gerwert, K. A Phosphoryl Transfer Intermediate in the GTPase Reaction of Ras in Complex with Its GTPase-Activating Protein. *Proc. Natl. Acad. Sci. U. S. A.* **2006**, *103*, 13911−13916.
(32) Kosloff, M.; Selinger, Z. GTPase Catalysis by Ras and Other G-Proteins: Insights from Substrate Directed Superimposition. *J. Mol. Biol.* **2003**, *331*, 1157−1170.
(33) Pasqualato, S.; Cherfils, J. Crystallographic Evidence for Substrate-Assisted GTP Hydrolysis by a Small GTP Binding Protein. *Structure* **2005**, *13*, 533−540.
(34) Wittinghofer, A. Phosphoryl Transfer in Ras Proteins, Conclusive or Elusive? *Trends Biochem. Sci.* **2006**, *31*, 20−23.
(35) Sprang, S. R.; Chen, Z.; Du, X. Structural Basis of Effector Regulation and Signal Termination in Heterotrimeric G_α Proteins. *Adv. Protein Chem.* **2007**, *74*, 1−65.
(36) Prakash, P.; Gorfe, A. A. Lessons from Computer Simulations of Ras Proteins in Solution and in Membranes. *Biochim. Biophys. Acta, Gen. Subj.* **2013**, *1830*, 5211−5218.
(37) Mishra, A. K.; Lambright, D. G. Small GTPases and their GAPs. *Biopolymers* **2016**, *105*, 431−448.
(38) Ligeti, E.; Welti, S.; Scheffzek, K. Inhibition and Termination of Physiological Responses by GTPase Activating Proteins. *Physiol. Rev.* **2012**, *92*, 237−272.
(39) Cherfils, J.; Zeghouf, M. Regulation of Small GTPases by GEFs, GAPs and GDIs. *Physiol. Rev.* **2013**, *93*, 269−309.
(40) Pape, T.; Wintermeyer, W.; Rodnina, M. V. Complete Kinetic Mechanism of Elongation Factor Tu-Dependent Binding of Aminoacyl-tRNA to the A Site of the *E. coli* Ribosome. *EMBO J.* **1998**, *17*, 7490−7497.
(41) Daviter, T.; Wieden, H. J.; Rodnina, M. V. Essential Role of Histidine 84 in Elongation Factor Tu for the Chemical Step of GTP Hydrolysis. *J. Mol. Biol.* **2003**, *332*, 689−699.
(42) Voorhees, R. M.; Schmeing, T. M.; Kelley, A. C.; Ramakrishnan, V. T. The Mechanism for Activation of GTP Hydrolysis on the Ribosome. *Science* **2010**, *330*, 835−838.
(43) Adamczyk, A. J.; Warshel, A. Converting Structural Information into an Allosteric-Energy-Based Picture for Elongation Factor Tu Activation by the Ribosome. *Proc. Natl. Acad. Sci. U. S. A.* **2011**, *108*, 9827−9832.
(44) Aleksandrov, A.; Field, M. Mechanism of Activation of Elongation Factor Tu by Ribosome: Catalytic Histidine Activates GTP by Protonation. *RNA* **2013**, *19*, 1218−1225.
(45) Maracci, C.; Peske, F.; Dannies, E.; Pohl, C.; Rodnina, M. V. Ribosome-Induced Tuning of GTP Hydrolysis by a Translational GTPase. *Proc. Natl. Acad. Sci. U. S. A.* **2014**, *111*, 14418−14423.
(46) Åqvist, J.; Kamerlin, S. C. L. The Conformational of a Catalytic Loop is Central to GTPase Activity on the Ribosome. *Biochemistry* **2015**, *54*, 546−556.
(47) Mann, D.; Teuber, C.; Tennigkeit, S. A.; Schröter, G.; Gerwert, K.; Kötting, C. Mechanism of the Intrinsic Arginine Finger in Heterotrimeric G Proteins. *Proc. Natl. Acad. Sci. U. S. A.* **2016**, *113*, E8041−E8050.
(48) Bos, J. L.; Rehmann, H.; Wittinghofer, A. GEFs and GAPs: Critical Elements in the Control of Small G-Proteins. *Cell* **2007**, *129*, 865−877.
(49) Scheffzek, K.; Ahmadian, M. R.; Kabsch, W.; Wiesmuller, L.; Lautwein, A.; Schmitz, F.; Wittinghofer, A. The Ras-RasGAP Complex: Structural Basis for GTPase Activation and its Loss in Oncogenic Ras Mutants. *Science* **1997**, *277*, 333−338.
(50) Berman, H. M.; Westbrook, J.; Feng, Z.; Gilliland, G.; Bhat, T. N.; Weissig, H.; Shindyalov, I. N.; Bourne, P. E. The Protein Data Bank. *Nucleic Acids Res.* **2000**, *28*, 235−242.
(51) Tesmer, J. J.; Berman, D. M.; Gilman, A. G.; Sprang, S. R. Structure of RGS4 Bound to AlF_4^-- Activated $G_{i\alpha1}$: stabilization of the transition state for GTP hydrolysis. *Cell* **1997**, *89*, 251−261.
(52) Resat, H.; Straatsma, T. P.; Dixon, D. A.; Miller, J. H. The Arginine Finger of RasGAP Helps Gln-61 Align the Nucleophilic Water in GAP-Stimulated Hydrolysis of GTP. *Proc. Natl. Acad. Sci. U. S. A.* **2001**, *98*, 6033−6038.
(53) Pai, E. F.; Krengel, U.; Petsko, G. A.; Goody, R. S.; Kabsch, W.; Wittinghofer, A. Refined Crystal Structure of the Triphosphate Conformation of H-ras p21 at 1.35 Å Resolution: Implications for the Mechanism of GTP Hydrolysis. *EMBO J.* **1990**, *9*, 2351−2359.
(54) Krengel, U.; Schlichting, I.; Scherer, A.; Schumann, R.; Frech, M.; John, J.; Kabsch, W.; Pai, E. F.; Wittinghofer, A. Three-Dimensional Structures of H-ras p21 Mutants: Molecular Basis for their Inability to Function as Signal Switch Molecules. *Cell* **1990**, *62*, 539−548.
(55) Langen, R.; Schweins, T.; Warshel, A. On the Mechanism of Guanosine Triphosphate Hydrolysis in Ras p21 Proteins. *Biochemistry* **1992**, *31*, 8691−8696.
(56) Prive, G. G.; Milburn, M. V.; Tong, L.; de Vos, A. M.; Yamaizumi, Z.; Nishimura, S.; Kim, S.-H. X-ray Crystal Structures of Transforming p21 Ras Mutants Suggest a Transition-State Stabilization Mechanism for GTP Hydrolysis. *Proc. Natl. Acad. Sci. U. S. A.* **1992**, *89*, 3649−3653.
(57) Schweins, T.; Langen, R.; Warshel, A. Why Have Mutagenesis Studies not Located the General Base in Ras p21? *Nat. Struct. Mol. Biol.* **1994**, *1*, 476−484.
(58) Sondek, J.; Lambright, D. G.; Noel, J. P.; Hamm, H. E.; Sigler, P. B. GTPase Mechanism of Gproteins from the 1.7-Å crystal structure of transducin α-GDP AlF_4^-. *Nature* **1994**, *372*, 276−279.
(59) Schweins, T.; Geyer, M.; Kalbitzer, H. R.; Wittinghofer, A.; Warshel, A. Linear Free Energy Relationships in the Intrinsic and GTPase Activating Protein-Stimulated Guanosine 5′-Triphosphate Hydrolysis of p21Ras. *Biochemistry* **1996**, *35*, 14225−14231.
(60) Ahmadian, M. R.; Zor, T.; Vogt, D.; Kabsch, W.; Selinger, Z.; Wittinghofer, A.; Scheffzek, K. Guanosine Triphosphate Stimulation of Oncogenic Ras Mutants. *Proc. Natl. Acad. Sci. U. S. A.* **1999**, *96*, 7065−7070.
(61) Grigorenko, B. L.; Nemukhin, A. V.; Topol, I. A.; Cachau, R. E.; Burt, S. K. QM/MM Modeling the Ras−GAP Catalyzed Hydrolysis of Guanosine Triphosphate. *Proteins: Struct., Funct., Genet.* **2005**, *60*, 495−503.

DOI: 10.1021/jacs.9b03193
J. Am. Chem. Soc. 2019, 141, 10684−10701

(62) Martín-García, F.; Mendieta-Moreno, J. I.; López-Vinas, E.; Gómez-Puertas, P.; Mendieta, J. The Role of Gln61 in HRas GTP Hydrolysis: A Quantum Mechanics/Molecular Mechanics Study. *Biophys. J.* **2012**, *102*, 152−157.
(63) Anand, B.; Majumdar, S.; Prakash, B. Structural Basis Unifying Diverse GTP Hydrolysis Mechanisms. *Biochemistry* **2013**, *52*, 1122−1130.
(64) Knihtila, R.; Holzapfel, G.; Weiss, K.; Meilleur, F.; Mattos, C. Neutron Crystal Structure of RAS GTPase Puts in Question the Protonation State of the GTP γ-Phosphate. *J. Biol. Chem.* **2015**, *290*, 31025−31036.
(65) Sprang, S. R. Activation of G proteins by GTP and the Mechanism of Gα-Catalyzed GTP Hydrolysis. *Biopolymers* **2016**, *105*, 449−462.
(66) Tripathi, R.; Glaves, R.; Marx, D. The GTPase hGBP1 Converts GTP to GMP in Two Steps *via* Proton Shuttle Mechanisms. *Chem. Sci.* **2017**, *8*, 371−380.
(67) Frasa, M. A.; Koessmeier, K. T.; Ahmadian, M. R.; Braga, V. M. Illuminating the Functional and Structural Repertoire of Human TBC/RABGAPs. *Nat. Rev. Mol. Cell Biol.* **2012**, *13*, 67−73.
(68) Flock, T.; Ravarani, C. N. J.; Sun, D.; Venkatakrishnan, A. J.; Kayikci, M.; Tate, C. G.; Veprintsev, D. B.; Babu, M. M. Universal Allosteric Mechanism for G_α Activation by GPCRs. *Nature* **2015**, *524*, 173−179.
(69) Dohlman, H. G.; Thorner, J. RGS Proteins and Signaling by Heterotrimeric G Proteins. *J. Biol. Chem.* **1997**, *272*, 3871−3874.
(70) Ross, E. M.; Wilkie, T. M. GTPase-Activating Proteins for Heterotrimeric G Proteins: Regulators of G protein signaling (RGS) and RGS-Like Proteins. *Annu. Rev. Biochem.* **2000**, *69*, 795−827.
(71) Wallin, G.; Kamerlin, S. C. L.; Åqvist, J. Energetics of Activation of GTP Hydrolysis on the Ribosome. *Nat. Commun.* **2013**, *4*, 1−10.
(72) Bora, R. P.; Plotnikov, N. V.; Lameira, J.; Warshel, A. Quantitative Exploration of the Molecular Origin of the Activation of GTPase. *Proc. Natl. Acad. Sci. U. S. A.* **2013**, *110*, 20509−20514.
(73) Khrenova, M. G.; Grigorenko, B. L.; Kolomeisky, A. B.; Nemukhin, A. V. Hydrolysis of Guanosine Triphosphate (GTP) by the Ras·GAP Protein Complex: Reaction Mechanism and Kinetic Scheme. *J. Phys. Chem. B* **2015**, *119*, 12838−12845.
(74) Cavalli, A.; Carloni, P. Enzymatic GTP Hydrolysis: Insights from an *Ab Initio* Molecular Dynamics Study. *J. Am. Chem. Soc.* **2002**, *124*, 3763−3768.
(75) Maegley, K. A.; Admiraal, S. J.; Herschlag, D. Ras-Catalyzed Hydrolysis of GTP: A New Perspective from Model Studies. *Proc. Natl. Acad. Sci. U. S. A.* **1996**, *93*, 8160−8166.
(76) Chung, H.-H.; Benson, D. R.; Schultz, P. G. Probing the Structure and Mechanism of Ras Protein with an Expanded Genetic Code. *Science* **1993**, *259*, 806−809.
(77) Dawson, R. M. C.; Elliott, D. C.; Elliott, W. H.; Jones, K. M. *Data for Biochemical Research*; Clarendon Press, 2002.
(78) Gorenstein, D.; Lee, Y.-G.; Kar, D. Kinetic Isotope Effects in the Reactions of Aryl-^{18}O-2, 4-Dinitrophenyl Dibenzyl Phosphate and Aryl-^{18}O-2, 4-Dinitrophenyl Phosphate. Evidence for Monomeric Metaphosphate. *J. Am. Chem. Soc.* **1977**, *99*, 2264−2267.
(79) Hengge, A. C.; Tobin, A. E.; Cleland, W. W. Studies of Transition-State Structures in Phosphoryl Transfer Reactions of Phosphodiesters of *p*-Nitrophenol. *J. Am. Chem. Soc.* **1995**, *117*, 5919−5926.
(80) Hengge, A. C. Isotope Effects in the Study of Phosphoryl and Sulfuryl Transfer Reactions. *Acc. Chem. Res.* **2002**, *35*, 105−112.
(81) Kirby, A. J.; Varvoglis, A. G. The Reactivity of Phosphate Esters. Monoester Hydrolysis. *J. Am. Chem. Soc.* **1967**, *89*, 415−423.
(82) Jin, Y.; Molt, R. W., Jr.; Waltho, J. P.; Richards, N.; Blackburn, G. M. ^{19}F NMR and DFT Analysis Reveal Structural and Electronic Transition State Features for RhoA-Catalyzed GTP Hydrolysis. *Angew. Chem., Int. Ed.* **2016**, *55*, 3318−3322.
(83) Warshel, A.; Weiss, R. M. An Empirical Valence Bond Approach for Comparing Reactions in Solutions and in Enzymes. *J. Am. Chem. Soc.* **1980**, *102*, 6218−6226.
(84) Warshel, A. *Computer Modeling of Chemical Reactions in Enzymes and Solutions*; John Wiley & Sons, Inc.: New York, 1991.
(85) Shurki, A.; Derat, E.; Barrozo, A.; Kamerlin, S. C. L. How Valence Bond Theory Can Help You Understand Your (Bio)chemical Reaction. *Chem. Soc. Rev.* **2015**, *44*, 1037−1052.
(86) Warshel, A.; Sharma, P. K.; Kato, M.; Xiang, Y.; Liu, H.; Olsson, M. H. M. Electrostatic Basis for Enzyme Catalysis. *Chem. Rev.* **2006**, *106*, 3210−3235.
(87) Åqvist, J.; Kazemi, M.; Isaksen, G. V.; Brandsdal, B. O. Entropy and Enzyme Catalysis. *Acc. Chem. Res.* **2017**, *50*, 199−207.
(88) Nagy, T.; Meuwly, M.; Duarte, F.; Pabis, A.; Kamerlin, S. C. L.; Plotnikov, N. V.; Harvey, J. N.; O'Connor, M.; Wglowacki, D. R.; Thaunay, F.; Calvo, F.; Ohanessian, G.; Clavaguéra, C.; Shurki, A.; Fuxreiter, M.; Mones, L.; Vianello, R.; Mavri, J. *Theory and Applications of the Empirical Valence Bond Approach: From Physical Chemistry to Chemical Biology*; John Wiley & Sons Ltd.: Chichester, 2017.
(89) Blaha-Nelson, D.; Krüger, D.; Szeler, K.; Ben-David, M.; Kamerlin, S. C. L. Active Site Hydrophobicity and the Convergent Evolution of Paraoxonase Activity in Structurally Divergent Enzymes: The Case of Serum Paraoxonase 1. *J. Am. Chem. Soc.* **2017**, *139*, 1155−1167.
(90) Marelius, J.; Kolmodin, K.; Feierberg, I.; Åqvist, J. Q: A Molecular Dynamics Program for Free Energy Calculations and Empirical Valence Bond Simulations. *J. Mol. Graphics Modell.* **1998**, *16*, 213−225.
(91) Jorgensen, W. L.; Maxwell, D. S.; Tirado-Rives, J. Development and Testing of the OPLS All-Atom Force Field on Conformational Energetics and Properties of Organic Liquids. *J. Am. Chem. Soc.* **1996**, *118*, 11225−11236.
(92) Mann, D.; Höweler, U.; Kötting, C.; Gerwert, K. Elucidation of Single Hydrogen Bonds in GTPases *via* Experimental and Theoretical Infrared Spectroscopy. *Biophys. J.* **2017**, *112* (1), 66−77.
(93) Duarte, F.; Bauer, P.; Barrozo, A.; Amrein, B. A.; Purg, M.; Åqvist, J.; Kamerlin, S. C. L. Force Field Independent Metal Parameters Using a Nonbonded Dummy Model. *J. Phys. Chem. B* **2014**, *118*, 4351−4362.
(94) *Release, S. 3: Macro Model version 9.1*; Schrödinger LLC: New York, 2013.
(95) Seminario, J. M. Calculation of Intramolecular Force Fields From Second-Derivative Tensors. *Int. J. Quantum Chem.* **1996**, *60*, 1271−1277.
(96) Bayly, C. I.; Cieplak, P.; Cornell, W.; Kollman, P. A. A Well-Behaved Electrostatic Potential Based Method Using Charge Restraints for Deriving Atomic Charges: The RESP Model. *J. Phys. Chem.* **1993**, *97*, 10269−10280.
(97) Frisch, M. J.; Trucks, G. W.; Schlegel, H. B.; Scuseria, G. E.; Robb, M. A.; Cheeseman, J. R.; Scalmani, G.; Barone, V.; Mennucci, B.; Petersson, G. A.; Nakatsuji, H.; Caricato, M.; Li, X.; Hratchian, H. P.; Izmaylov, A. F.; Bloino, J.; Zheng, G.; Sonnenberg, J. L.; Hada, M.; Ehara, M.; Toyota, K.; Fukuda, R.; Hasegawa, J.; Ishida, M.; Nakajima, T.; Honda, Y.; Kitao, O.; Nakai, H.; Vreven, T.; Montgomery, J. A., Jr.; Peralta, J. E.; Ogliaro, F.; Bearpark, M.; Heyd, J. J.; Brothers, E.; Kudin, K. N.; Staroverov, V. N.; Keith, T.; Kobayashi, R.; Normand, J.; Raghavachari, K.; Rendell, A.; Burant, J. C.; Iyengar, S. S.; Tomasi, J.; Cossi, M.; Rega, N.; Millam, J. M.; Klene, M.; Knox, J. E.; Cross, J. B.; Bakken, V.; Adamo, C.; Jaramillo, J.; Gomperts, R.; Stratmann, R. E.; Yazyev, O.; Austin, A. J.; Cammi, R.; Pomelli, C.; Ochterski, J. W.; Martin, R. L.; Morokuma, K.; Zakrzewski, V. G.; Voth, G. A.; Salvador, P.; Dannenberg, J. J.; Dapprich, S.; Daniels, A. D.; Farkas, O.; Foresman, J. B.; Ortiz, J. V.; Cioslowski, J.; Fox, D. J. *Gaussian 09; Revision E.01*; Gaussian, Inc.: Wallingford, CT, 2013.
(98) Case, D. A.; Ben-Shalom, I. Y.; Brozell, S. R.; Cerutti, D. S.; Cheatham, I. T. E.; Cruzeiro, V. W. D.; Darden, T. A.; Duke, R. E.; Ghoreishi, D.; Gilson, M. K.; Gohlke, H.; Goetz, A. W.; Greene, D.; Harris, R.; Homeyer, N.; Izadi, S.; Kovalenko, A.; Kurtzman, T.; Lee, T. S.; LeGrand, S.; Li, P.; Lin, C.; Liu, J.; Luchko, T.; Luo, R.; Mermelstein, D. J.; Merz, K. M.; Miao, Y.; Monard, G.; Nguyen, C.;

DOI: 10.1021/jacs.9b03193
J. Am. Chem. Soc. 2019, 141, 10684−10701

Nguyen, H.; Omelyan, I.; Onufriev, A.; Pan, F.; Qi, R.; Roe, D. R.; Roitberg, A.; Sagui, C.; Schott-Verdugo, S.; Shen, J.; Simmerling, C. L.; Smith, J.; Salomon-Ferrer, R.; Swails, J.; Walker, R. C.; Wang, J.; Wei, H.; Wolf, R. M.; Wu, X.; Xiao, L.; York, D. M.; Kollman, P. A. *AMBER 2018*; University of California, San Francisco, CA, 2018.
(99) Meagher, K. L.; Redman, L. T.; Carlson, H. A. Development of Polyphosphate Parameters for use with the AMBER Force Field. *J. Comput. Chem.* **2003**, *24*, 1016−1025.
(100) Scheidig, A. J.; Burmester, C.; Goody, R. S. The Pre-Hydrolysis State of p21Ras in Complex with GTP: New Insights into the Role of Water Molecules in the GTP Hydrolysis Reaction of Ras-like Proteins. *Structure* **1999**, *7*, 1311−1324.
(101) Coleman, D.; Berghuis, A.; Lee, E; Linder, M.; Gilman, A.; Sprang, S. R. Structures of Active Conformations of Gi Alpha 1 and the Mechanism of GTP Hydrolysis. *Science* **1994**, *265*, 1405−1412.
(102) Müller, M. P.; Peters, H.; Blümer, J.; Blankenfeldt, W.; Goody, R. S.; Itzen, A. The Legionella Effector Protein DrrA AMPylates the Membrane Traffic Regulator Rab1b. *Science* **2010**, *329*, 946−949.
(103) Jorgensen, W. L.; Chandrasekhar, J.; Madura, J. D.; Impey, R. W.; Klein, M. L. Comparison of Simple Potential Functions for Simulating Liquid Water. *J. Chem. Phys.* **1983**, *79*, 926−935.
(104) King, G.; Warshel, A. A Surface Constrained All-Atom Solvent Model for Effective Simulations of Polar Solutions. *J. Chem. Phys.* **1989**, *91*, 3647−3661.
(105) Søndergaard, C. R.; Olsson, M. H. M.; Rostkowski, M.; Jensen, J. H. Improved Treatment of Ligands and Coupling Effects in Empirical Calculation and Rationalization of pK_a Values. *J. Chem. Theory Comput.* **2011**, *7*, 2284−2295.
(106) Berendsen, H. J. C.; Postma, J. P. M.; Vangunsteren, W. F.; Dinola, A.; Haak, J. R. Molecular-Dynamics with Coupling to an External Bath. *J. Chem. Phys.* **1984**, *81*, 3684−3690.
(107) Lee, F. S.; Warshel, A. A Local Reaction Field Method for Fast Evaluation of Long-Range Electrostatic Interactions in Molecular Simulations. *J. Chem. Phys.* **1992**, *97*, 3100−3107.
(108) Ryckaert, J. P.; Ciccotti, G.; Berendsen, H. J. C. Numerical-Integration of Cartesian Equations of Motion of a System with Constraints - Molecular-Dynamics of N-Alkanes. *J. Comput. Phys.* **1977**, *23*, 327−341.
(109) Kötting, C.; Gerwert, K. Time-Resolved FTIR Studies Provide Activation Free Energy, Activation Enthalpy and Activation Entropy for GTPase Reactions. *Chem. Phys.* **2004**, *307*, 227−232.
(110) Humphrey, W.; Dalke, A.; Schulten, K. VMD: Visual Molecular Dynamics. *J. Mol. Graphics* **1996**, *14*, 33−38.
(111) Pettersen, E. F.; Goddard, T. D.; Huang, C. C.; Couch, G. S.; Greenblatt, D. M.; Meng, E. C.; Ferrin, T. E. UCSF Chimera - A Visualization System for Exploratory Research and Analysis. *J. Comput. Chem.* **2004**, *25*, 1605−1612.
(112) Durrant, J. D.; de Oliveira, C. A. F.; McCammon, J. A. POVME: An Algorithm for Measuring Binding-Pocket Volumes. *J. Mol. Graphics Modell.* **2011**, *29*, 773−776.
(113) Durrant, J. D.; Votapka, L.; Sørensen, J.; Amaro, R. E. POVME 2.0: An Enhanced Tool for Determining Pocket Shape and Volume Characteristics. *J. Chem. Theory Comput.* **2014**, *10*, 5047−5056.
(114) McGibbon, R. T.; Beauchamp, K. A.; Harrigan, M. P.; Klein, C.; Swails, J. M.; Hernández, C. X.; Schwantes, C. R.; Wang, L. P.; Lane, T. J.; Pande, V. J. MDTraj: A Modern Open Library for the Analysis of Molecular Dynamics Trajectories. *Biophys. J.* **2015**, *109*, 1528−1532.
(115) Baxa, M. C.; Haddadian, E. J.; Jumper, J. M.; Freed, K. F.; Sosnick, T. R. Loss of Conformational Entropy in Protein Folding Calculated Using Realistic Ensembles and its Implications for NMR-Based Calculations. *Proc. Natl. Acad. Sci. U. S. A.* **2014**, *111*, 15396−15401.
(116) Grigorenko, B. L.; Rogov, A. V.; Nemukhin, A. V. Mechanism of Triphosphate Hydrolysis in Aqueous Solution: QM/MM Simulations in Water Clusters. *J. Phys. Chem. B* **2006**, *110*, 4407−4412.
(117) Glaves, R.; Mathias, G.; Marx, D. Mechanistic Insights into the Hydrolysis of a Nucleoside Triphosphate Model in Neutral and Acidic Solution. *J. Am. Chem. Soc.* **2012**, *134*, 6995−7000.
(118) Rudack, T.; Xia, F.; Schlitter, J.; Kötting, C.; Gerwert, K. The Role of Magnesium for Geometry and Charge in GTP Hydrolysis, Revealed by Quantum Mechanics/Molecular Mechanics Simulations. *Biophys. J.* **2012**, *103*, 293−302.
(119) Plotnikov, N. V.; Prasad, B. R.; Chakrabarty, S.; Chu, Z. T.; Warshel, A. Quantifying the Mechanism of Phosphate Monoester Hydrolysis in Aqueous Solution by Evaluating the Relevant *Ab Initio* QM/MM Free Energy Surfaces. *J. Phys. Chem. B* **2013**, *117*, 12807−12819.
(120) Wang, C.; Huang, W.; Liao, J.-L. QM/MM Investigation of ATP Hydrolysis in Aqueous Solution. *J. Phys. Chem. B* **2015**, *119*, 3720−3726.
(121) Kiani, F. A.; Fischer, S. Effects of Protonation on the Hydrolysis of Triphosphate in Vacuum and the Implications for Catalysis by Nucleotide Hydrolyzing Enzymes. *BMC Biochem* **2016**, *17*, 12.
(122) van Beek, B.; van Bochove, M. A.; Hamlin, T. A.; Bickelhaupt, F. M. Nucleophilic Substitution at Di- and Triphosphates: Leaving Group Ability of Phosphate *vs* Diphosphate. *Electron. Struct.* **2019**, *1*, 024001.
(123) John, J.; Frech, M.; Wittinghofer, A. Biochemical Properties of H-Ras Encoded p21 Mutants and Mechanism of the Autophosphorylation Reaction. *J. Biol. Chem.* **1988**, *263*, 11792−11799.
(124) Lan, K. L.; Zhong, H.; Nanamori, M.; Neubig, R. R. Rapid Kinetics of Regulator of G-protein Signaling (RGS)-Mediated $G_{\alpha i}$ and $G_{\alpha o}$ Deactivation. *J. Biol. Chem.* **2000**, *275*, 33497−33503.
(125) Koripella, K.; Holm, M.; Dourado, D.; Mandava, C. S.; Flores, S.; Sanyal, S. A Conserved Histidine in Switch-II of EF-G Moderates Release of Inorganic Phosphate. *Sci. Rep.* **2015**, *5*, 1−10.
(126) Zeidler, W.; Egle, C.; Ribeiro, S.; Wagner, A.; Katunin, V.; Kreutzer, R.; Rodnina, M.; Wintermeyer, W.; Sprinzl, M. Site-Directed Mutagenesis of Thermus-Thermophilus Elongation-Factor Tu - Replacement of His85, Asp81 and Arg300. *Eur. J. Biochem.* **1995**, *229*, 596−604.
(127) Frech, M.; Darden, T. A.; Pedersen, L. G.; Foley, C. K.; Charifson, P. S.; Anderson, M. W.; Wittinghofer, A. Role of Glutamine-61 in the Hydrolysis of GTP by p21h-Ras: An Experimental and Theoretical Study. *Biochemistry* **1994**, *33*, 3237−3244.
(128) Buhrman, G.; Holzapfel, G.; Fetics, S.; Mattos, C. Allosteric Modulation of Ras Positions Q61 for a Direct Role in Catalysis. *Proc. Natl. Acad. Sci. U. S. A.* **2010**, *107*, 4931−4936.
(129) Du, X.; Black, G. E.; Lecchi, P.; Abramson, F. P.; Sprang, S. R. Kinetic Isotope Effects in Ras-Catalyzed GTP Hydrolysis: Evidence for a Loose Transition State. *Proc. Natl. Acad. Sci. U. S. A.* **2004**, *101*, 8858−8863.
(130) Lee, F. S.; Chu, Z.-T.; Bolger, M. B.; Warshel, A. Calculations of Antibody-Antigen Interactions: Microscopic and Semi-Microscopic Evaluation of the Free Energies of Binding of Phosphorylcholine Analogs to McPC603. *Protein Eng., Des. Sel.* **1992**, *5*, 215−228.
(131) Muegge, I.; Tao, H.; Warshel, A. A Fast Estimate of Electrostatic Group Contributions to the Free Energy of Protein-Inhibitor Binding. *Protein Eng., Des. Sel.* **1997**, *10*, 1363−1372.
(132) Purg, M.; Elias, M.; Kamerlin, S. C. L. Similar Active Sites and Mechanisms do not Lead to Cross-Promiscuity in Organophosphate Hydrolysis: Implications for Biotherapeutic Engineering. *J. Am. Chem. Soc.* **2017**, *139*, 17533−17546.
(133) Kulkarni, Y. S.; Liao, Q.; Petrović, D.; Krüger, D. M.; Strodel, B.; Amyes, T. L.; Richard, J. P.; Kamerlin, S. C. L. Enzyme Architecture: Modeling the Operation of a Hydrophobic Clamp in Catalysis by Triosephosphate Isomerase. *J. Am. Chem. Soc.* **2017**, *139*, 10514−10525.
(134) Ahmadian, M. R.; Stege, P.; Scheffzek, K.; Wittinghofer, A. Confirmation of the Arginine-Finger Hypothesis for the GAP-Stimulated GTP-Hydrolysis Reaction of Ras. *Nat. Struct. Biol.* **1997**, *4*, 686−689.

DOI: 10.1021/jacs.9b03193
J. Am. Chem. Soc. 2019, 141, 10684−10701

(135) Kötting, C.; Kallenbach, A.; Suveyzdis, Y.; Wittinghofer, A.; Gerwert, K. The GAP Arginine Finger Movement into the Catalytic Site of Ras Increases the Activation Entropy. *Proc. Natl. Acad. Sci. U. S. A.* **2008**, *105*, 6260−6265.
(136) Kötting, C.; Gerwert, K. What Vibrations Tell Us About GTPases. *Biol. Chem.* **2015**, *396*, 131−144.
(137) Mohamed, M. F.; Hollfelder, F. Efficient, Crosswise Catalytic Promiscuity Among Enzymes That Catalyze Phosphoryl Transfer. *Biochim. Biophys. Acta, Proteins Proteomics* **2013**, *1834*, 417−424.
(138) Pabis, A.; Duarte, F.; Kamerlin, S. C. L. Promiscuity in the Enzymatic Catalysis of Phosphate and Sulfate Transfer. *Biochemistry* **2016**, *55*, 3061−3081.
(139) Hunter, J. D. Matplotlib: A 2D Graphics Environment. *Comput. Sci. Eng.* **2007**, *9*, 90−95.
(140) Tubiana, T.; Carvaillo, J. C.; Boulard, Y.; Bressanelli, S. TTClust: A Versatile Molecular Simulation Trajectory Clustering Program with Graphical Summaries. *J. Chem. Inf. Model.* **2018**, *58*, 2178−2182.
(141) Nagy, G. N.; Suardíaz, R.; Lopata, A.; Ozohanics, O.; Vékey, K.; Brooks, B. R.; Leveles, I.; Tóth, J.; Vértessy, B. G.; Rosta, E. Structural Characterization of Arginine Fingers: Identification of an Arginine Finger for the Pyrophosphatase dUTPases. *J. Am. Chem. Soc.* **2016**, *138*, 15035−15045.
(142) Rudack, T.; Jenrich, S.; Brucker, S.; Vetter, I. R.; Gerwert, K.; Kötting, C. Catalysis of GTP Hydrolysis by Small GTPases at Atomic Detail by Integration of X-ray Crystallography, Experimental, and Theoretical IR Spectroscopy. *J. Biol. Chem.* **2015**, *290*, 24079−24090.
(143) Low, P. S.; Bada, J. L.; Somero, G. N. Temperature Adaptation of Enzymes: Roles of the Free Energy, the Enthalpy, and the Entropy of Activation. *Proc. Natl. Acad. Sci. U. S. A.* **1973**, *70*, 430−432.
(144) Lienhard, G. E. Enzymatic Catalysis and Transition-State Theory. *Science* **1973**, *180*, 149−154.
(145) Cook, D. B.; McKenna, J. A Contribution to the Theory of Enzyme Catalysis. The Potential Importance of Vibrational Activation Entropy. *J. Chem. Soc., Perkin Trans. 2* **1974**, *2*, 1223−1225.
(146) Page, M. I. Entropy, Binding Energy, and Enzymic Catalysis. *Angew. Chem., Int. Ed. Engl.* **1977**, *16*, 449−459.
(147) Young, L.; Post, C. B. Catalysis by Entropic Guidance from Enzymes. *Biochemistry* **1996**, *35*, 15129−15133.
(148) Kast, P.; Asif-Ullah, M.; Hilvert, D. Is Chorismate Mutase a Prototypic Entropy Trap? - Activation Parameters for the *Bacillus Subtilis* Enzyme. *Tetrahedron Lett.* **1996**, *37*, 2691−2694.
(149) Zhang, X.; Houk, K. N. Why Enzymes Are Proficient Catalysts: Beyond the Pauling Paradigm. *Acc. Chem. Res.* **2005**, *38*, 379−385.
(150) Ottosson, J.; Rotticci-Mulder, J. C.; Rotticci, D.; Hult, K. Rational Design of Enantioselective Enzymes Requires Considerations of Entropy. *Protein Sci.* **2001**, *10*, 1769−1774.
(151) Jackson, C. J.; Foo, J. L.; Tokuriki, N.; Afriat, L.; Carr, P. D.; Kim, H. K.; Schenk, G.; Tawfik, D. S.; Ollis, D. L. Conformational Sampling, Catalysis, and Evolution of the Bacterial Phosphotriesterase. *Proc. Natl. Acad. Sci. U. S. A.* **2009**, *106*, 21631−21636.
(152) Schopf, P.; Mills, M. J.; Warshel, A. The Entropic Contributions in Vitamin B12 Enzymes Still Reflect the Electrostatic Paradigm. *Proc. Natl. Acad. Sci. U. S. A.* **2015**, *112*, 4328−4333.
(153) Kazemi, M.; Himo, F.; Åqvist, J. Enzyme Catalysis by Entropy without Circe Effect. *Proc. Natl. Acad. Sci. U. S. A.* **2016**, *113*, 2406−2411.
(154) Bora, R. P.; Warshel, A. Perspective: Defining and Quantifying the Role of Dynamics in Enzyme Catalysis. *J. Chem. Phys.* **2016**, *144*, 180901.
(155) Bhowmick, A.; Sharma, S. C.; Honma, H.; Head-Gordon, T. The Role of Side Chain Entropy and Mutual Information for Improving the *De Novo* Design of Kemp Eliminases KE07 and KE70. *Phys. Chem. Chem. Phys.* **2016**, *18*, 19386−19396.
(156) Arango-Restrpo, A.; Rubi, J. M.; Barragán, D. Enzymatic Evolution Driven by Entropy Production. *Bio Rxiv* **2018**, DOI: 10.1101/319814.
(157) Wang, Y.; Manu, V. S.; Kim, J.; Li, G.; Ahuja, L. G.; Aoto, P.; Taylor, S. S.; Veglia, G. Globally Correlated Conformational Entropy Underlies Positive and Negative Cooperativity in a Kinase's Enzymatic Cycle. *Nat. Commun.* **2019**, *10*, 799.
(158) Åqvist, J.; Kamerlin, S. C. L. Conserved Motifs in Different Classes of GTPases Dictate their Specific Modes of Catalysis. *ACS Catal.* **2016**, *6*, 1737−1743.
(159) de Vivo, M.; Dal Peraro, M.; Klein, M. L. Phosphodiester Cleavage in Ribonuclease H Occurs via an Associative Two-Metal-Aided Catalytic Mechanism. *J. Am. Chem. Soc.* **2008**, *130*, 10955−10962.
(160) Rosta, E.; Nowotny, M.; Yang, W.; Hummer, G. Catalytic Mechanism of RNA Backbone Cleavage by Ribonuclease H from Quantum Mechanics/Molecular Mechanics Simulations. *J. Am. Chem. Soc.* **2011**, *133*, 8934−8941.
(161) Palermo, G.; Stenta, M.; Cavalli, A.; Dal Peraro, M.; de Vivo, M. Molecular Simulations Highlight the Role of Metals in Catalysis and Inhibition of Type II Topoisomerase. *J. Chem. Theory Comput.* **2013**, *9*, 857−862.
(162) Rosta, E.; Yang, W.; Hummer, G. Calcium Inhibition of Ribonuclease H1 Two-Metal Ion Catalysis. *J. Am. Chem. Soc.* **2014**, *136*, 3137−3144.
(163) Ganguly, A.; Thaplyal, P.; Rosta, E.; Bevilacqua, P. C.; Hammes-Schiffer, S. Quantum Mechanical/Molecular Mechanical Free Energy Simulations of the Self-Cleavage Reaction in the Hepatitis Delta Virus Ribozyme. *J. Am. Chem. Soc.* **2014**, *136*, 1483−1496.
(164) Radak, B. K.; Lee, T.-S.; Harris, M. E.; York, D. M. Assessment of Metal-Assisted Nucleophile Activation in the Hepatitis Delta Virus Ribozyme from Molecular Simulation and 3D-RISM. *RNA* **2015**, *21*, 1566−1577.
(165) Palermo, G.; Cavalli, A.; Klein, M. L.; Alfonso-Prieto, M.; Dal Peraro, M.; De Vivo, M. Catalytic Metal Ions and Enzymatic Processing of DNA and RNA. *Acc. Chem. Res.* **2015**, *48*, 220−228.
(166) Casalino, L.; Palermo, G.; Rothlisberger, G.; Magistrato, A. Who Activates the Nucleophile in Ribozyme Catalysis? An Answer from the Splicing Mechanism of Group II Introns. *J. Am. Chem. Soc.* **2016**, *138*, 10374−10377.
(167) Admiraal, S. J.; Herschlag, D. Mapping the Transition State for ATP Hydrolysis: Implications for Enzyme Catalysis. *Chem. Biol.* **1995**, *2*, 729−739.
(168) Liao, Q.; Kulkarni, Y.; Sengupta, U.; Petrović, D.; Mulholland, A. J.; van der Kamp, M. W.; Strodel, B.; Kamerlin, S. C. L. Loop Motion in Triosephosphate Isomerase Is Not a Simple Open and Shut Case. *J. Am. Chem. Soc.* **2018**, *140*, 15889−15903.
(169) Cohen, S. G.; Vaidya, V. M.; Schultz, R. M. Active Site of α-Chymotrypsin Activation by Association-Desolvation. *Proc. Natl. Acad. Sci. U. S. A.* **1970**, *66*, 249−256.
(170) Wolfenden, R. Waterlogged Molecules. *Science* **1983**, *222*, 1087−1093.
(171) Dewar, M. J.; Storch, D. M. Alternate View of Enzyme Reactions. *Proc. Natl. Acad. Sci. U. S. A.* **1985**, *82*, 2225−2229.
(172) Cannon, W. R.; Benkovic, S. J. Solvation, Reorganization Energy, and Biological Catalysis. *J. Biol. Chem.* **1998**, *273*, 26257−26260.
(173) Lohman, D. C.; Edwards, D. R.; Wolfenden, R. Catalysis by Desolvation: The Catalytic Prowess of SAM-Dependent Halide-Alkylating Enzymes. *J. Am. Chem. Soc.* **2013**, *135*, 14473−14475.
(174) Richard, J. P.; Amyes, T. L.; Goryanova, B.; Zhai, X. Enzyme Architecture: On the Importance of Being in a Protein Cage. *Curr. Opin. Chem. Biol.* **2014**, *21*, 1−10.
(175) Warshel, A.; Åqvist, J.; Creighton, S. Enzymes Work by Solvation Substitution Rather than by Desolvation. *Proc. Natl. Acad. Sci. U. S. A.* **1989**, *86*, 5820−5824.
(176) Sigala, P. A.; Fafarman, A. T.; Bogard, P. E.; Boxer, S. G.; Herschlag, D. Do Ligand Binding and Solvent Exclusion Alter the Electrostatic Character within the Oxyanion Hole of an Enzymatic Active Site? *J. Am. Chem. Soc.* **2007**, *129*, 12104−12105.

DOI: 10.1021/jacs.9b03193
J. Am. Chem. Soc. 2019, 141, 10684−10701

(177) Lameira, J.; Bora, R. P.; Chu, Z. T.; Warshel, A. Methyltransferases do not Work by Compression, Cratic, or Desolvation Effects, but by Electrostatic Preorganization. *Proteins: Struct., Funct., Genet.* **2015**, *83*, 318−330.
(178) Araújo, E.; Lima, A. H.; Lameira, J. Catalysis by Solvation Rather than the Desolvation Effect: Exploring the Catalytic Efficiency of SAM-Dependent Chlorinase. *Phys. Chem. Chem. Phys.* **2017**, *19*, 21350−21356.
(179) Cox, A. D.; Fesik, S. W.; Kimmelman, A. C.; Luo, J.; Der, C. J. Drugging the Undruggable Ras: Mission Possible? *Nat. Rev. Drug Discovery* **2014**, *13*, 828−851.
(180) Cromm, P. M.; Spiegel, J.; Grossmann, T. N.; Waldmann, H. Direct Modulation of Small GTPase Activity and Function. *Angew. Chem., Int. Ed.* **2015**, *54*, 13516−13537.
(181) Lu, S.; Jang, H.; Gu, S.; Zhang, J.; Nussinov, R. Drugging Ras GTPase: A Comprehensive Mechanistic and Signaling Structural View. *Chem. Soc. Rev.* **2016**, *45*, 4929−4952.
(182) Li, W. J.; Rudack, T.; Gerwert, K.; Grater, F.; Schlitter, J. Exploring the Multidimensional Free Energy Surface of Phosphoester Hydrolysis with Constrained QM/MM Dynamics. *J. Chem. Theory Comput.* **2012**, *8*, 3596−3604.
(183) Xia, F.; Rudack, T.; Cui, Q.; Kötting, C.; Gerwert, K. Detailed Structure of the $H_2PO_4^-$- Guanosine Diphosphate Intermediate in Ras-GAP Decoded from FTIR Experiments by Biomolecular Simulations. *J. Am. Chem. Soc.* **2012**, *134*, 20041−20044.
(184) Du, X.; Sprang, S. R. Transition State Structures and the Roles of Catalytic Residues in GAP-Facilitated GTPase of Ras As Elucidated by ^{18}O Kinetic Isotope Effects. *Biochemistry* **2009**, *48*, 4538−4547.
(185) Petrović, D.; Szeler, K.; Kamerlin, S. C. L. Challenges and Advances in the Computational Modeling of Biological Phosphate Hydrolysis. *Chem. Comm* **2018**, *54*, 3077−3089.
(186) Lu, S.; Jang, H.; Nussinov, R.; Zhang, J. The Structural Basis of Oncogenic Mutations G12, G13 and Q61 in Small GTPase K-Ras4B. *Sci. Rep.* **2016**, *6*, 1−15.

DOI: 10.1021/jacs.9b03193
J. Am. Chem. Soc. 2019, 141, 10684−10701

Supporting Information for:

GTP Hydrolysis Without an Active Site Base:

A Unifying Mechanism for Ras and Related GTPases

Ana R. Calixto[1,‡], Cátia Moreira[1,‡], Anna Pabis[2], Carsten Kötting[3], Klaus Gerwert[3], Till Rudack[3,*] and Shina C. L. Kamerlin[1,*]

1. Department of Chemistry – BMC, Uppsala University, Box 576, S-751 23 Uppsala, Sweden. 2. Department of Cell and Molecular Biology, Uppsala University, BMC Box 596, S-751 24 Uppsala, Sweden. 3. Department of Biophysics, Ruhr University Bochum, 44801 Bochum, Germany.

[‡] These authors contributed equally.

Corresponding author email addresses: till.rudack@rub.de and lynn.kamerlin@kemi.uu.se

Table of Contents

S1. Supplementary Figures

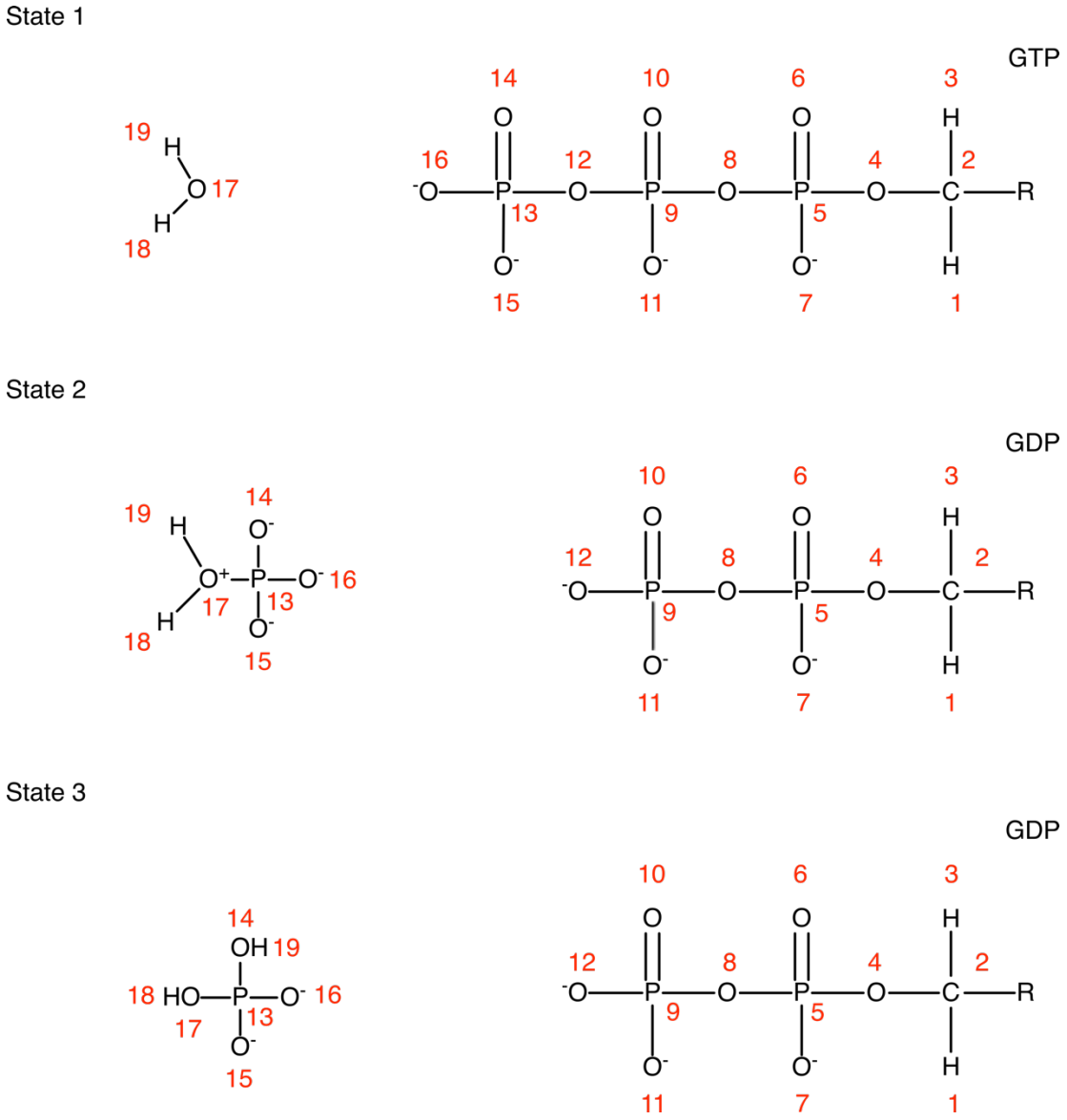

Figure S1. The valence bond states used to describe the solvent-assisted mechanism in our empirical valence bond (EVB) simulations of both the GTPase-catalyzed and non-enzymatic hydrolysis of GTP in aqueous solution and in the relevant enzyme active sites. For clarity, only the triphosphate of the GTP is indicated in this figure, as the remainder of the molecule was not part of the EVB region during our simulations. The atom numbering corresponds to the EVB parameter tables, shown in **Tables S15** to **S29**.

State 1

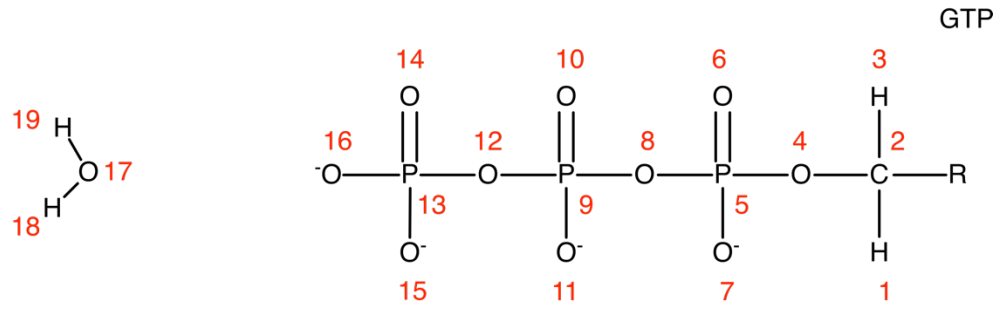

State 2

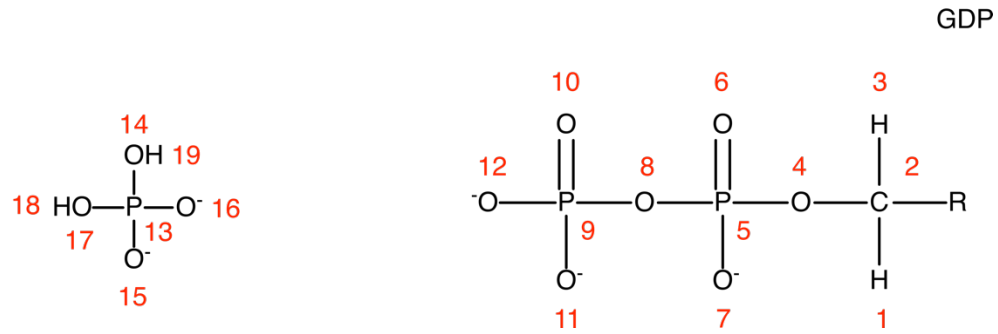

Figure S2. The valence bond states used to describe the substrate-assisted mechanism in our empirical valence bond (EVB) simulations of both the GTPase-catalyzed and non-enzymatic hydrolysis of GTP in aqueous solution and in the relevant enzyme active sites. For clarity, only the triphosphate of the GTP is indicated in this figure, as the remainder of the molecule was not part of the EVB region during our simulations. The atom numbering corresponds to the EVB parameter tables, shown in **Tables S15** to **S29**.

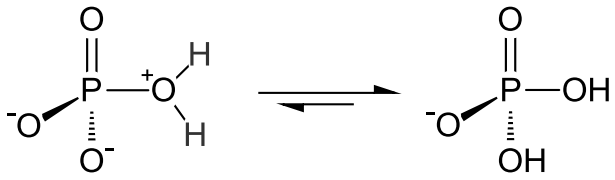

Figure S3. Transient intermediate formed during the solvent-assisted hydrolysis of GTP (left), which is expected to quickly tautomerize to form the more stable final product (right).[1]

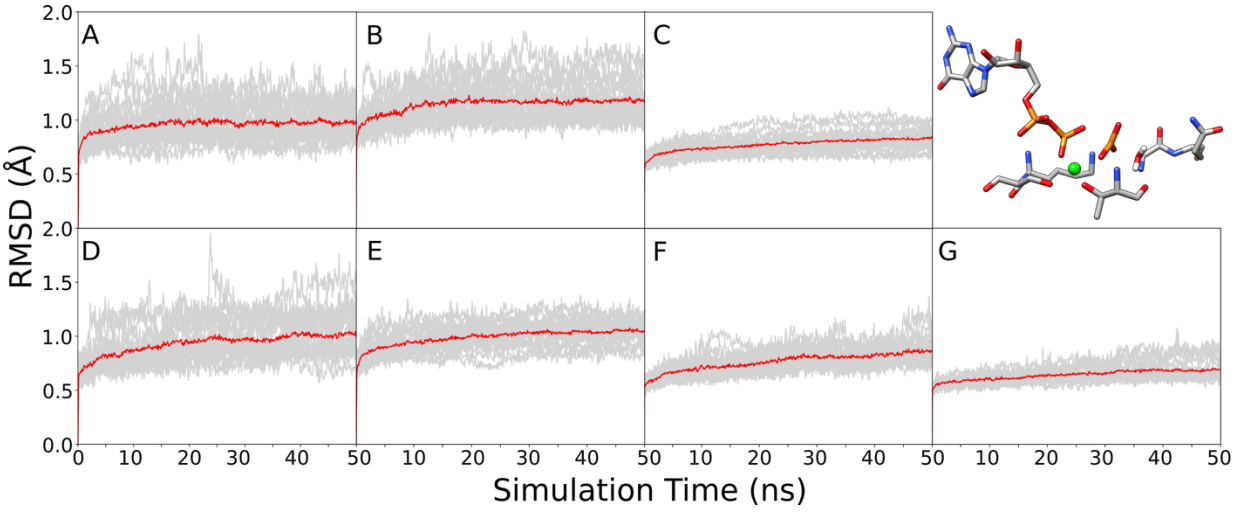

Figure S4. The root mean square deviations (RMSD, Å) of all backbone atoms during 20 x 50ns (1 μs total) of equilibration of the transition state (λ = 0.5) for the solvent-assisted hydrolysis of GTP by (**A**) wild-type Ras, (**B**) Q61H Ras, (**C**) RasGAP, (**D**) Rab, (**E**) RabGAP, (**F**) $G_{\alpha i}$ and (**G**) $G_{\alpha i}$-RGS4. Snapshots were taken every 100ps, and the RMSD values were calculated using MDtraj.[2] The grey shaded lines indicate the data from each individual trajectory for each system, and the solid red lines indicate the average RMSD over all trajectories for each system. Shown here is also a representative structure of the solvent-assisted transition state for Ras-catalyzed hydrolysis of GTP, extracted from our EVB simulations of this reaction.

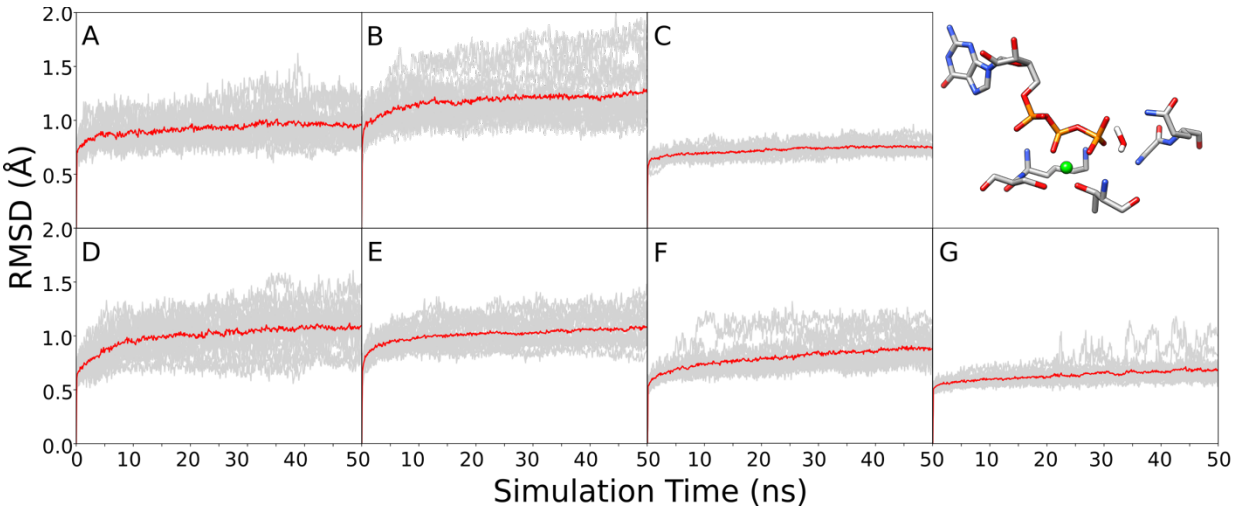

Figure S5. The root mean square deviations (RMSD, Å) of all backbone atoms during 20 x 50ns (1 μs total) of equilibration of the transition state (λ = 0.5) for the substrate-assisted hydrolysis of GTP by (**A**) wild-type Ras, (**B**) Q61H Ras, (**C**) RasGAP, (**D**) Rab, (**E**) RabGAP, (**F**) $G_{\alpha i}$ and (**G**) $G_{\alpha i}$-RGS4. Snapshots were taken every 100ps, and the RMSD values were calculated using MDtraj.[2] The grey shaded lines indicate the data from each individual trajectory for each system, and the solid red lines indicate the average RMSD over all trajectories for each system. Shown here is also a representative structure of the substrate-assisted transition state for Ras-catalyzed hydrolysis of GTP, extracted from our EVB simulations of this reaction.

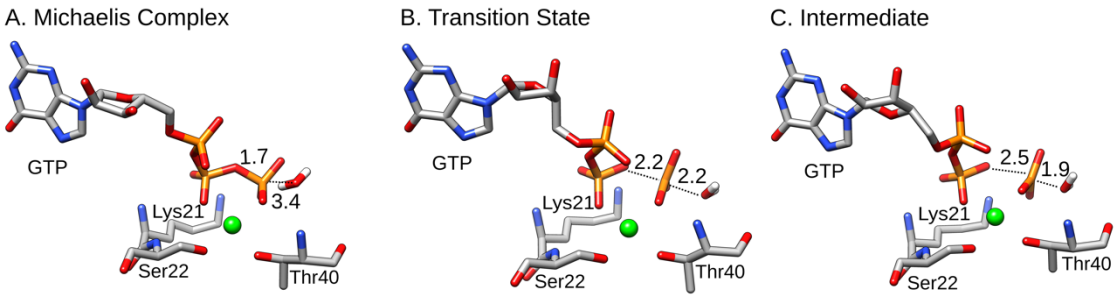

Figure S6. Structures of key stationary points, extracted from our empirical valence bond simulations of the Rab-catalyzed solvent-assisted hydrolysis of GTP. Shown here are (**A**) the Michaelis complex, (**B**) the transition state for the phosphoryl transfer reaction, and (**C**) the short-lived intermediate. Note that, as described in the main text, we only modelled the final tautomerization step (**Figure S3**) in the case of the non-enzymatic reaction, and the Ras- and RasGAP-catalyzed reactions, as this step is fast and not rate-limiting (**Figure 3**). The P-O distances annotated on this figure (in Å) are average distances over all replicas, as presented in **Table 1**, and the structures shown in this figure were selected because they have P-O distances that are very similar to the average distances across all the EVB trajectories. The corresponding free energies for this reaction can be found in **Figure 3** and **Table S3**. Shown here are the substrate, nucleophilic water molecule, Mg^{2+} ion, and key catalytic residues. The remainder of the protein has been omitted for clarity.

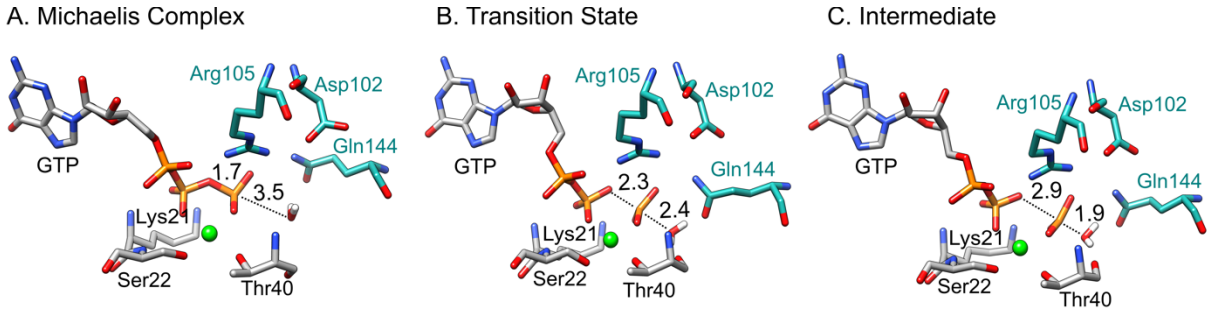

Figure S7. Structures of key stationary points, extracted from our empirical valence bond simulations of the RabGAP-catalyzed solvent-assisted hydrolysis of GTP. Shown here are (**A**) the Michaelis complex, (**B**) the transition state for the phosphoryl transfer reaction, and (**C**) the short-lived intermediate. Note that, as described in the main text, we only modelled the final tautomerization step (**Figure S3**) in the case of the non-enzymatic reaction, and the Ras- and RasGAP-catalyzed reactions, as this step is fast and not rate-limiting (**Figure 3**). The P-O distances annotated on this figure (in Å) are average distances over all replicas, as presented in **Table 1**, and the structures shown in this figure were selected because they have P-O distances that are very similar to the average distances across all the EVB trajectories. The corresponding free energies for this reaction can be found in **Figure 3** and **Table S3**. Shown here are the substrate, nucleophilic water molecule, Mg^{2+} ion, and key catalytic residues. The remainder of the protein has been omitted for clarity.

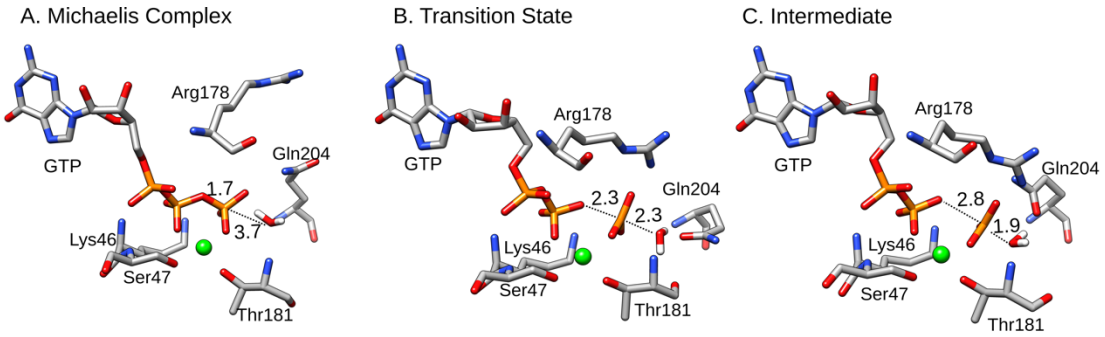

Figure S8. Structures of key stationary points, extracted from our empirical valence bond simulations of the $G_{\alpha i}$-catalyzed solvent-assisted hydrolysis of GTP. Shown here are (**A**) the Michaelis complex, (**B**) the transition state for the phosphoryl transfer reaction, and (**C**) the short-lived intermediate. Note that, as described in the main text, we only modelled the final tautomerization step (**Figure S3**) in the case of the non-enzymatic reaction, and the Ras- and RasGAP-catalyzed reactions, as this step is fast and not rate-limiting (**Figure 3**). The P-O distances annotated on this figure (in Å) are average distances over all replicas, as presented in **Table 1**, and the structures shown in this figure were selected because they have P-O distances that are very similar to the average distances across all the EVB trajectories. The corresponding free energies for this reaction can be found in **Figure 3** and **Table S3**. Shown here are the substrate, nucleophilic water molecule, Mg^{2+} ion, and key catalytic residues. The remainder of the protein has been omitted for clarity.

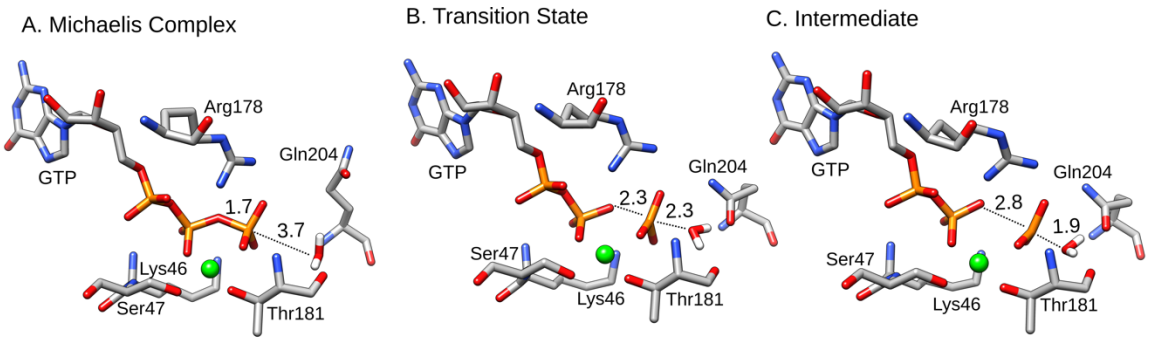

Figure S9. Structures of key stationary points, extracted from our empirical valence bond simulations of the $G_{\alpha i}$-RGS4-catalyzed solvent-assisted hydrolysis of GTP. Shown here are (**A**) the Michaelis complex, (**B**) the transition state for the phosphoryl transfer reaction, and (**C**) the short-lived intermediate. Note that, as described in the main text, we only modelled the final tautomerization step (**Figure S3**) in the case of the non-enzymatic reaction, and the Ras- and RasGAP-catalyzed reactions, as this step is fast and not rate-limiting (**Figure 3**). The P-O distances annotated on this figure (in Å) are average distances over all replicas, as presented in **Table 1** and the structures shown in this figure were selected because they have P-O distances that are very similar to the average distances across all the EVB trajectories. The corresponding free energies for this reaction can be found in **Figure 3** and **Table S3**. Shown here are the substrate, nucleophilic water molecule, Mg^{2+} ion, and key catalytic residues. The remainder of the protein has been omitted for clarity.

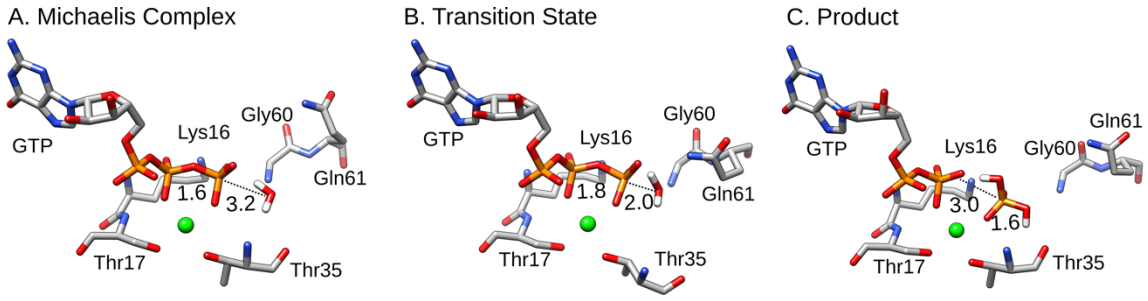

Figure S10. Structures of key stationary points, extracted from our empirical valence bond simulations of the Ras-catalyzed substrate-assisted hydrolysis of GTP. Shown here are (**A**) the Michaelis complex, (**B**) the transition state for the phosphoryl transfer reaction, and (**C**) the product complex. The P-O distances annotated on this figure (in Å) are average distances over all replicas, as presented in **Table S7**, and the structures shown in this figure were selected because they have P-O distances that are very similar to the average distances across all the EVB trajectories. The corresponding free energies for this reaction can be found in **Figure 3** and **Table S3**. Shown here are the substrate, nucleophilic water molecule, Mg^{2+} ion, and key catalytic residues. The remainder of the protein has been omitted for clarity.

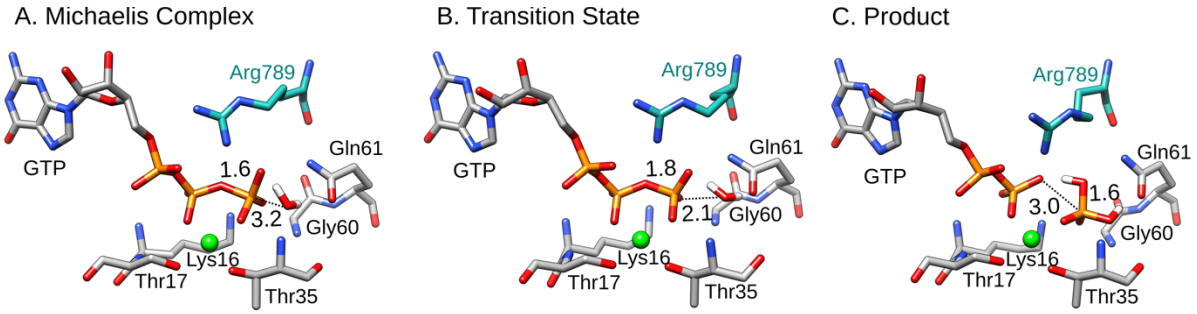

Figure S11. Structures of key stationary points, extracted from our empirical valence bond simulations of the RasGAP-catalyzed substrate-assisted hydrolysis of GTP. Shown here are (**A**) the Michaelis complex, (**B**) the transition state for the phosphoryl transfer reaction, and (**C**) the product complex. The P-O distances annotated on this figure (in Å) are average distances over all replicas, as presented in **Table S7**, and the structures shown in this figure were selected because they have P-O distances that are very similar to the average distances across all the EVB trajectories. The corresponding free energies for this reaction can be found in **Figure 3** and **Table S3**. Shown here are the substrate, nucleophilic water molecule, Mg^{2+} ion, and key catalytic residues. The remainder of the protein has been omitted for clarity.

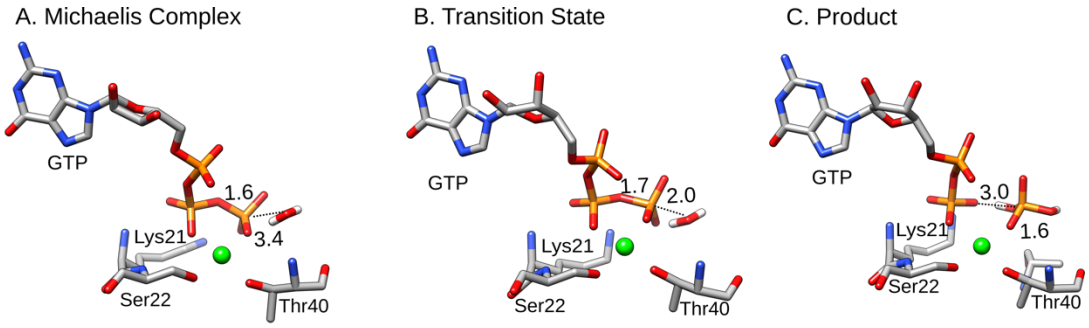

Figure S12. Structures of key stationary points, extracted from our empirical valence bond simulations of the Rab-catalyzed substrate-assisted hydrolysis of GTP. Shown here are (**A**) the Michaelis complex, (**B**) the transition state for the phosphoryl transfer reaction, and (**C**) the product complex. The P-O distances annotated on this figure (in Å) are average distances over all replicas, as presented in **Table S7**, and the structures shown in this figure were selected because they have P-O distances that are very similar to the average distances across all the EVB trajectories. The corresponding free energies for this reaction can be found in **Figure 3** and **Table S3**. Shown here are the substrate, nucleophilic water molecule, Mg^{2+} ion, and key catalytic residues. The remainder of the protein has been omitted for clarity.

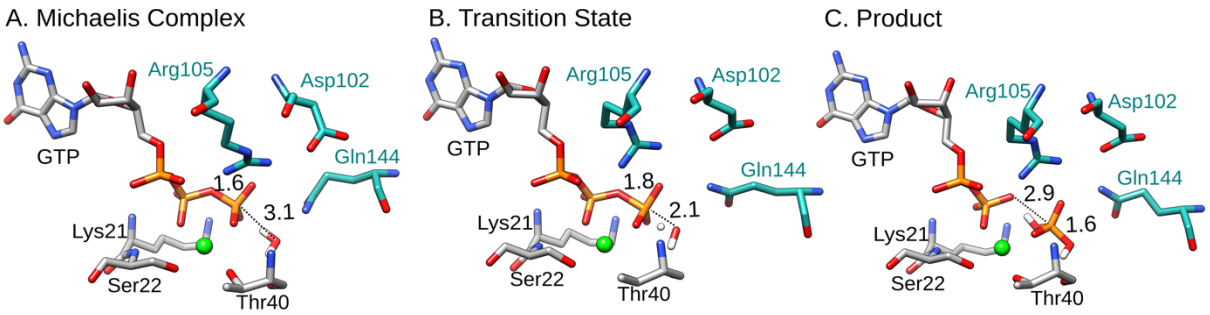

Figure S13. Structures of key stationary points, extracted from our empirical valence bond simulations of the RabGAP-catalyzed substrate-assisted hydrolysis of GTP. Shown here are (**A**) the Michaelis complex, (**B**) the transition state for the phosphoryl transfer reaction, and (**C**) the product complex. The P-O distances annotated on this figure (in Å) are average distances over all replicas, as presented in **Table S7**, and the structures shown in this figure were selected because they have P-O distances that are very similar to the average distances across all the EVB trajectories. The corresponding free energies for this reaction can be found in **Figure 3** and **Table S3**. Shown here are the substrate, nucleophilic water molecule, Mg^{2+} ion, and key catalytic residues. The remainder of the protein has been omitted for clarity.

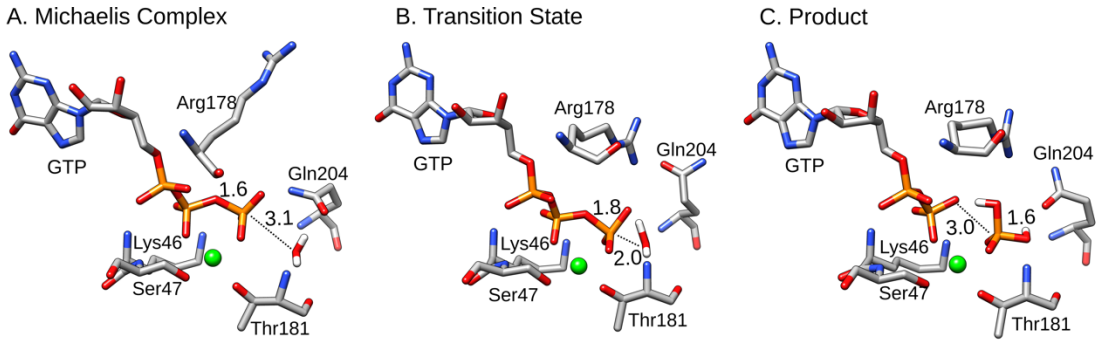

Figure S14. Structures of key stationary points, extracted from our empirical valence bond simulations of the $G_{\alpha i}$-catalyzed substrate-assisted hydrolysis of GTP. Shown here are (**A**) the Michaelis complex, (**B**) the transition state for the phosphoryl transfer reaction, and (**C**) the product complex. The P-O distances annotated on this figure (in Å) are average distances over all replicas, as presented in **Table S7**, and the structures shown in this figure were selected because they have P-O distances that are very similar to the average distances across all the EVB trajectories. The corresponding free energies for this reaction can be found in **Figure 3** and **Table S3**. Shown here are the substrate, nucleophilic water molecule, Mg^{2+} ion, and key catalytic residues. The remainder of the protein has been omitted for clarity.

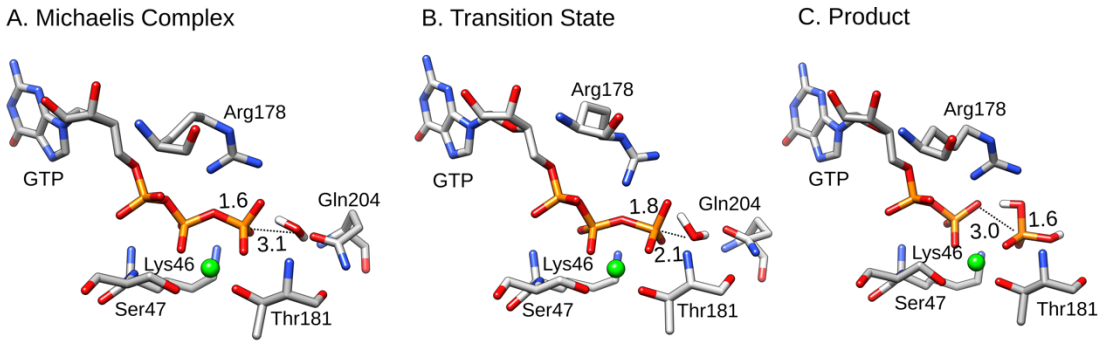

Figure S15. Structures of key stationary points, extracted from our empirical valence bond simulations of the $G_{\alpha i}$-RGS4-catalyzed substrate-assisted hydrolysis of GTP. Shown here are (**A**) the Michaelis complex, (**B**) the transition state for the phosphoryl transfer reaction, and (**C**) the product complex. The P-O distances annotated on this figure (in Å) are average distances over all replicas, as presented in **Table S7**, and the structures shown in this figure were selected because they have P-O distances that are very similar to the average distances across all the EVB trajectories. The corresponding free energies for this reaction can be found in **Figure 3** and **Table S3**. Shown here are the substrate, nucleophilic water molecule, Mg^{2+} ion, and key catalytic residues. The remainder of the protein has been omitted for clarity.

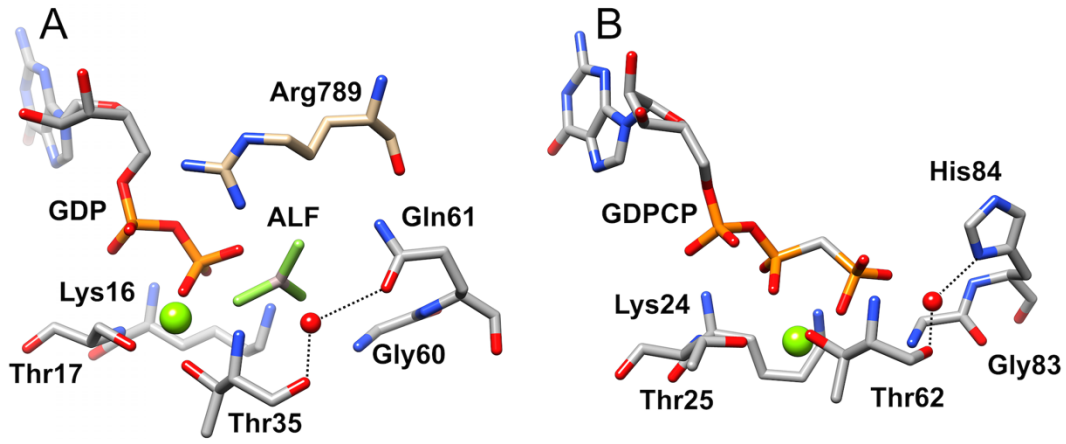

Figure S16. Comparison of the active sites of (**A**) the RasGAP complex (PDB ID: 1WQ1[3]) and (**B**) elongation factor thermounstable (EF-Tu) (PDB ID: 4V5L[4]), showing the active site residue, His84, present in EF-Tu in the same structural position as the residue Gln61 found in Ras and the RasGAP complex.

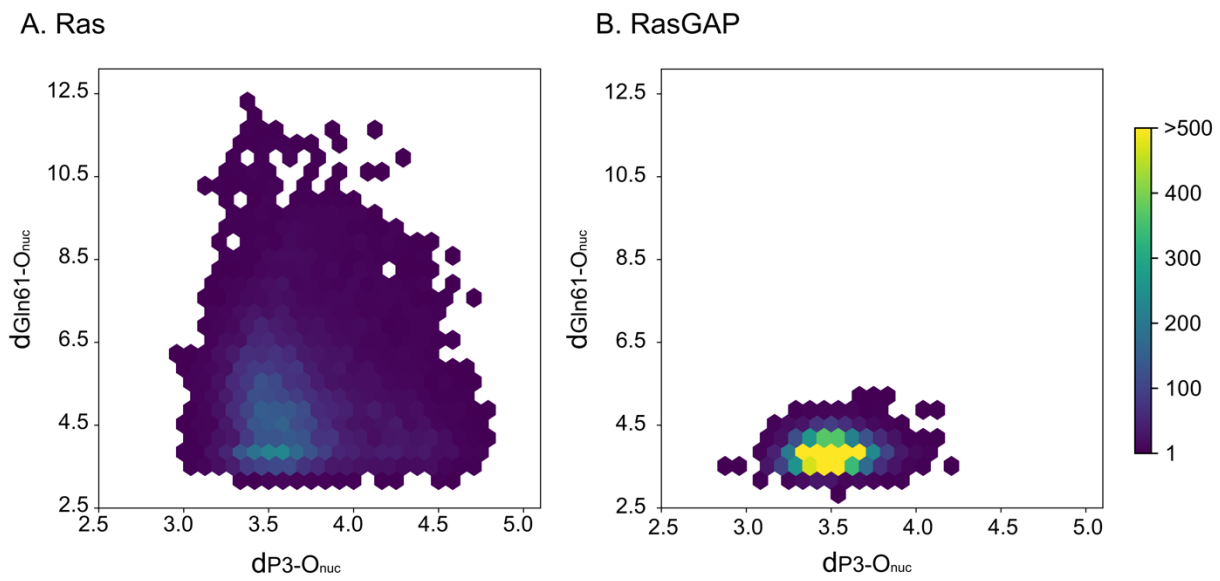

Figure S17. Conformational space of the nucleophilic water molecule sampled during 20 x 50ns (1 μs total) simulations of the Michaelis complexes of **(A)** Ras and **(B)** RasGAP, and defined as a function of the distance between the phosphorus atom of the γ-phosphate of the GTP (P3) and the oxygen atom of the nucleophilic water molecule (O_{nuc}, *x*-axis), and between the Cδ atom of the Gln61 side chain and the oxygen atom of the nucleophilic water molecule (O_{nuc}, *y*-axis). Simulations at the Michaelis complex were performed using the same protocol as for the equilibrations at the transition state, as described in the **Methodology** section, and using the same restraints as were applied in our EVB simulations (again, see the **Methodology** section). Snapshots were extracted for analysis every 100 ps.

S2. Supplementary Tables

Table S1. Overview of the different crystal structures used in this study, indicating the PDB ID, the resolution of the structure (in Å), any substrate or transition state analogues present in the structure (ligand) and any chemical modifications performed on the analogues, where present (modification).

PDB ID	Resolution (Å)	Ligand[a]	Modification[b]
1QRA[5]	1.6	GTP	-
1WQ1[3]	2.5	GDP; AF3	Al to P; F to O; bond between GDP and Al.
1GIA[6]	2.0	GSP	S to O
3NKV[7]	1.7	GNP	N to O
4HLQ[8]	3.3	GDP; BEF	Be to P; F to O; bond between GDP and Be.
621P[9]	2.4	GNP	N to O

[a] Here, the relevant ligands are guanosine-5´-triphosphate (GTP), guanosine-5´-diphosphate (GDP), 5´-guanosine-diphosphate-monothiophosphate (GSP), phophoaminophosphonic acid-guanylate ester (GNP), aluminum fluoride, AlF_3 (AF3), and beryllium fluoride, BeF_3^- (BEF). [b] All modifications were reverted to GTP, as described in the **Methodology** section.

Table S2. List of residues in their ionized states, as well as the protonation patterns of histidine residues, during the simulations.

Type	**Residue Number**[a]
Ras	
Asp	30, 33, 38, 54, 57, 69, 92, 119, 154
Glu	3, 31, 37, 62, 63, 76, 91, 98, 126, 143, 153, 162
Lys	5, 16, 42, 88, 101, 104, 117, 147
Arg	41, 68, 73, 97, 102, 123, 149
His-δ	94
His-ε	27, 166
RasGAP	
Asp	30, 33, 38, 54, 57, 69, 92, 119, 154, 748*, 775*, 782*, 972*
Glu	3, 31, 37, 62, 63, 76, 91, 98, 126, 143, 153, 162, 777*, 781*, 783*, 799*, 829*, 945*, 950*, 954*
Lys	5, 16, 42, 88, 101, 104, 117, 147, 803*, 834*, 884*, 935*, 949*, 961*, 964*
Arg	41, 68, 73, 97, 102, 123, 149, 749*, 776*, 789*, 892*, 894*, 903*, 913*, 928*
His-δ	94, 736*, 762*, 965*, 1005*
His-ε	27, 166, 743*, 811*, 812*, 847*, 883*, 986*, 999*, 1021*
Rab1	
Asp	16, 30, 31, 44, 63, 89, 92, 107, 124
Glu	35, 68, 94, 105, 149, 159
Lys	10, 21, 46, 100, 116, 122, 128, 129, 153
Arg	27, 48, 69, 71, 108
His-δ	-
His-ε	82
RabGAP	
Asp	16, 30, 31, 44, 63, 89, 92, 107, 124, 95*, 102*, 128*, 148*, 179*, 183*
Glu	35, 68, 94, 105, 149, 159, 116*, 120*, 124*
Lys	10, 21, 46, 100, 116, 122, 128, 129, 153, 94*, 186*

Arg	27, 48, 69, 71, 108, 90*, 104*, 105*, 108*, 109*, 119*
His-δ	141*, 187*, 227*, 277*
His-ε	82, 37*, 147*, 172*, 173*, 204*, 234*, 246*, 276*
$G_{\alpha i}$	
Asp	150, 158, 173, 200, 229, 231, 237, 251, 272, 328
Glu	43, 58, 65, 115, 116, 145, 186, 207, 216, 236, 238, 239, 245, 275, 276, 308
Lys	35, 46, 51, 54, 70, 180, 197, 209, 210, 248, 270, 271, 277, 280, 312, 317
Arg	86, 90, 142, 144, 161, 176, 178, 205, 208, 242
His-δ	213, 322
His-ε	57, 188, 195, 244
$G_{\alpha i}$-RGS4	
Asp	150, 158, 173, 200, 229, 231, 237, 251, 272, 328, 90*, 130*, 150*, 163*
Glu	43, 58, 65, 116, 145, 186, 207, 216, 236, 238, 239, 245, 275, 276, 297, 308, 61*, 83*, 86*, 87*, 117*, 126*, 135*, 136*, 151*, 161*
Lys	35, 46, 51, 54, 180, 197, 209, 210, 248, 270, 271, 277, 280, 317, 77*, 81*, 125*, 154*, 155*, 162*, 170*
Arg	86, 90, 142, 144, 161, 176, 178, 205, 208, 242, 134*, 139*, 166*, 167*
His-δ	213, 322, 69*
His-ε	57, 188, 195, 244

[a] Residues denoted with a star come from the GAP/RGS proteins. All residues not included in this table were kept in their unionized forms as they were outside the simulation sphere (see the **Methodology** section for further details).

Table S3. A comparison of calculated and experimental rates and activation free energies for the hydrolysis of GTP by a range of GTPases.[a]

System	k_{cat} (s^{-1})[b]	T_{exp} (K)[b]	$\Delta G^{\ddagger}_{exp}$	Solvent-Assisted		Substrate-Assisted	
				$\Delta G^{\ddagger}_{calc}$	ΔG^{0}_{calc}	$\Delta G^{\ddagger}_{calc}$	ΔG^{0}_{calc}
Water	--	298.15	27.9	27.9± 0.3	19.0 ± 0.5	37.2 ± 0.3	-7.4 ± 0.9
Ras	4.7 x 10^{-4}	310.15	22.9	23.9 ± 0.3	17.7 ± 0.5	30.8 ± 0.2	-13.8 ± 0.7
RasGAP	19.1	298.15	15.7	14.9 ± 0.4	7.8 ± 0.5	28.7 ± 0.3	-13.5 ± 0.6
Ras-Q61H	3.2 x 10^{-5}	310.15	24.6	24.8 ± 0.5	18.9 ± 0.6	31.7± 0.4	-11.4 ± 0.9
Rab	1.5 x 10^{-5}	293.15	23.6	24.0 ± 0.4	21.9 ± 0.4	36.9± 0.7	2.1± 0.8
RabGAP	0.9	268	17.2	14.0 ± 0.5	4.5 ± 0.8	23.6 ± 0.5	-19.7 ± 0.8
$G_{\alpha i}$	0.028	293.15	19.2	21.1 ± 0.5	15.8 ± 0.6	29.4 ± 0.3	-14.2 ± 0.7
$G_{\alpha i}$-RGS4	5.0	293.15[b]	16.2	16.5 ± 0.6	9.8 ± 0.7	29.6 ± 0.3	-14.4 ± 0.5

[a] $\Delta G^{\ddagger}_{exp}$ and $\Delta G^{\ddagger}_{calc}$ denote experimental and calculated activation free energies, respectively, and ΔG^{0}_{calc} denotes the calculated reaction free energies. All energies are shown in kcal mol^{-1}, and the calculated values are averages and standard error of the mean (s.e.m.) over 20 individual trajectories for each system, obtained as described in the **Methodology** section. The experimental values were derived from the corresponding experimentally measured k_{cat} (s^{-1}) using transition state theory. [b] The experimental k_{cat} values were obtained from ref. [10] for Ras and RasGAP, ref. [9] for Ras-Q61H, ref. [11] for $G_{\alpha i}$ and $G_{\alpha i}$-RGS4, and ref. [8] for Rab and RabGAP. T_{exp} denotes the temperature (in K) used in the experiment for the measurements. All simulations were performed at 300K. The activation free energy for the non-enzymatic reaction in water was taken from ref. [12]. As the experiments were performed at different temperatures, the corresponding temperatures used in the experiments are also provided in this table. All simulations were performed at 300 K. Finally, the EVB simulations for the non-enzymatic hydrolysis of GTP *via* a solvent-assisted pathway were calibrated to the experimental value, and the differences between the substrate- and solvent-assisted pathways in the non-enzymatic reaction were taken from our previous quantum chemical study,[13] as described in the **Methodology** section.

Table S4. Calculated activation and reaction free energies for the tautomerization step shown in **Figure S3**, during the non-enzymatic, Ras-catalyzed, and RasGAP-catalyzed hydrolyses of GTP.[a]

	$\Delta G^{\ddagger}_{calc}$	ΔG^{0}_{calc}
Water	4.0 ± 0.3	-26.4 ±0.6
Ras	3.3 ± 0.3	-30.2 ± 0.6
RasGAP	4.7 ± 0.3	-23.8 ± 0.6

[a] $\Delta G^{\ddagger}_{calc}$ and ΔG^{0}_{calc} denote the calculated activation and reaction free energies, respectively. All energies are shown in kcal mol^{-1}, and the calculated values are averages and standard error of the mean (s.e.m.) over 20 individual trajectories for each system, obtained as described in the **Methodology** section. In **Figure 3** of the main text, these values have been added to the energy of the intermediate (ΔG^{0}_{calc}) obtained from the preceding phosphoryl transfer step (**Table S3**) in order to obtain the full corrected free energy profile for these reactions.

Table S5. Average calculated phosphorus-oxygen distances to the departing leaving group ($P\text{-}O_{lg}$) and to the incoming nucleophile ($P\text{-}O_{nuc}$) at the reactant complexes and transition states for non-enzymatic GTP hydrolysis *via* solvent- and substrate-assisted mechanisms.[a]

	Solvent-Assisted	**Substrate-Assisted**
Michaelis Complex		
$P\text{-}O_{lg}$	1.71 ± 0.01	1.63 ± 0.00
$P\text{-}O_{nuc}$	4.03 ± 0.02	3.32 ± 0.01
O_{nuc} - O_{lg}	5.72 ± 0.02	4.80 ± 0.01
(First) Transition State		
$P\text{-}O_{lg}$	2.56 ± 0.01	1.82 ± 0.01
$P\text{-}O_{nuc}$	2.26 ± 0.01	2.05 ± 0.01
O_{nuc} - O_{lg}	4.82 ± 0.01	3.84 ± 0.01
Intermediate/Product		
$P\text{-}O_{lg}$	3.90 ± 0.02	3.42 ± 0.02
$P\text{-}O_{nuc}$	1.88 ± 0.01	1.58 ± 0.00
O_{nuc} - O_{lg}	5.76 ± 0.02	4.69 ± 0.03

[a] All values are averages and standard error of the mean over 400 individual snapshots, extracted from 20 independent empirical valence bond simulations, obtained as described in the **Methodology** section.

Table S6. Average calculated phosphorus-oxygen distances to the departing leaving group ($P\text{-}O_{lg}$) and to the incoming nucleophile ($P\text{-}O_{nuc}$) for the tautomerization step at the transition states and product states for non-enzymatic (water) as well as Ras- and RasGAP-catalyzed GTP hydrolysis.[a]

	Water	**Ras**	**RasGAP**
Second Transition State			
$P\text{-}O_{lg}$	3.81± 0.02	3.33 ± 0.02	3.31 ± 0.01
$P\text{-}O_{nuc}$	1.87 ± 0.00	1.87 ± 0.00	1.86. ± 0.00
O_{nuc} - O_{lg}	5.08 ± 0.06	5.17 ± 0.02	4.92 ± 0.01
Product			
$P\text{-}O_{lg}$	3.50 ± 0.02	3.22 ± 0.02	3.19 ± 0.01
$P\text{-}O_{nuc}$	1.65 ± 0.00	1.65 ± 0.00	1.64 ± 0.00
O_{nuc} - O_{lg}	4.60 ± 0.05	4.74 ± 0.01	4.70 ± 0.01

[a] All values are averages and standard error of the mean over 400 individual snapshots, extracted from 20 independent empirical valence bond simulations, obtained as described in the **Methodology** section.

Table S7. Average calculated phosphorus-oxygen distances to the departing leaving group ($P\text{-}O_{lg}$) and to the incoming nucleophile ($P\text{-}O_{nuc}$) at the Michaelis complexes, transition states and products for GTPase-catalyzed GTP hydrolysis *via* a substrate-assisted pathway.[a]

	Ras	**RasGAP**	**Ras Q61H**	**Rab**	**RabGAP**	**$G_{\alpha i}$**	**$G_{\alpha i}$-RGS4**
Michaelis Complex							
$P\text{-}O_{lg}$	1.63 ± 0.00	1.64 ± 0.00	1.63 ± 0.00	1.62 ± 0.00	1.62 ± 0.00	1.63 ± 0.00	1.62 ± 0.00
$P\text{-}O_{nuc}$	3.22 ± 0.01	3.21 ± 0.01	3.30 ± 0.01	3.45 ± 0.01	3.07 ± 0.01	3.14 ± 0.01	3.12 ± 0.01
O_{nuc} - O_{lg}	4.73 ± 0.01	4.68 ± 0.01	4.80 ± 0.01	3.62 ± 0.03	4.61 ± 0.01	4.66 ± 0.01	4.58 ± 0.01
Transition State							
$P\text{-}O_{lg}$	1.84 ± 0.01	1.85 ± 0.01	1.84 ± 0.01	1.75 ± 0.01	1.80 ± 0.01	1.85 ± 0.01	1.84 ± 0.01
$P\text{-}O_{nuc}$	2.04 ± 0.01	2.10 ± 0.01	2.05 ± 0.01	2.01 ± 0.01	2.12 ± 0.01	2.05 ± 0.01	2.08 ± 0.01
O_{nuc} - O_{lg}	3.85 ± 0.01	3.92 ± 0.01	3.86 ± 0.01	3.74 ± 0.01	3.90 ± 0.01	3.88 ± 0.01	3.89 ± 0.01
Product							
$P\text{-}O_{lg}$	2.97 ± 0.01	3.02 ± 0.01	2.98 ± 0.01	2.96 ± 0.01	2.93 ± 0.01	3.02 ± 0.01	2.98 ± 0.01
$P\text{-}O_{nuc}$	1.58 ± 0.00	1.58 ± 0.00	1.58 ± 0.00	1.57 ± 0.00	1.58 ± 0.00	1.58 ± 0.00	1.58 ± 0.00
O_{nuc} - O_{lg}	4.45 ± 0.01	4.50 ± 0.01	4.47 ± 0.01	3.87 ± 0.01	4.44 ± 0.01	4.52 ± 0.01	4.46 ± 0.01

[a] All values are averages and standard error of the mean over 400 individual snapshots, extracted from 20 independent empirical valence bond simulations, obtained as described in the **Methodology** section. For the corresponding values for the non-enzymatic reaction in aqueous solution, as well as the GTPase-catalyzed reaction proceeding through a solvent-assisted mechanism, see **Tables S5** and **Table 1** of the main text.

Table S8. Average distances between the Arg finger provided by the GAP (or the instrinc Arg, in the case of $G_{\alpha i}$) and the leaving group oxygen (O_{lg}) at the Michaelis complexes, transition states and products for GTPase-catalyzed substrate-assisted GTP hydrolysis.[a]

	RasGAP	**RabGAP**	**$G_{\alpha i}$**	**$G_{\alpha i}$-RGS4**
Michaelis Complex				
Arg:H_{ε}-O_{lg}	5.97 ± 0.02	6.06 ± 0.02	5.28 ± 0.09	5.54 ± 0.02
Arg:$H_{\eta 11}$-O_{lg}	**2.72 ± 0.01**	3.26 ± 0.02	7.63 ± 0.08	**2.21 ± 0.01**
Arg:$H_{\eta 12}$-O_{lg}	2.89 ± 0.01	**2.26 ± 0.02**	7.68 ± 0.07	3.20 ± 0.01
Arg:$H_{\eta 21}$-O_{lg}	4.78 ± 0.03	5.24 ± 0.02	**5.16 ± 0.12**	4.78 ± 0.02
Arg:$H_{\eta 22}$-O_{lg}	5.88 ± 0.02	3.64 ± 0.02	6.30 ± 0.11	3.31 ± 0.01
Transition State				
Arg:H_{ε}-O_{lg}	6.03 ± 0.02	6.01 ± 0.02	5.34 ± 0.10	5.64 ± 0.02
Arg:$H_{\eta 11}$-O_{lg}	**2.76 ± 0.01**	3.28 ± 0.01	7.50 ± 0.09	**1.98 ± 0.01**
Arg:$H_{\eta 12}$-O_{lg}	3.01 ± 0.02	**2.11 ± 0.01**	7.56 ± 0.07	3.26 ± 0.01
Arg:$H_{\eta 21}$-O_{lg}	4.93 ± 0.03	5.14 ± 0.03	**5.14 ± 0.13**	4.76 ± 0.01
Arg:$H_{\eta 22}$-O_{lg}	6.00 ± 0.02	3.52 ± 0.02	6.20 ± 0.12	3.25 ± 0.01
Product				
Arg:H_{ε}-O_{lg}	5.57 ± 0.02	5.70 ± 0.02	**5.48 ± 0.09**	5.47 ± 0.01
Arg:$H_{\eta 11}$-O_{lg}	**2.49 ± 0.01**	3.10 ± 0.01	7.37 ± 0.09	**1.66 ± 0.01**
Arg:$H_{\eta 12}$-O_{lg}	2.90 ± 0.02	**1.74 ± 0.01**	7.36 ± 0.08	3.14 ± 0.01
Arg:$H_{\eta 21}$-O_{lg}	4.74 ± 0.03	4.87 ± 0.02	**5.49 ± 0.12**	4.53 ± 0.01
Arg:$H_{\eta 22}$-O_{lg}	5.66 ± 0.02	2.36 ± 0.01	6.37 ± 0.12	3.07 ± 0.01

[a] H_{ε} is the hydrogen at the N_{ε} nitrogen atom of Arg. $H_{\eta 11}$, $H_{\eta 12}$ and $H_{\eta 21}$, $H_{\eta 22}$ are the hydrogen atoms at $N_{\eta 1}$ and $N_{\eta 2}$ nitrogens of Arg, respectively. All values are averages and standard error of the mean over 400 individual snapshots, extracted from 20 independent empirical valence bond simulations, obtained as described in the **Methodology** section. The corresponding values for the solvent-assisted mechanism can be found in **Table 2** of the main text. The closest interactions, in each case, are highlighted in bold.

Table S9. Calculated activation and reaction free energies for Ras-catalyzed GTP hydrolysis *via* solvent and substrate assisted pathways, with and without a 10 kcal mol^{-1} $Å^{-2}$ harmonic positional restraint placed on the Gln61 side chain.[a]

	$\Delta G^{\ddagger}_{calc}$	ΔG^{0}_{calc}
Solvent-assisted pathway		
Flexible Gln61	23.9 ± 0.3	17.7 ± 0.5
Restrained Gln61	17.6 ± 0.5	11.2 ± 0.5
Substrate-assisted pathway		
Flexible Gln61	30.8 ± 0.2	-13.8 ± 0.7
Restrained Gln61	29.6 ± 0.3	-13.8 ± 1.1

[a] $\Delta G^{\ddagger}_{calc}$ and ΔG^{0}_{calc} denote the calculated activation and reaction free energies, respectively. All energies are shown in kcal mol^{-1}, and the calculated values are averages and standard error of the mean (s.e.m.) over 20 individual trajectories for each system, obtained as described in the **Methodology** section.

Table S10. Loss of conformational entropy of the catalytic glutamine residue upon protein folding of different GTPases considered in this work, calculated using the Predicting Loss of Protein S(entropy) (PLOPS)[14] webserver.[a]

System	Residue	TΔS Backbone	TΔS Sidechain	TΔS Total
Ras	Q61	1.15	0.39	1.54
RasGAP	Q61	1.15	1.00	2.15
Rab	Q67	1.15	0.44	1.59
RabGAP	Q144	1.15	0.99	2.14
$G_{\alpha i}$	Q204	1.15	0.75	1.90
$G_{\alpha i}$-RGS4	Q204	1.15	0.96	2.11

[a] All values are presented in kcal mol^{-1}. Note that as PLOPS calculates entropy *loss* upon protein folding, a more positive TΔS value in this table indicates that the side chain is more ordered in the folded state of the protein. The PLOPS webserver can be accessed at https://godzilla.uchicago.edu/pages/PLOPS/live/index.html.

Table S11. Metal-ligand distances in the initial crystal structures and during our simulations of solvent- and substrate-assisted GTP hydrolysis catalyzed by different GTPases.[a]

	Ras	**RasGAP**	**Ras Q61H**	**Rab**	**RabGAP**	**$G_{\alpha i}$**	**$G_{\alpha i}$-RGS4**
Initial crystal structures							
Ser:OG [b]	2.16	2.09	2.09	2.17	2.19	2.13	2.13
Thr:OG1 [b]	2.18	2.16	2.21	2.20	2.15	2.12	2.13
GTP:O- [b]	2.12	2.06	2.11	2.10	2.10	2.04	2.05
GTP:Ob [b]	2.11	2.07	2.10	2.03	2.08	2.06	2.16
HOH 1 [b]	2.09	2.11	2.19	2.15	2.14	2.14	2.09
HOH 2 [b]	2.16	2.12	2.11	2.14	2.13	2.10	2.17
Solvent-assisted pathway							
Ser:OG [b]	2.15 ± 0.05	2.14 ± 0.05	2.14 ± 0.05	2.14 ± 0.01	2.15 ± 0.01	2.15 ± 0.05	2.14 ± 0.04
Thr:OG1 [b]	2.17 ± 0.05	2.16 ± 0.05	2.16 ± 0.05	2.16 ± 0.01	2.17 ± 0.01	2.17 ± 0.05	2.15 ± 0.05
GTP:O- [b]	2.08 ± 0.04	2.08 ± 0.04	2.08 ± 0.04	2.10 ± 0.00	2.10 ± 0.00	2.08 ± 0.04	2.08 ± 0.04
GTP:Ob [b]	2.11 ± 0.04	2.10 ± 0.04	2.10 ± 0.04	2.08 ± 0.00	2.08 ± 0.00	2.11 ± 0.04	2.11 ± 0.04
HOH 1 [b]	2.13 ± 0.05	2.12 ± 0.04	2.13 ± 0.05	2.13 ± 0.00	2.14 ± 0.00	2.12 ± 0.05	2.12 ± 0.04
HOH 2 [b]	2.12 ± 0.05	2.13 ± 0.05	2.13 ± 0.05	2.12 ± 0.00	2.13 ± 0.00	2.13 ± 0.05	2.13 ± 0.05
Substrate-assisted pathway							
Ser:OG [b]	2.14 ± 0.05	2.13 ± 0.05	2.14 ± 0.05	2.12 ± 0.00	2.14 ± 0.01	2.15 ± 0.05	2.14 ± 0.05
Thr:OG1 [b]	2.16 ± 0.05	2.15 ± 0.05	2.16 ± 0.05	2.13 ± 0.00	2.16 ± 0.01	2.16 ± 0.05	2.15 ± 0.05
GTP:O- [b]	2.08 ± 0.04	2.06 ± 0.04	2.08 ± 0.04	2.11 ± 0.00	2.10 ± 0.00	2.08 ± 0.04	2.06 ± 0.04
GTP:Ob [b]	2.11 ± 0.04	2.11 ± 0.04	2.11 ± 0.04	2.07 ± 0.00	2.07 ± 0.00	2.11 ± 0.04	2.11 ± 0.04
HOH 1 [b]	2.13 ± 0.05	2.12 ± 0.04	2.13 ± 0.05	2.14 ± 0.00	2.14 ± 0.00	2.12 ± 0.05	2.12 ± 0.04
HOH 2 [b]	2.12 ± 0.05	2.13 ± 0.05	2.13 ± 0.05	2.16 ± 0.01	2.14 ± 0.00	2.13 ± 0.05	2.14 ± 0.05

[a] Values for both solvent- and substrate-assisted mechanism are averages and standard error of the mean over 10 000 individual snapshots, extracted every 100ps from the 20x50ns independent simulations (1μs total), obtained as described in the **Methodology** section. Values for the initial structure were obtained from the corresponding PDB structures used for our simulations, specifically, 1QRA[5, 15] (Ras), 1WQ1[3, 15] (RasGAP), 1GIA[6, 15] ($G_{\alpha i}$-subunit), 3NKV[7, 15] (Rab), chains I and J from 4HLQ[8, 15] (Rab1GAP), 621P[9, 15] (Ras Q61H variant). In the case of the $G_{\alpha i}$-RGS4 complex, a refined crystal structure was used as a starting point for the simulations.[16] [b] In all systems, the octahedral coordination sphere of Mg^{2+} is formed by two oxygen atoms belonging to the side chain residues of the

GTPase, namely a Ser and a Thr, two oxygens of the GTP triphosphate moiety (where Ob denotes the oxygen bridging the β,γ-phosphate and O^- denotes a non-bridging oxygen from the β-phosphate) and the oxygen atoms of two water molecules. The relevant sidechains in each system are the side chains of Ser17 and Thr35 in wild-type and Q61H mutant Ras and RasGAP, the side chains of Ser22 and Thr40 in Rab and RabGAP, the side chains of Ser14 and Thr148 in $G_{\alpha i}$, and the side chains of Ser47 and Thr181 in $G_{\alpha i}$-RGS4.

Table S12. Average number of water molecules found within 6Å of phosphorus atom of the γ-phosphate group of GTP (upper section), and the average number of hydrogen bonds formed between key species, as annotated, at the Michaelis complexes, transition states and intermediates of solvent-assisted GTPase-catalyzed GTP hydrolysis.[a]

	Ras	**RasGAP**	**Rab**	**RabGAP**	**$G_{\alpha i}$**	**$G_{\alpha i}$-RGS4**
Average number of water molecules within 6Å of the phosphorus atom of the γ-phosphate of GTP[b]						
Michaelis Complex	8.28 ± 0.08	2.05 ± 0.01	7.02 ± 0.08	2.76 ± 0.05	4.90 ± 0.06	3.46 ± 0.06
First Transition State	8.26 ± 0.09	2.00 ± 0.00	6.42 ± 0.07	2.86 ± 0.05	5.25 ± 0.07	3.22 ± 0.05
Intermediate	8.94 ± 0.09	2.00 ± 0.00	6.13 ± 0.07	3.05 ± 0.05	5.30 ± 0.08	3.39 ± 0.05
Average number of hydrogen bonds formed between the γ-phosphate and the solvent molecules[b]						
Michaelis Complex	2.76 ± 0.06	0.04± 0.01	1.59 ± 0.05	0.14 ± 0.02	0.85 ± 0.04	0.61 ± 0.04
First Transition State	2.01 ± 0.04	-	1.50 ± 0.03	0.18 ± 0.01	0.53 ± 0.03	0.14 ± 0.02
Intermediate	1.87 ± 0.04	-	1.29 ± 0.03	0.17 ± 0.03	0.29 ± 0.03	0.17 ± 0.02
Average number of hydrogen bonds formed between the γ-phosphate and the GTPase						
Michaelis Complex	1.60 ± 0.04	2.65 ± 0.04	2.76 ± 0.04	3.34 ± 0.04	2.98 ± 0.04	2.88 ± 0.04
First Transition State	2.01 ± 0.04	3.64 ± 0.04	3.33 ± 0.05	3.75 ± 0.04	3.20 ± 0.04	3.53 ± 0.03
Intermediate	2.11 ± 0.04	3.78 ± 0.02	3.45 ± 0.05	4.03 ± 0.03	3.37 ± 0.04	3.79 ± 0.04
Average number of hydrogen bonds formed between the carbonyl oxygen of the active site Gln and the nucleophilic water molecule						
Michaelis Complex	0.16 ± 0.02	0.74 ± 0.02	-	0.60 ± 0.04	0.63 ± 0.03	0.39 ± 0.02
First Transition State	0.25 ± 0.02	0.84 ± 0.02	0.71 ± 0.02	0.91 ± 0.03	0.83 ± 0.02	0.77 ± 0.02
Intermediate	0.31 ± 0.02	0.90 ± 0.01	0.80 ± 0.02	0.90 ± 0.03	0.88 ± 0.02	0.75 ± 0.02

[a] All values are averages and standard error of the mean over 400 individual snapshots, extracted from 20 independent empirical valence bond simulations, obtained as described in the **Methodology** section. The corresponding values for the substrate-assisted mechanism can be found in **Table S13**. [b] The nucleophilic water molecule is excluded from these numbers. Note that "-" in this table indicates that no hydrogen bonds were found for this system.

Table S13. Average number of water molecules found within 6Å of phosphorus atom of the γ-phosphate group of GTP (upper section), and the average number of hydrogen bonds formed between key species, as annotated, at the Michaelis complexes, transition states and products of substrate-assisted GTPase-catalyzed GTP hydrolysis.[a]

	Ras	**RasGAP**	**Rab**	**RabGAP**	**$G_{\alpha i}$**	**$G_{\alpha i}$-RGS4**
Average number of water molecules within 6Å of the phosphorus atom of the γ-phosphate of GTP[b]						
Michaelis Complex	8.22 ± 0.08	2.21 ± 0.02	6.53 ± 0.07	3.12 ± 0.05	5.46 ± 0.07	3.62 ± 0.04
Transition State	7.61 ± 0.09	2.18 ± 0.02	6.24 ± 0.07	2.77 ± 0.04	4.86 ± 0.06	3.22 ± 0.03
Product	7.67 ± 0.08	2.30 ± 0.03	8.50 ± 0.11	2.96 ± 0.05	5.33± 0.07	3.20 ± 0.04
Average number of hydrogen bonds formed between the γ-phosphate and the solvent molecules[b]						
Michaelis Complex	2.32 ± 0.04	0.07 ± 0.01	1.40 ± 0.04	0.22 ± 0.02	1.06 ± 0.05	0.85 ± 0.02
Transition State	1.41 ± 0.04	0.04 ± 0.01	1.25 ± 0.03	0.12 ± 0.02	0.37 ± 0.03	0.50 ± 0.02
Product	0.81 ± 0.03	0.07 ± 0.01	1.85 ± 0.06	0.05 ± 0.01	0.25 ± 0.02	0.17 ± 0.02
Average number of hydrogen bonds formed between the γ-phosphate and the GTPase						
Michaelis Complex	1.62 ± 0.03	2.77 ± 0.04	2.83 ± 0.05	3.25 ± 0.04	2.45 ± 0.04	2.24 ± 0.03
Transition State	1.95 ± 0.03	2.79 ± 0.03	2.74 ± 0.05	3.17 ± 0.04	2.63 ± 0.04	2.48 ± 0.03
Product	2.21 ± 0.03	2.60 ± 0.04	1.36 ± 0.05	3.68 ± 0.03	2.64 ± 0.04	2.66 ± 0.03
Average number of hydrogen bonds formed between the carbonyl oxygen of the active site Gln and the nucleophilic water molecule						
Michaelis Complex	-	0.45 ± 0.02	-	0.44 ± 0.04	0.09 ± 0.01	0.27 ± 0.02
Transition State	0.02 ± 0.01	0.56 ± 0.02	0.08 ± 0.01	0.51 ± 0.03	0.01 ± 0.00	0.41 ± 0.02
Product	0.04 ± 0.01	0.66 ± 0.02	0.31 ± 0.02	0.52 ± 0.03	0.10 ± 0.01	0.80 ± 0.02

[a] All values are averages and standard error of the mean over 400 individual snapshots, extracted from 20 independent empirical valence bond simulations, obtained as described in the **Methodology** section. The corresponding values for the solvent-assisted mechanism can be found in **Table S12**. [b] The nucleophilic water molecule is excluded from these numbers. Note that "-" in this table indicates that no hydrogen bonds were found for this system.

S3. Empirical Valence Bond Parameters

Table S14. EVB off-diagonal element (H_{ij}) and gas phase shift (α_i) parameters, calibrated as described in the main text.

Mechanism	Reaction	H_{ij} (kcal mol^{-1})	α_i (kcal mol^{-1})
Solvent-assisted	Phosphate Hydrolysis	77.36	262.42
Solvent-assisted	Tautomerization	25.70	-197.35
Substrate -assisted	GTP hydrolysis	50.94	46.69

Table S15. List of the atom types and van der Waals parameters used to describe atoms constituting the reacting part of the system.

Type	A_i (kcal$^{1/2}$ mol$^{1/2}$ Å^6)	B_i (kcal$^{1/2}$ mol$^{1/2}$ Å^3)	C_i (kcal mol^{-1})	α_i (Å^2)	$A_{1\text{-}4}$ (kcal$^{1/2}$ mol$^{1/2}$Å^3)	$B_{1\text{-}4}$ (kcal$^{1/2}$ mol$^{1/2}$ Å^3)	Mass (a.u.)
CT	944.52	22.03			667.88	15.58	12.01
HC	69.58	4.91			49.20	3.47	1.01
HO	0.01	0.04	5	2.5	0.00	0.03	1.01
HW	0.00	0.00	5	2.5	0.00	0.00	1.01
Olg	873.79	27.96	500	2.0	617.86	19.76	16.00
OH	401.02	17.32	53	2.5	283.56	12.25	16.00
OP1	873.79	27.96	53	2.5	617.86	19.76	16.00
OP2	626.39	23.67	53	2.5	442.92	16.74	16.00
OW	726.89	24.39	53	2.5	539.44	17.25	16.00
OW2	726.89	24.39	60	2.5	539.44	17.25	16.00
O1	445.13	18.25	150	2.0	314.76	12.91	16.00
O2	873.79	27.96	150	2.0	617.86	19.76	16.00
P1	2447.79	46.79	45	1.4	1730.85	33.09	30.97
P2	2447.79	46.79	40	1.5	1730.85	33.09	30.97
P3	2447.79	46.79	43	2.5	1730.85	33.09	30.97

[a] For all atoms except the reacting atoms, a standard 6-12 Lennard-Jones potential was used. In the case of the reacting atoms, which change bonding patterns between atoms *i* and *j*, an alternate function of the form $V_{react} = C_i C_j \exp(-\alpha_i \alpha_j r_{ij})$ was used to prevent artificial repulsion between these atoms as bonding patterns change. r_{ij} denotes the distance (Å) between atoms *i* and *j*. Note that this was only applied to atoms that change bonding patterns during the reaction, and not to all atoms in the system. For atom type assignment see **Table S16**.

Table S16. Atom types in the different VB states (**Figure S1** and **S2**) used to describe GTP hydrolysis *via* both solvent- and substrate-assisted mechanisms.[a]

Atom number	State 1_{solv}	State 2_{solv}	State 3_{solv}	State 1_{sub}	State 2_{sub}
1	HC	HC	HC	HC	HC
2	CT	CT	CT	CT	CT
3	HC	HC	HC	HC	HC
4	O1	O1	O1	O1	O1
5	P1	P1	P1	P1	P1
6	OP1	OP1	OP1	OP1	OP1
7	OP1	OP1	OP1	OP1	OP1
8	O1	O1	O1	O1	O1
9	P1	P1	P1	P1	P1
10	OP1	OP1	OP1	OP1	OP1
11	OP1	OP1	OP1	OP1	OP1
12	O1	Olg	Olg	O1	O2
13	P1	P2	P2	P3	P3
14	OP1	OP2	OH	OP1	OH
15	OP1	OP2	OP2	OP1	OP2
16	OP1	OP2	OP2	OP1	OP2
17	OW2	OH	OH	OW	OH
18	HW	HO	HO	HW	HO
19	HW	HO	HO	HW	HO

[a] See **Figure S1 and S2** for the atom numbering, **Table S15** for the corresponding van der Waals parameters and **Table S17** for the corresponding partial charges. The subscripts solv and sub denote solvent- and substrate-assisted mechanisms, respectively.

Table S17. Atomic partial charges in the different VB states (**Figure S1** and **S2**) used to describe GTP hydrolysis *via* both solvent- and substrate-assisted mechanisms.[a]

Atom number	State 1_{solv}	State 2_{solv}	State 3_{solv}	State 1_{sub}	State 2_{sub}
1	0.067907	0.067909	0.067909	0.067907	0.067909
2	0.055805	0.055807	0.055807	0.055805	0.055807
3	0.067907	0.067909	0.067909	0.067907	0.067909
4	-0.598641	-0.657813	-0.657813	-0.598641	-0.657813
5	1.253323	1.493096	1.493096	1.253323	1.493096
6	-0.879813	-0.947275	-0.947275	-0.879813	-0.947275
7	-0.879813	-0.947275	-0.947275	-0.879813	-0.947275
8	-0.568844	-0.634516	-0.634516	-0.568844	-0.634516
9	1.385334	1.367380	1.367380	1.385334	1.367380
10	-0.889312	-0.955074	-0.955074	-0.889312	-0.955074
11	-0.889312	-0.955074	-0.955074	-0.889312	-0.955074
12	-0.532148	-0.955074	-0.955074	-0.532148	-0.955074
13	1.265125	1.389070	1.565000	1.265125	1.565000
14	-0.952506	-0.861224	-0.692500	-0.952506	-0.692500
15	-0.952506	-0.861224	-0.970000	-0.952506	-0.970000
16	-0.952506	-0.861224	-0.970000	-0.952506	-0.970000
17	-0.834000	-0.647508	-0.692500	-0.834000	-0.692500
18	0.417000	0.421055	0.380000	0.417000	0.380000
21	0.417000	0.421055	0.380000	0.417000	0.380000

[a] For the corresponding atom numbering, see **Figure S1 and S2**, and for details of how these charges were derived, see the main text. The subscripts solv and sub denote solvent- and substrate-assisted mechanisms, respectively.

Table S18. Bond types and corresponding parameters for the covalent bonds of the reacting part of the system.[a]

Bond type	D (kcal mol^{-1})	α (Å^{-2})	r_0 (Å)	K_b (kcal mol^{-1} Å^{-2})	r_0 (Å)
0	Not Set				
1	60.0	1.5	1.610		
2	95.0	2.0	1.610		
3	95.0	1.5	1.880		
4	110.0	2.0	0.940		
5	245.8	1.5	0.957		
6	245.8	1.5	0.975		
7				460.0	1.660
8				460.0	1.670
9				460.0	1.690
10				460.0	1.967
11				717.0	1.600
12				717.0	1.610
13				1000.0	1.963
14				1104.8	0.975
15				1106.0	0.945
16				1106.0	0.957
17				1046.5	1.510
18				1050.0	1.480
19				1050.0	1.500
20				1050.0	1.540

[a] The bonds between non-reacting atoms are described using harmonic potentials, $V_{\text{harmonic}} = 0.5K_b\,(r_{ij} - r_0)^2$, while bonds between reacting atoms are described using Morse potentials $V_{\text{Morse}} = D\,\{1 - \exp[-\alpha\,(r_{ij} - r_0)]\}^2$. The bond-type assignments for the initial phosphoryl transfer reaction in the solvent-assisted mechanism, the subsequent tautomerization step, and for the substrate-assisted mechanism, are shown in **Tables S19 – S21**, respectively.

Table S19. Bond types used to describe the covalent bonds of the reacting part of the system, for the initial phosphoryl transfer step during solvent-assisted GTP hydrolysis (for the VB states see **Figure S1**).[a]

Atom number		**Bond type**	
#1	**#2**	**State 1**	**State 2**
12	13	1	0
13	17	0	3
8	9	8	7
4	5	9	8
5	8	11	12
9	10	19	20
9	11	19	20
9	12	11	20
13	14	20	17
13	15	20	17
13	16	20	17
17	18	16	14
17	19	16	14

[a] See **Figure S1** for the atom numbering.

Table S20. Bond types used to describe the covalent bonds of the reacting part of the system, for the tautomerization step during solvent-assisted GTP hydrolysis (for the VB states see **Figure S1**).[a]

Atom number		Bond type	
#1	**#2**	**State 2**	**State 3**
17	19	6	0
14	19	0	4
13	14	17	10
13	15	17	18
13	16	17	18
13	17	13	10
17	18	14	15
8	9	7	7
4	5	8	8
5	8	12	12
9	10	20	20
9	11	20	20
9	12	20	20

[a] See **Figure S1** for the atom numbering.

Table S21. Bond types used to describe the covalent bonds of the reacting part of the system, for GTP hydrolysis *via* a substrate-assisted mechanism, using the VB states described in **Figure S2**.[a]

Atom number		Bond type	
#1	**#2**	**State 1**	**State 2**
12	13	1	0
17	19	5	0
14	19	0	4
13	17	0	2
8	9	8	7
4	5	9	8
5	8	11	12
9	10	19	20
9	11	19	20
9	12	11	20
13	14	20	10
13	15	20	18
13	16	20	18
17	18	16	15

[a] See **Figure S2** for the atom numbering.

Table S22. Angle types and the corresponding parameters used for bending adjacent bonds in the reacting part of the system.[a]

Angle type	K_a (kcal mol^{-1} rad^{-2})	Θ (°)
0	Not Set	
1	47.80	110.50
2	90.00	102.60
3	90.00	108.50
4	97.70	112.07
5	99.52	105.88
6	155.20	98.09
7	163.52	118.05
8	239.00	98.50
9	200.00	104.52
10	200.00	108.23
11	280.00	119.90
12	280.00	122.50

[a] The angle potential is described using the potential $V_{angle} = 0.5\ \Sigma K_a(\Theta-\Theta_0)^2$. The angle-type assignments for the initial phosphoryl transfer reaction in the solvent-assisted mechanism, the subsequent tautomerization step, and for the substrate-assisted mechanism, are shown in **Tables S23 – S25**, respectively.

Table S23. Angle types used to describe the covalent bonds of the reacting part of the system, for the initial phosphoryl transfer step during solvent-assisted GTP hydrolysis (for the VB states see **Figure S1**).[a]

Atom number			Angle type	
#1	**#2**	**#3**	**State 1**	**State 2**
12	13	14	10	0
12	13	15	10	0
12	13	16	10	0
9	12	13	1	0
14	13	17	0	6
15	13	17	0	6
16	13	17	0	6
13	17	18	0	4
13	17	19	0	4
6	5	8	2	10
10	9	12	10	12
14	13	15	12	7
14	13	16	12	7
7	5	8	2	10
11	9	12	10	12
15	13	16	12	7
8	9	12	8	10
4	5	8	4	2
18	17	19	9	5

[a]See **Figure S1** for the atom numbering.

Table S24. Angle types used to describe the covalent bonds of the reacting part of the system, for the tautomerization step during solvent-assisted GTP hydrolysis (for the VB states see **Figure S1**).[a]

Atom number			Angle type	
#1	**#2**	**#3**	**State 2**	**State 3**
14	13	17	6	2
15	13	17	6	10
16	13	17	6	10
13	17	19	4	0
13	17	18	4	3
14	13	15	7	10
14	13	16	7	10
15	13	16	7	11
19	17	19	5	0
13	14	19	0	3
10	9	12	12	12
7	5	8	10	10
11	9	12	12	12
8	9	12	10	10
4	5	8	2	2

[a] See **Figure S1** for the atom numbering.

Table S25. Angle types used to describe the covalent bonds of the reacting part of the system, for GTP hydrolysis *via* a substrate-assisted mechanism, using the VB states described in **Figure S2**.[a]

Atom number			Angle type	
#1	**#2**	**#3**	**State 1**	**State 2**
12	13	14	10	0
12	13	15	10	0
12	13	16	10	0
9	12	13	1	0
18	17	19	9	0
14	13	17	0	2
15	13	17	0	10
16	13	17	0	10
13	14	19	0	3
13	17	18	0	3
6	5	8	2	10
10	9	12	10	12
14	13	15	12	10
14	13	16	12	10
7	5	8	2	10
11	9	12	10	12
15	13	16	12	11
8	9	12	8	10
4	5	8	8	2

[a] See **Figure S2** for the atom numbering.

Table S26. Torsion types and the corresponding parameters for rotation of dihedrals in the reacting part of the system.[a]

Torsion type	K_φ (kcal mol^{-1} rad^{-2})	n	φ_0 (°)
0	Not Set		
1	0.00000	1.0	0.0
2	0.02271	-5.0	0.0
3	0.19778	-4.0	180.0
4	0.45949	-3.0	0.0
5	-0.24857	-2.0	180.0
6	-2.26757	1.0	0.0
7	0.15476	-3.0	0.0
8	0.0006	1.0	0.0
9	-0.00224	-5.0	0.0
10	0.00209	-4.0	180.0
11	0.59826	-3.0	0.0
12	-0.08724	-2.0	180.0
13	1.35188	1.0	0.0
14	-0.09097	-5.0	0.0
15	0.15685	-4.0	180.0
16	0.58482	-3.0	0.0
17	-0.89627	-2.0	180.0
18	-0.35761	1.0	0.0
19	0.00762	-5.0	0.0
20	0.06603	-4.0	180.0
21	0.15341	-3.0	0.0
22	-0.08246	-2.0	180.0
23	-0.75615	1.0	0.0
24	0.01509	-5.0	0.0
25	0.13175	-4.0	180.0
26	0.30608	-3.0	0.0
27	-0.16611	-2.0	180.0
28	-1.51141	1.0	0.0

[a] The torsion angle potential is described using the potential $V_{torsion} = K_\varphi(1+\cos(n\varphi-\varphi_0))$. The torsion-type assignments for the initial phosphoryl transfer reaction in the solvent-assisted mechanism, the subsequent tautomerization step, and for the substrate-assisted mechanism, are shown in **Tables S27 – S29**, respectively.

Table S27. Torsion types used to describe the covalent bonds of the reacting part of the system, for the initial phosphoryl transfer step during solvent-assisted GTP hydrolysis (for the VB states see **Figure S1**).[a]

Atom number				Torsion type	
#1	**#2**	**#3**	**#4**	**State 1**	**State 2**
10	9	12	13	1	0
11	9	12	13	1	0
8	9	12	13	2	0
8	9	12	13	3	0
8	9	12	13	4	0
8	9	12	13	5	0
8	9	12	13	6	0
9	12	13	14	7	0
9	12	13	14	8	0
9	12	13	15	7	0
9	12	13	15	8	0
9	12	13	16	7	0
9	12	13	16	8	0
14	13	17	18	0	1
14	13	17	19	0	1
15	13	17	18	0	1
15	13	17	19	0	1
16	13	17	18	0	1
16	13	17	19	0	1
2	4	5	8	9	14
2	4	5	8	10	15
2	4	5	8	11	16
2	4	5	8	12	17
2	4	5	8	13	18
4	5	8	9	19	24
4	5	8	9	20	25
4	5	8	9	21	26
4	5	8	9	22	27
4	5	8	9	23	28
5	8	9	12	2	0
5	8	9	12	3	0
5	8	9	12	4	0
5	8	9	12	5	0
5	8	9	12	6	1

[a] See **Figure S1** for the atom numbering.

Table S28. Torsion types used to describe the covalent bonds of the reacting part of the system, for the tautomerization step during solvent-assisted GTP hydrolysis (for the VB states see **Figure S1**).[a]

Atom number				Torsion type	
#1	**#2**	**#3**	**#4**	**State 2**	**State 3**
14	13	17	18	1	1
14	13	17	19	1	0
15	13	17	18	1	1
15	13	17	19	1	0
16	13	17	18	1	1
16	13	17	19	1	0
17	13	14	19	0	1
15	13	14	19	0	1
16	13	14	19	0	1
2	4	5	8	14	14
2	4	5	8	15	15
2	4	5	8	16	16
2	4	5	8	17	17
2	4	5	8	18	18
4	5	8	9	24	24
4	5	8	9	25	25
4	5	8	9	26	26
4	5	8	9	27	27
4	5	8	9	28	28
5	8	9	12	1	1

[a] See **Figure S1** for the atom numbering.

Table S29. Torsion types used to describe the covalent bonds of the reacting part of the system, for GTP hydrolysis *via* a substrate-assisted mechanism, using the VB states described in **Figure S2**.[a]

Atom number				Torsion type	
#1	**#2**	**#3**	**#4**	**State 1**	**State 2**
10	9	12	13	1	0
11	9	12	13	1	0
8	9	12	13	2	0
8	9	12	13	3	0
8	9	12	13	4	0
8	9	12	13	5	0
8	9	12	13	6	0
9	12	13	14	7	0
9	12	13	14	8	0
9	12	13	15	7	0
9	12	13	15	8	0
9	12	13	16	7	0
9	12	13	16	8	0
14	13	17	18	0	1
14	13	17	19	0	1
15	13	17	18	0	1
15	13	17	19	0	1
16	13	17	18	0	1
16	13	17	19	0	1
2	4	5	8	9	14
2	4	5	8	10	15
2	4	5	8	11	16
2	4	5	8	12	17
2	4	5	8	13	18
4	5	8	9	19	24
4	5	8	9	20	25
4	5	8	9	21	26
4	5	8	9	22	27
4	5	8	9	23	28
5	8	9	12	2	0
5	8	9	12	3	0
5	8	9	12	4	0
5	8	9	12	5	0
5	8	9	12	6	1

[a] See **Figure S2** for the atom numbering.

S4. References

1. Duarte, F.; Åqvist, J.; Williams, N. H.; Kamerlin, S. C. L., Resolving Apparent Conflicts Between Theoretical and Experimental Models of Phosphate Monoester Hydrolysis. *J. Am. Chem. Soc.* **2014,** *137*, 1081-1093.

2. McGibbon, R. T.; Beauchamp, K. A.; Harrigan, M. P.; Klein, C.; Swails, J. M.; Hernández, C. X.; Schwantes, C. R.; Wang, L. P.; Lane, T. J.; Pande, V. J., MDTraj: A Modern Open Library for the Analysis of Molecular Dynamics Trajectories. *Biophys. J.* **2015,** *109*, 1528-1532.

3. Scheffzek, K.; Ahmadian, M. R.; Kabsch, W.; Wiesmuller, L.; Lautwein, A.; Schmitz, F.; Wittinghofer, A., The Ras-RasGAP Complex: Structural Basis for GTPase Activation and its Loss in Oncogenic Ras Mutants. *Science* **1997,** *277*, 333-338.

4. Voorhees, R. M.; Schmeing, T. M.; Kelley, A. C.; Ramakrishnan, V. T., The Mechanism for Activation of GTP Hydrolysis on the Ribosome. *Science* **2010,** *835-838*.

5. Scheidig, A. J.; Burmester, C.; Goody, R. S., The Pre-Hydrolysis State of p21Ras in Complex with GTP: New Insights into the Role of Water Molecules in the GTP Hydrolysis Reaction of Ras-like Proteins. *Structure* **1999,** *7*, 1311-1324.

6. Coleman, D. E.; Berghuis, A. M.; Lee, E.; Linder, M. E.; Gilman, A. G., Structures of Active Conformations of Gi Alpha 1 and the Mechanism of GTP Hydrolysis. *Science* **1994,** *265*, 1405-1412.

7. Müller, M. P.; Peters, H.; Blümer, J.; Blankenfeldt, W.; Goody, R. S.; Itzen, A., The Legionella Effector Protein DrrA AMPylates the Membrane Traffic Regulator Rab1b. *Science* **2010,** *329*, 946-949.

8. Gavriljuk, K.; Gazdag, E.-M.; Itzen, Y.; Kötting, C.; Goody, R. S.; Gerwert, K., Catalytic Mechanism of a Mammalian Rab*RabGAP Complex in Atomic Detail. *Proc. Natl. Acad. Sci. U. S. A.* **2012,** *109*, 21348-21353.

9. Krengel, U.; Schlichting, I.; Scherer, A.; Schumann, R.; Frech, M.; John, J.; Kabsch, W.; Pai, E. F.; Wittinghofer, A., Three-Dimensional Structures of H-ras p21 Mutants: Molecular Basis for their Inability to Function as Signal Switch Molecules. *Cell* **1990,** *62*, 539-548.

10. Schweins, T.; Geyer, M.; Scheffzek, K.; Warshel, A.; Robert, K.; Wittinghofer, A., Substrate-Assisted Catalysis as a Mechanism for GTP Hydrolysis of p21Ras and Other GTP-Binding Proteins. *Nat. Struct. Biol.* **1995,** *2*, 36-44.

11. Lan, K. L.; Zhong, H.; Nanamori, M.; Neubig, R. R., Rapid Kinetics of Regulator of G-protein Signaling (RGS)-Mediated $G_{\alpha i}$ and $G_{\alpha o}$ Deactivation. *J. Biol. Chem.* **2000,** *275*, 33497-33503.

12. Kötting, C.; Gerwert, K., Time-Resolved FTIR Studies Provide Activation Free Energy, Activation Enthalpy and Activation Entropy for GTPase Reactions. *Chem. Phys.* **2004,** *307*, 227-232.

13. Barrozo, A.; Blaha-Nelson, D.; Williams, N. H.; Kamerlin, S. C. L., The Effect of Magnesium Ions on Triphosphate Hydrolysis. *Pure Appl. Chem.* **2017,** *89*, 715-727.

14. Baxa, M. C.; Haddadian, E. J.; Jumper, J. M.; Freed, K. F.; Sosnick, T. R., Loss of Conformational Entropy in Protein Folding Calculated Using Realistic Ensembles and its Implications for NMR-Based Calculations. *Proc. Natl. Acad. Sci. U. S. A.* **2014,** *111*, 15396-15401.

15. Berman, H. M.; Westbrook, J.; Feng, Z.; Gilliland, G.; Bhat, T. N.; Weissig, H.; Shindyalov, I. N.; Bourne, P. E., The Protein Data Bank. *Nucleic Acids Res.* **2000,** *28*, 235-242.

16. Mann, D.; Teuber, C.; Tennigkeit, S. A.; Schröter, G.; Gerwert, K.; Kötting, C., Mechanism of the Intrinsic Arginine Finger in Heterotrimeric G Proteins. *Proc. Natl. Acad. Sci. U. S. A.* **2016,** *113*, E8041-E8050.